LASER DOPPLER FLOWMETERS--A SPECTRAL ANALYSIS

A THESIS

Presented to

The Faculty of the Graduate Division

by

William Taylor Mayo, Jr.

In Partial Fulfillment

of the Requirements for the Degree

Doctor of Philosophy

in the School of Electrical Engineering

Georgia Institute of Technology

May, 1969

In presenting the dissertation as a partial fulfillment of the requirements for an advanced degree from the Georgia Institute of Technology, I agree that the Library of the Institute shall make it available for inspection and circulation in accordance with its regulations governing materials of this type. I agree that permission to copy from, or to publish from, this dissertation may be granted by the professor under whose direction it was written, or, in his absence, by the Dean of the Graduate Division when such copying or publication is solely for scholarly purposes and does not involve potential financial gain. It is understood that any copying from, or publication of, this dissertation which involves potential financial gain will not be allowed without written permission.

_____

/ /

7/25/68

LASER DOPPLER FLOWMETERS--A SPECTRAL ANALYSIS

Approved:

Chairman

Date approved by Chairman: May 30, 1969

ACKNOWLEDGMENTS

Dr. W. B. Jones, Jr., was my advisor for my Master's thesis, my course work, and the initial phases of my Doctoral research. He suggested the area of research and provided helpful guidance. Discussion of the problem with Frank Morris, another of Dr. Jones' graduate students, contributed to the formulation of the statistical approach developed in Chapter III. After Dr. Jones' departure from Georgia Tech, Dr. F. K. Hurd became my advisor, and both he and Dr. A. M. Bush provided me with suggestions and helpful criticism in the final stages of the research and in the writing of the thesis. Dr. J. W. Hooper served as the third member of my reading committee.

A National Science Foundation Co-op Fellowship provided financial support during my Master's work and through the first year of my Doctoral research. The following year I was supported by a Teaching and Research Assistantship provided by Dr. B. J. Dasher, the Director of the School of Electrical Engineering. D. M. Meadows then took an interest in my work which resulted in a research position at the Lockheed-Georgia Systems Sciences Research Laboratories. The major portion of the experimental research was conducted at the Lockheed-Georgia facilities.

Barbara Bradley, Beverly Thomas, and my wife Mary Ann contributed to the typing of rough drafts; Hal Bramlett made the final drawings; and Betty Sims and Doris Lunsford typed the final version of the thesis.

My wife Mary Ann and my son Taylor endured many nights and weekends while I studied.

To all these individuals, and to many others, I owe a debt which cannot be paid. I can only offer my deepest thanks.

TABLE OF CONTENTS

LIST OF TABLES

LIST OF ILLUSTRATIONS

Figure Page

SUMMARY

The objectives of this thesis research have been: to provide theoretical insight concerning the effects of the optical subsystem of an optical heterodyne laser Doppler flowmeter on the measurement volume dimensions, the system alignment, the signal bandwidth, and the signal-to-noise ratio; to design improved laser flowmeter optical systems; to experimentally verify the feasibility of improved systems and to verify some of the predicted variations of signal bandwidth and signal-to-noise ratio.

The method of attack has been to formulate a general static model of the laser flowmeter from which the signal current could be determined in terms of the positions of the scatterers. The flow velocity has been assumed constant in space and time to isolate signal spectral effects dependent on the optical system from those dependent on the flow field. A three-dimensional Poisson "shot-noise" random process has been developed and used to formulate a stochastic model of the flowmeter signal current.

In the development of the generalized heterodyne flowmeter optics model a theorem concerning optical heterodyne detection has been proved which states that the effect on the signal current of any finite set of passive transmission filters, used to alter the signal and/or reference beam radiation, may be obtained with an equivalent reference beam with no filters present. The response of the generalized

equivalent flowmeter optical system has been determined analytically and used to determine optimum systems employing elliptical Gaussian beams. The variation of the signal bandwidth, the signal-to-noise ratio and the measurement volume dimensions have been expressed as algebraic functions of the parameters of the optimized system.

The theoretical analysis has led to the development of a simplified practical optical system which requires almost no heterodyne alignment and is insensitive to stress or vibration. In addition, a new type of laser flowmeter, which operates on the principles of interference patterns, has been discovered and analyzed briefly. This system is capable of making velocity measurements in situations for which a heterodyne flowmeter employing a reference beam is not applicable.

Some of the predictions of the heterodyne flowmeter analysis have been verified experimentally, and the feasibility of the new flowmeter optical systems has been demonstrated.

CHAPTER I

INTRODUCTION

Motivation for Problem

Principles of Laser Flowmeters

An optical heterodyne laser Doppler flowmeter[1-15] is an electro-optical system capable of measuring localized vector velocities of liquids and gases in real time without disturbing the flow field. A wide variety of specific optical and electronic subsystems have been developed since the first feasibility experiment was reported by Yeh and Cummins in 1964.[1] All of these systems function by detecting the Doppler frequency shift of coherent light scattered by a dilute suspension of microscopic contaminant particles moving with the fluid. Since electronic systems do not have optical frequency response, the Doppler shift is detected by mixing the scattered wave with an optical local oscillator reference beam at a square-law photodetector surface.† This heterodyne detection process[16-19] translates the frequency modulation to the electronic frequency range at the photodetector output. Vector velocity measurements can be obtained by using three detectors and reference beams in different locations to determine independent velocity components. The region over which the measurement occurs may

---

†All photodetectors respond to incident power, which is proportional to the square of the total incident field.

be restricted to very small volumes by focussing the incident and scattered beams.

Figure 1(a) illustrates the Doppler effect. A plane wave of frequency f_o is incident in the direction of unit vector $\bar{u}_o$ on a scatterer moving with non-relativistic velocity $\bar{v}$. The locally plane scattered radiation far from the scatterer, with local direction of propagation given by unit vector $\bar{u}_s$, has frequency $f_s = f_o + f_d$, where

$$f_d = \frac{K}{2\pi} (\bar{u}_s - \bar{u}_o) \cdot \bar{v} \tag{1}$$

and

$$K = \frac{2\pi}{\lambda} = \frac{2\pi f_o}{c} \tag{2}$$

For a typical scattering angle, $\theta = 10°$, and typical wavelength, $\lambda = 0.633$ microns, Equation (1) implies a Doppler sensitivity of 275 KHz/ft/sec.

Figure 1(b) illustrates the optical heterodyne detection process. A beam splitter is usually used to superpose the two optical waves because effective mixing does not occur unless the wavefronts of the two beams are aligned parallel to within a fraction of a wavelength over the entire detection aperture. (For example, for a 1 mm square aperture, the allowable misalignment angle is less than 0.633 milliradians if $\lambda = 0.633$ microns.)

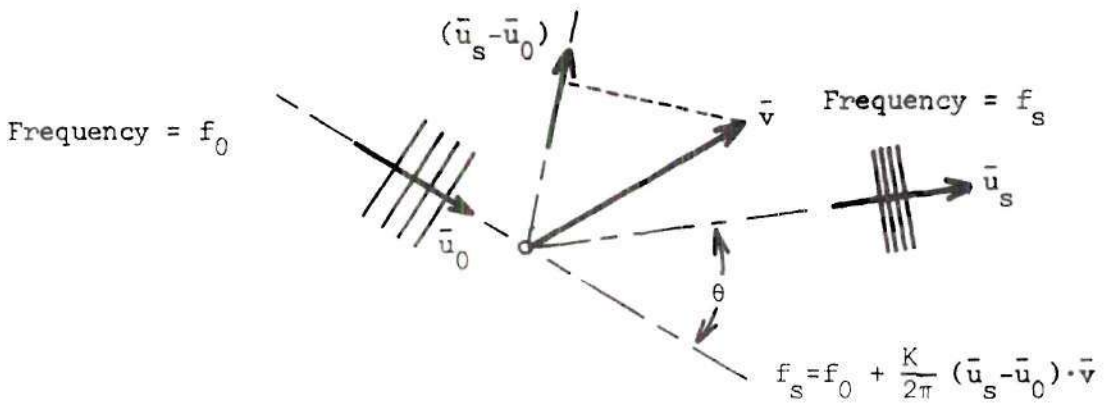

(a) The Doppler Effect

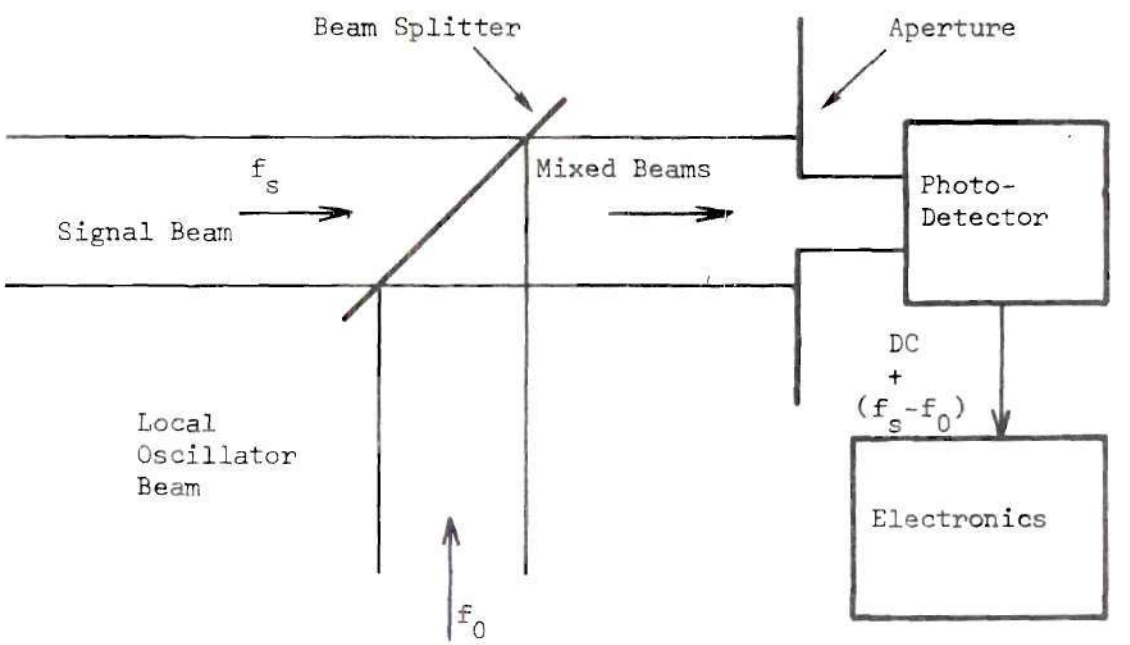

(b) Optical Heterodyne Receiver

Figure 1. Basic Principles of Heterodyne Flowmeters

Types of Flowmeter Optical Systems

In the feasibility experiments performed by Yeh and Cummins[1] collimated beams were used. Figure 2 illustrates an optical system developed primarily by J. W. Foreman[2-5] and others at Brown Engineering Laboratories, Huntsville, Alabama, which localizes the measurement by focussing. Others[6-10] have used essentially this same optical system with minor variations of the optical elements. The vector velocity instrument reported by Rolfe and Huffaker,[6,7,11] for example, makes use of essentially three such arrangements with a single scattering beam.

Figure 3 illustrates another heterodyne system reported by Goldstein[12,13] et al. which has also been used with minor variations by others.[14] Although quite different in appearance from the Foreman system, the Goldstein system merely adds the signal and reference beams in a different manner so that a combining beam splitter is unnecessary.

A system has been reported by Bond[15] in which two signal waves scattered in different directions are mixed rather than having one scattered wave mixed with a strong local oscillator reference beam. This "symmetrical heterodyne" system should not properly be said to employ optical heterodyne detection without qualification because the excellent noise rejection properties usually associated with optical heterodyne detection are not present. In this presentation, the phrase "heterodyne flowmeter" will by definition refer only to systems employing a strong reference beam. The "symmetrical heterodyne" system will be excluded as belonging to a separate class not to be

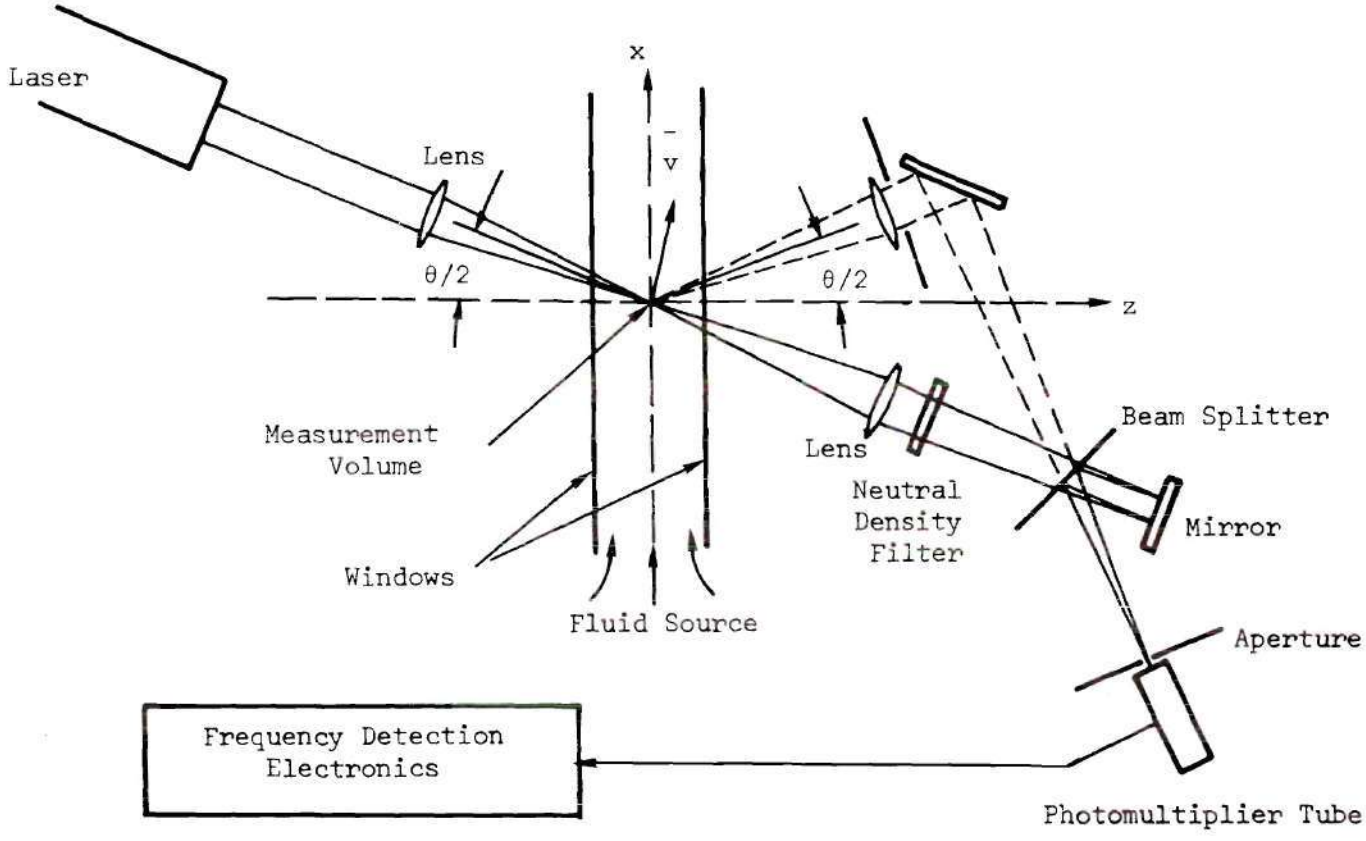

Figure 2. Laser Doppler Flowmeter

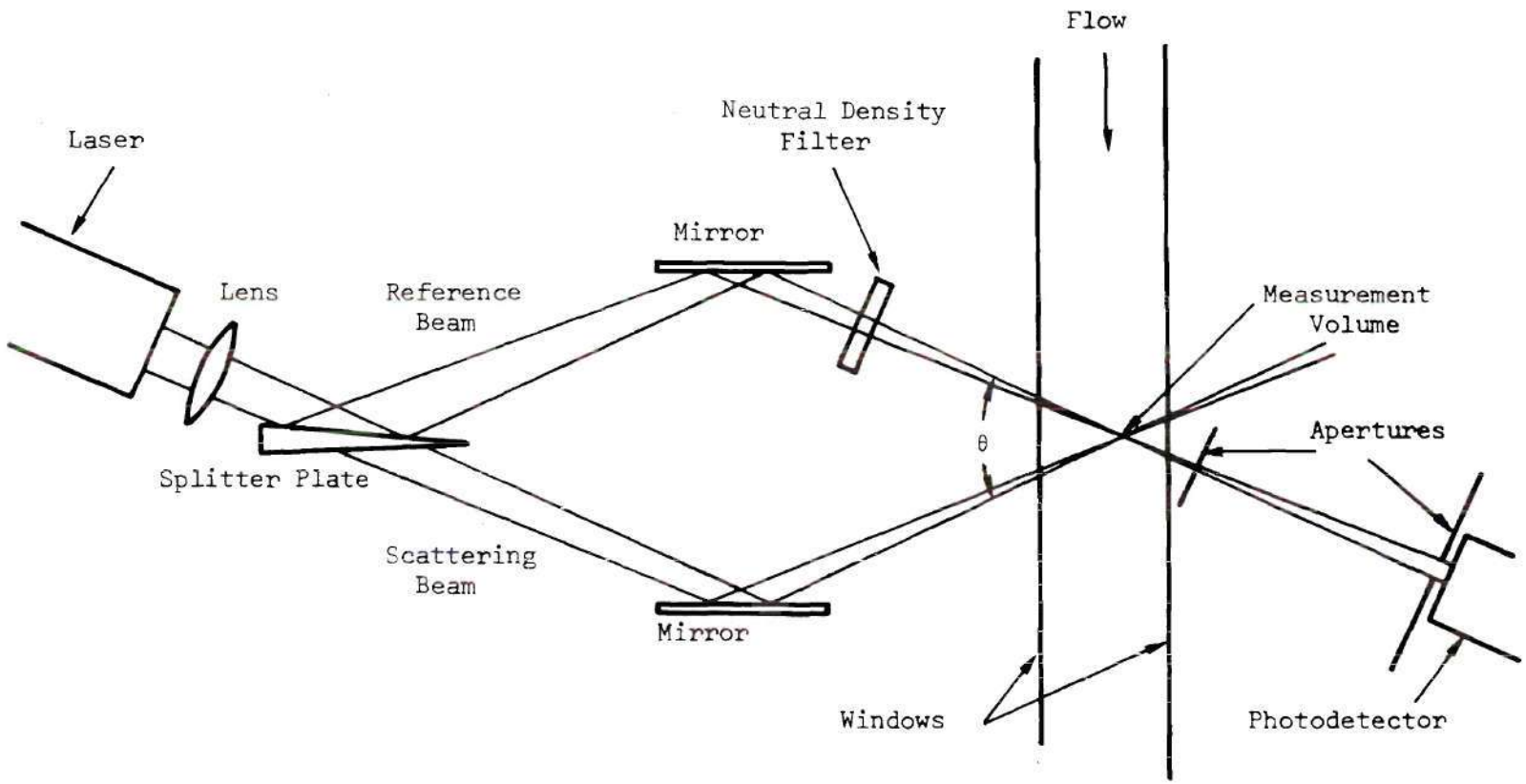

Figure 3. Heterodyne Flowmeter without Combining Beam Splitter (After Goldstein).

considered although it may deserve more theoretical analysis than has yet been reported.

A laser Doppler particle-velocity measurement system has been reported by James, Babcock and Seiffert[20] which utilizes an optical interferometric frequency detection system rather than an electronic system. The sensitivity of such optical frequency detectors is so limited, however, that only very high velocities such as those occurring in rocket exhausts may be measured.

Primary Optical System Considerations

Optical heterodyne detection requires that a reference wave be critically aligned with the scattered signal wave so that effective mixing can occur. In addition vibration of optical components can produce undesirable Doppler shifts which are detected along with those caused by scatterer motion. Laser Doppler flowmeters are therefore usually difficult to align and are sensitive to vibration effects.

The dimensions of the volume over which an average velocity is measured is determined by choices of lenses, apertures, the scattering angle, and the incident beam dimensions. The measurement volume dimensions are critically important in some measurements, such as those where high velocity gradients exist.

Since in most applicatins the incident and scattered light is focussed, rather than collimated, a spread of scattering angles exists and the signal is smeared out in temporal spectrum over a range of frequencies. This effect may alternately be thought of as resulting from the finite time a scattering particle remains in the scattering

volume. Regardless of viewpoint, the spectral spread of the signal caused by the optical configuration is undesirable since electronic frequency detection systems can most conveniently handle narrow-band signals. This spectral spreading becomes a serious problem in high velocity wind tunnel or rocket exhaust measurements where it is desirable to keep the Doppler shift sensitivity as low as possible by reducing the scattering angle in order that electronic bandwidths will not be exceeded.

The optical system also affects the signal-to-noise ratio of the photo-detector output. This is intuitively obvious since spreading the signal in spectrum requires wider bandwidths and hence allows more broad-band noise to be detected. It is similarly obvious that apertures commonly used for signal and reference beam control purposes can reduce the potential signal-to-noise ratio by blocking useful optical power from reaching the photo-detector.

In summary, the most important considerations of the design of a laser flowmeter optical system are: the difficulty of alignment and sensitivity to vibration and stress; the dimensions of the measurement volume; the spectral spread of the signal; and the effects of the optics on signal-to-noise ratio.

Need for Fundamental Analysis

The development of laser flowmeters as reported in the literature has been largely experimental. A few theoretical analyses have been presented of various aspects of system design and behavior, but to date no one has undertaken a fundamental systems analysis of

flowmeter optical systems to determine optimum design and basic limitations. As a result overly complicated and inefficient systems are currently being used by investigators who do not agree about what their systems are actually measuring. This lack of agreement is evident, for example, from the different opinions concerning the measurement volume dimensions. Although several treatments of the signal spectral broadening exist, none are sufficiently general or fundamental in approach. The relationship between signal-to-noise ratio and the optical system requires a statistical analysis which has not yet been forthcoming.

Description of the Problem

Statement of Objectives

The primary objectives of the work presented in this thesis have been:

(1) To provide theoretical insight concerning the effects of the optical subsystems of optical-heterodyne laser Doppler flowmeters on the measurement volume dimensions, the system alignment, the signal bandwidth, and the signal-to-noise ratio.

(2) To determine a class of optimum optical systems and predict variations of measurement volume dimensions, signal bandwidth and signal-to-noise ratio in terms of the variables of this class of systems.

(3) To design improved laser flowmeter optical systems.

(4) To experimentally verify the feasibility of improved systems and some of the predicted signal bandwidth and signal-to-noise ratio variations.

Method of Attack

The theoretical method of attack has been to formulate a general static model of the laser flowmeter from which the signal current could be determined in terms of the positions of the scatterers by application of the results of modern coherent-optics theory. The principal assumption has been that the time varying signal current is obtained when the equation of motion of the scatterers is substituted for positions since distances involved are small and only particle velocities much less than that of light are considered. The flow velocity has been assumed constant in space and time to isolate signal spectral effects dependent on the optical system alone from those dependent on the flow field. The theory of random processes has been used to formulate a stochastic model of the signal current, based on the assumption that the scattering centers are initially statistically uniformly distributed in space.

Experimentally, flowmeter signals have been observed and measured in the time domain with oscilloscopes and in the frequency domain with spectrum analyzers and analog spectral averaging techniques. The experiments were restricted to low-velocity constant-flow conditions using smoke as the scattering medium in air.

Scope

The material presented in this thesis has been arranged in three major categories: theoretical analysis of optical heterodyne laser flowmeters, presented in Chapters II, III, and IV; design and analysis of new types of flowmeter optical systems, in Chapters V and VI; and experimental verification in Chapter VII. The theoretical work relies

heavily on the results of the recent systems approach to optics using two-dimensional Fourier transform theory. Readers not familiar with this field may wish to consult excellent texts† which have become available in the last year.

In Chapter II a three-dimensional linear system model is postulated for the heterodyne laser flowmeter and shown to be equivalent in general to any of the present art systems employing a heterodyne reference beam. The system impulse response is determined and used to define the measurement volume extent. The response function expressions are also interpreted to determine the functional form of an optimum class of incident beam field distributions.

Chapter III is devoted to the statistical nature of heterodyne flowmeter signals and noise. A three-dimensional shot noise process is formulated and specialized to describe the signals obtained from constant-velocity scattering particles uniformly statistically distributed in space. The signal power spectrum is determined as a general integral expression and used with optical heterodyne noise theory to determine general signal-to-noise ratio expressions. Optical heterodyne noise theory is also extended to include the adverse effects of laser amplitude fluctuation noise on low-frequency modulation systems.

The general integral expressions derived in Chapters II and III are evaluated and interpreted in Chapter IV for a specialized class of optimum flowmeters. The resulting expressions reveal the trade-offs

---

†*Fourier Optics* by Goodman[21] is highly recommended for an introduction. Another book by Papoulis[22] gives a more extensive system treatment.

involved in maximizing the signal-to-noise ratio while minimizing the spectral width and measurement volume dimensions.

In Chapter V a new heterodyne flowmeter optical system implementation is described and analyzed which is a significant practical improvement over previously used systems in applications requiring low scattering angles.

Chapter VI describes an unexpected development suggested by the theoretical analysis. The new type of flowmeter described and analyzed there should most properly be called an "interference flowmeter" since its behavior is more easily described in terms of interference theory than in terms of Doppler shifts and optical heterodyne detection. The analysis of this system is specialized somewhat and less detailed than that of Chapters II-IV. However, the system is shown to have great potential for unique applications.

In Chapters VII experiments are described in which some of the effects of optical system variations on the signal bandwidth and the signal-to-noise were studied; the data is compared with theory. The experiments also demonstrated the feasibility of the new flowmeter optical systems described in Chapters V and VI.

The final chapter is devoted to summarizing conclusions drawn from the thesis work and outlining future work suggested by it.

CHAPTER II

A GENERALIZED HETERODYNE LASER FLOWMETER OPTICAL SYSTEM

Introduction

The plane-wave Doppler formula given in Chapter I has been used in a ray-optics sense as a basis for analysis by previous laser flowmeter investigators. In the present chapter, the Doppler formula is just one result of the basic diffraction theory analysis of flowmeter optical systems which is presented. After a statement of assumptions and an explanation of notation, a general theorem, which is applicable to heterodyne flowmeters, concerning optical heterodyne detection is presented and proved. With the use of this theorem and some results of coherent optics, a general flowmeter model is postulated and analyzed. The analysis reveals the limitations on measurement volume dimensions, provides a basis for optimum optical design, and gives the system response in a form useful for the signal-to-noise and spectral-width analysis of Chapter III.

Assumptions of the Model

For purposes of analysis, independent point scattering from a dilute suspension of scatterers is assumed. Experimentally, both particles with dimensions small compared with a wavelength (Rayleigh scattering) and particles with dimensions comparable to a wavelength (Mie scattering) have been used by other investigators. Rayleigh scattering is isotropic in the plane normal to the electric field. Mie

scattering is highly forward directed, but the radiation pattern is assumed constant over the small solid angular collecting apertures usually associated with laser flowmeters. The suspensions of scatterers are assumed to be dilute so that independent single scattering occurs with negligible attenuation or distortion of the incident beams.

The propagation of optical beams will be described using the scalar diffraction theory of monochromatic light. Two assumptions are implicit here. The first is that possible polarization effects of the scattering process or reflections from mirrors can be neglected. The heterodyne detection process only detects radiation with the same polarization as the reference beam. Polarization thus affects the effective value of the scattering coefficient assigned to the scatterer, but the absolute value of the scattering coefficient is not to be considered here.

The assumption of monochromatic light is valid for gas laser sources with regard to any dispersion which might be produced by the optical elements. The finite bandwidth of laser sources can be shown not to affect a laser flowmeter having equal path lengths for the reference and scattered radiation. The tolerance on the equality of the path lengths depends on the temporal coherence of the source. Foreman[5] has discussed the effects of path length difference when a multiple axial mode laser is used. In the present work, the path length difference will be assumed small enough that the source may be assumed monochromatic.

All optical elements, such as lenses, mirrors, and optically flat surfaces, are assumed to be ideal, aberration-free elements.

The last general assumption is the quasistatic assumption. The assumption is that for scatterer velocities much less than the speed of light, the time varying scattered field may be determined by calculating the amplitude and phase of the scattered wave in terms of the static positions of the scatterers.

Integral Notation

In recent years the electrical engineering community has been increasingly active in the field of coherent optics. It has now become common to describe the propagation of optical-frequency electromagnetic radiation in terms of two-dimensional Fourier transform integrals, convolution integrals, and correlation integrals, i.e. in the mathematical language of systems and communications theory. This type of systems approach is used in this dissertation. Occasions will arise where it is also necessary to use one and three-dimensional Fourier integrals, convolution integrals, and correlation integrals. In some of these instances the clarity of the mathematical expressions is improved by the use of multi-dimensional short-hand notation for the integrals analogous to the standard one-dimensional notation commonly used in communications theory. Definitions are given below for the notation which will be used.

In order that the definitions[†] need not be given three separate

---

[†]For much more extensive discussions of these topics, see Goodman,[21] Papoulis,[22] and Stroke.[24]

times, the symbols $\bar{r}$ and $\bar{f}$ are used here to imply either one, two, or three-dimensional arguments with $d\bar{r}$ and $d\bar{f}$ implying iterated integrals of the proper dimension.

The Fourier transform, $G(\bar{f})$, of a complex-valued function $g(\bar{r})$ is obtained by an integral operation denoted by $T[g(\bar{r})]$ as[†]

$$G(\bar{f}) = \int g(\bar{r})e^{-2\pi\bar{r}\cdot\bar{f}}\, d\bar{r} = T[g(\bar{r})] \tag{1}$$

and is assumed to exist. The inverse transform operation $IT[G(\bar{f})]$ recovers the original function as

$$g(\bar{r}) = \int G(\bar{f})e^{2\pi\bar{r}\cdot\bar{f}}\, d\bar{f} = IT[G(\bar{f})] \tag{2}$$

The factor 2π has been placed in the exponent. Thus $\bar{f}$ is a frequency variable, not a radian frequency variable, and the only difference between the transform and inverse transform operations is the sign of the exponent.

The convolution of two functions $g_1(\bar{r})$ and $g_2(\bar{r})$ is a commutative operation denoted by an asterisk and defined by

$$g_1(\bar{r}) * g_2(\bar{r}) = \int g_1(\bar{a})\, g_2(\bar{r}-\bar{a})\, d\bar{a} \tag{3}$$

[†]The limits of integration on all integrals in this dissertation will be minus infinity to plus infinity unless shown otherwise. Upper case letters will be used to denote frequency domain functions and lower case letters will be used to denote time or space domain functions.

The correlation of two functions $g_1(\bar{r})$ and $g_2(\bar{r})$ is denoted by the symbol $\oplus$ and is defined by

$$g_1(\bar{r}) \oplus g_2(\bar{r}) = \int g_1(\bar{a})\, g_2(\bar{r}+\bar{a})\, d\bar{a} \tag{4}$$

The results of the correlation and convolution operations are in general not the same. For example, the correlation operation is not commutative in general. However, if $g_1(\bar{r})$ is an *even* function, i.e. if

$$g_1(\bar{r}) = g_1(-\bar{r}), \tag{5}$$

then the distinction between convolution and correlation vanishes, i.e.

$$g_1(\bar{r}) \oplus g_2(\bar{r}) = g_1(\bar{r}) * g_2(\bar{r}) \tag{6}$$

if $g_1(\bar{r})$ is even.

Most of the usual Fourier transform theorems, valid for one-dimensional transforms, also apply to multi-dimensional transforms. Goodman,[21] Papoulis,[22] and Stroke[24] each give lists of these theorems for the two-dimensional case. One of the less well-known theorems given in a slightly different form by Stroke[24] is the correlation theorem which states that[†]

[†]The superscript asterisk denotes "complex conjugate."

$$g_1^*(\bar{r}) \oplus g_2(\bar{r}) = IT[G_1^*(\bar{f})\, G_2(\bar{f})] \tag{7}$$

If one sets $\bar{r}$ equal to zero in this equation, the result is a multi-dimensional Parseval's theorem, i.e.

$$\int g_1^*(\bar{a})\, g_2(\bar{a})\, d\bar{a} = \int G_1^*(\bar{f})\, G_2(\bar{f})\, d\bar{f} \tag{8}$$

Some Results of Coherent Optics

In this section several pertinent results of coherent optics are reviewed. These results provide the mathematical basis for the description of optical propagation in a laser Doppler flowmeter.

At a point (x,y,z = 0) in a beam of monochromatic light propagating primarily in the z direction,† a real optical disturbance, u^r, proportional to the electric or magnetic field, may be expressed as

$$u^r(x,y,z=0,t) = \mathrm{Re}\left[u(x,y,z=0)e^{-j2\pi f_o t}\right] \tag{9}$$

where f_o is the optical frequency and u(x,y,z=0) is the *complex*†† amplitude of $u^r(x,y,z=0,t)$. The Re[ ] notation denotes "real part of," and, as usual in electrical engineering practice, the Re[ ] and the exponential time variation will be assumed henceforth. The quantity

---

†Low spatial frequency content, or paraxial assumption.

††The superscript r is used to denote strictly real functions in cases where confusion might arise. No special notation is used for complex quantities.

$u(x,y,z=0)$ is normalized so that the intensity, $I = |u(x,y,z=0)|^2$, is the average power per unit area passing through the z=0 plane.

The propagation of paraxial scalar fields from the z=0 plane to the z=d plane may be determined by Fresnel diffraction approximations and produces a diffracted field $u(x,y,z=d)$ given by a convolution integral as

$$u(x,y,d) = \frac{e^{jKd}}{j\lambda d} \iint u(a,b,o) e^{\frac{jK}{2d}\left[(x-a)^2 + (y-b)^2\right]} da\, db \qquad (10)$$

$$= h(x,y,d) * u(x,y,o)$$

where $h(x,y,d)$ is a "black box" impulse response representing the effects of propagation given by

$$h(x,y,d) = \frac{e^{jKd}}{j\lambda d} \; e^{\frac{jK}{2d}(x^2+y^2)} \qquad (11)$$

In a manner completely analogous to that used for time invariant linear systems, propagation may be described in a spatial frequency domain by using the two-dimensional Fourier transforms of the functions in (10), with respect to x and y, to obtain

$$U(f_x,f_y,d) = H(f_x,f_y,d)\, U(f_x,f_y,0) \qquad (12)$$

where

$$H(f_x,f_y,d) = T[h(x,y,d] = e^{jKd}\, e^{-j\pi\lambda d(f_x^2+f_y^2)} \qquad (13)$$

The field complex amplitudes may be recovered from the spatial frequency domain by the Fourier inverse integral operation. Thus

$$u(x,y,d) = IT[U(f_x,f_y,d)] = \iint U(f_x,f_y,d)e^{j2\pi(f_x x+f_y y)}\, df_x\, df_y \quad (14)$$

The propagation function has an inverse given by

$$H^{-1}(f_x,f_y,d) = H^{*}(f_x,f_y,d) \quad (15)$$

so

$$U(f_x,f_y,0) = H^{*}(f_x,f_y,d)\, U(f_x,f_y,d) \quad (16)$$

From Equation (7) one sees that the inverse propagation may be represented in the space domain by a correlation integral as

$$u(x,y,0) = h^{*}(x,y,d) \circledast u(x,y,d) \quad (17)$$

Since the propagation function h(x,y,d) is an even function, Equation (17) may be alternately written as

$$u(x,y,0) = h^{*}(x,y,d) * u(x,y,d) \quad (18)$$

When the distance of propagation from one z plane to another is sufficiently large, the Fraunhoffer approximation of the diffraction integral applies. To see this, one expands Equation (10) as

$$u(x,y,d) = \frac{e^{jKd}}{j\lambda d} e^{\frac{jK}{2d}(x^2+y^2)} \iint u(a,b,0) e^{\frac{jK}{2d}(a^2+b^2)} e^{-\frac{jK}{d}(ax+by)} da\, db \quad (19)$$

If a maximum radius $(x^2+y^2)_{max}$ is assigned to the beam in the z=0 plane, then for

$$d >> \frac{K}{2}\left(x^2+y^2\right)_{max} \quad (20)$$

one obtains the Fraunhoffer approximation or far field case. Then

$$u(x,y,d) \approx \frac{e^{jKd}}{j\lambda d} e^{\frac{jK}{2d}(x^2+y^2)} \iint u(a,b,0) e^{-j2\pi\left(a\frac{x}{\lambda d} + b\frac{y}{\lambda d}\right)} da\, db \quad (21)$$

$$= \frac{e^{jKd}}{j\lambda d} e^{\frac{jK}{d}\left(x^2+y^2\right)} U\left(\frac{x}{\lambda d}, \frac{y}{\lambda d}, 0\right)$$

i.e., the far field is a scaled Fourier transform of the z=0 field, except for a multiplying phase function.

The effect of inserting "thin" passive optical elements, such as lens or apertures, normal to a propagating beam is to multiply the complex amplitude in the plane of the element by a complex transmission function t(x,y) such that

$$|t(x,y)| \leq 1 \quad (22)$$

Since the transmission element will change the functional form of the propagating field, subscripts will be used to denote which side of the

element is being considered. For example, if $u_o(x,y,z)$ is incident on a filter $t_1(x,y)$ at $z = d$, then $u_o(x,y,d)$ is the complex amplitude at $z = d^-$ just prior to the element, and

$$u_1(x,y,d) = u_o(x,y,d)\ t(x,y) \tag{23}$$

is the complex amplitude of $u_1(x,y,z)$ at $z = d^+$ just past the element. A list of several common optical elements and their associated transmission functions are given in Table 1.

Table 1. Transmission Functions for Common Optical Elements

Description	t(x,y)
1. Spherical lens; focal length = F	$e^{\frac{-jK}{2F}(x^2+y^2)}$
2. Cylindrical lens; x focal length = F_x, y focal length = ∞	$e^{\frac{-jK}{2F_x}x^2}$
3. Prism: deflection angle θ measured from z axis toward x axis	$e^{jK\ x\ \sin\theta}$
4. Circular aperture, radius R	$1,\ x^2 + y^2 < R^2$ $0,\ x^2 + y^2 > R^2$
5. General passive filter	$t^r(x,y)e^{j\phi(x,y)},\ \|t\| < 1$

A specific result of optics theory concerning the use of a spherical lens will be useful later. The complex amplitude of a beam

incident in the positive z direction is $u_o(x,y)$ in the front focal plane of the lens. The lens diameter is assumed larger than any appreciable part of the incident beam and may therefore be considered infinite. The propagation integrals and the quadratic phase function $t(x,y)$, given in Table 1 for a spherical lens, may be used to determine the complex amplitude $u_1(x,y,z)$ in any z-plane past the lens as

$$u_1(x,y,z) = \frac{e^{jKz}}{\lambda F} \iint u_o(a,b) e^{\frac{-jKz}{2F^2}(a^2+b^2)} e^{-j2\pi\left(a\frac{x}{\lambda F} + b\frac{y}{\lambda F}\right)} da\, db \qquad (24)$$

where the z=0 plane is the back focal plane of the lens and where a constant phase term has been neglected. For the special case in which z=0, the complex amplitude in the back focal plane is given by[†]

$$u_1(x,y,0) = \frac{1}{\lambda F} U_o\left(\frac{x}{\lambda F}, \frac{y}{\lambda F}, -2F\right) \qquad (25)$$

i.e., by an exact scaled Fourier transform of the complex amplitude incident in the front focal plane.

The Optical Heterodyne Reference Beam as a Spatial Filter

In most cases, flowmeter investigators have found it desirable to use transmission filters such as lenses and apertures at various

---

[†]Equation (25) is derived by Goodman[21]. Equation (24) may be derived from (25) by using the propagation law. Alternately, Vander Lugt[23] presents an even more general result of which (24) is a special case, but the notation is different and some of the constants are not preserved.

places in the scattered wave before and after it is added to the heterodyne reference wave. This has been done to shield the photodetector from stray light, to aid in the alignment of the optics, and to restrict the transverse dimensions and angular extent of the scattered radiation. These arrangements of transmission filters will be called "spatial filters" in the present discussion.

Some shielding of the photodetector is necessary and some spatial filter arrangements do make it easier to obtain the critical heterodyne alignment. Unfortunately, these spatial filters also affect the position and extent of the measurement volume, the signal bandwidth, and the signal-to-noise ratio (SNR), and it would be quite difficult to analyze every conceivable system and determine an optimum arrangement. The purpose of this section is to show that *in any optical heterodyne receiver employing spatial filtering of the signal wave, the same filtering may be achieved by choosing an equivalent reference beam and then using only apertures, lenses, etc., which do not prevent any appreciable portion of the reference beam power from reaching the photodetector*. One sees immediately that such a result will allow the optimum filtering to be determined with respect to the reference wave alone without analyzing endless optical configurations. The detailed proof of the hypothesis given above is given in Appendix A, but the motivation for it is presented below.

Figure 1(b) illustrated a simple optical heterodyne receiver. Others[19] have pointed out that, since the photodetector responds to incident power which is conserved by lossless propagation, the signal

current is not altered by moving the position of the detector or inserting phase filters, such as lenses, into the mixed beams after the last aperture, so long as all the optical power is still intercepted by the detector. The total power† P(t) incident on a detector plane $z = z_d$ is given by a surface integral of the intensity, i.e.[19]

$$P(t) = \iint \left| u_s(x,y,z_d,t) + u_r(x,y,z_d) \right|^2 dxdy \tag{26}$$

where $u_r(x,y,z_d)$ is a monochromatic reference wave of finite transverse extent, having much greater total power than the signal wave†† $u_s(x,y,z_d,t)$. The signal wave varies slowly in time compared with the optical frequency. Neglecting the small term proportional to the intensity of the signal beam alone, the real photocurrent i(t) is given by

$$i(t) = i_{dc} + i_s(t) + i_s^*(t) \tag{27}$$

where the DC current is real,

$$i_{dc} = N \iint \left| u_r(x,y,z_d) \right|^2 dxdy \tag{28}$$

---

†The power P(t) is a running time average power. The averaging time is long compared with the optical period but short compared with the time in which the complex envelope of the signal wave changes appreciably.

††Note that $u_s(x,y,z_d,t)$ is the complex envelope of the very narrow band signal radiation.

and a complex signal current is given as

$$i_s(t) = N \iint u_s(x,y,z_d,t)u_r^*(x,y,z_d)dxdy \qquad (29)$$

where N is the product of the detector quantum efficiency η and the electronic charge e, divided by the photon energy hf_o. The DC term given by (28) determines the system noise and will be discussed further in Chapter III. The complex signal current term given by (29) is of interest here.

Equation (29) reveals the well-known fact that the reference beam behaves as an aperture in the sense that only that part of the signal wave incident on photodetector area with non-zero incident reference beam may be detected. Thus a reference beam of small transverse extent behaves as a low-pass filter in the *space* domain.

It is also well known that the signal and reference beams must be closely aligned in direction of propagation, but no one seems to have described this fact in the following general manner:†

$$i_s(t) = N \iint U_s(f_x,f_y,z_d,t)U_r^*(f_x,f_y,z_d)df_xdf_y \qquad (30)$$

This result is obtained from (29) by use of a two-dimensional Parseval's theorem, given by (8). Equation (29) states that no signal current is

---

†This expression in the spatial frequency domain can be used to show that placing the detector at $z_d + d$ instead of at z_d has no effect on the signal current, since $|H(f_x,f_y,d)|^2 = 1$.

produced by portions of the signal wave not in the same *spatial frequency* domain as to the reference beam. The spatial frequency spectrum is, for paraxial radiation, a decomposition in terms of plane waves with direction cosines given by $(\lambda f_x, \lambda f_y, 1)$. Thus a reference beam whose spatial frequency spectrum is restricted to small values behaves as a low-pass filter in the spatial frequency (angular direction) domain of the signal wave.

The reference beam has been shown to restrict both the transverse extent and the angular extent of the detected portion of the signal wave passing through any single z plane after mixing. This fact motivates the general hypothesis, proved in Appendix A, that the effects on the signal current of any number of transmission filters in different z planes of the signal and/or reference waves may be replaced by a single equivalent reference beam, with all filters removed. Therefore, in marked contrast to the usual collection of lenses and apertures located in front of the photo-detector, the generalized heterodyne flowmeter configuration presented in the next section has no spatial filtering of the signal radiation. It must be emphasized that the results of the rest of this chapter pertain to the *equivalent* reference beam, described in Appendix A.

Description of a Generalized Heterodyne Flowmeter Model

Figure 4 illustrates schematically the generalized flowmeter model which is to be analyzed. A strong incident scattering beam with finite transverse extent has complex amplitude $u_{io}(x',y)$ in an input plane as shown. In another input plane, the comparatively

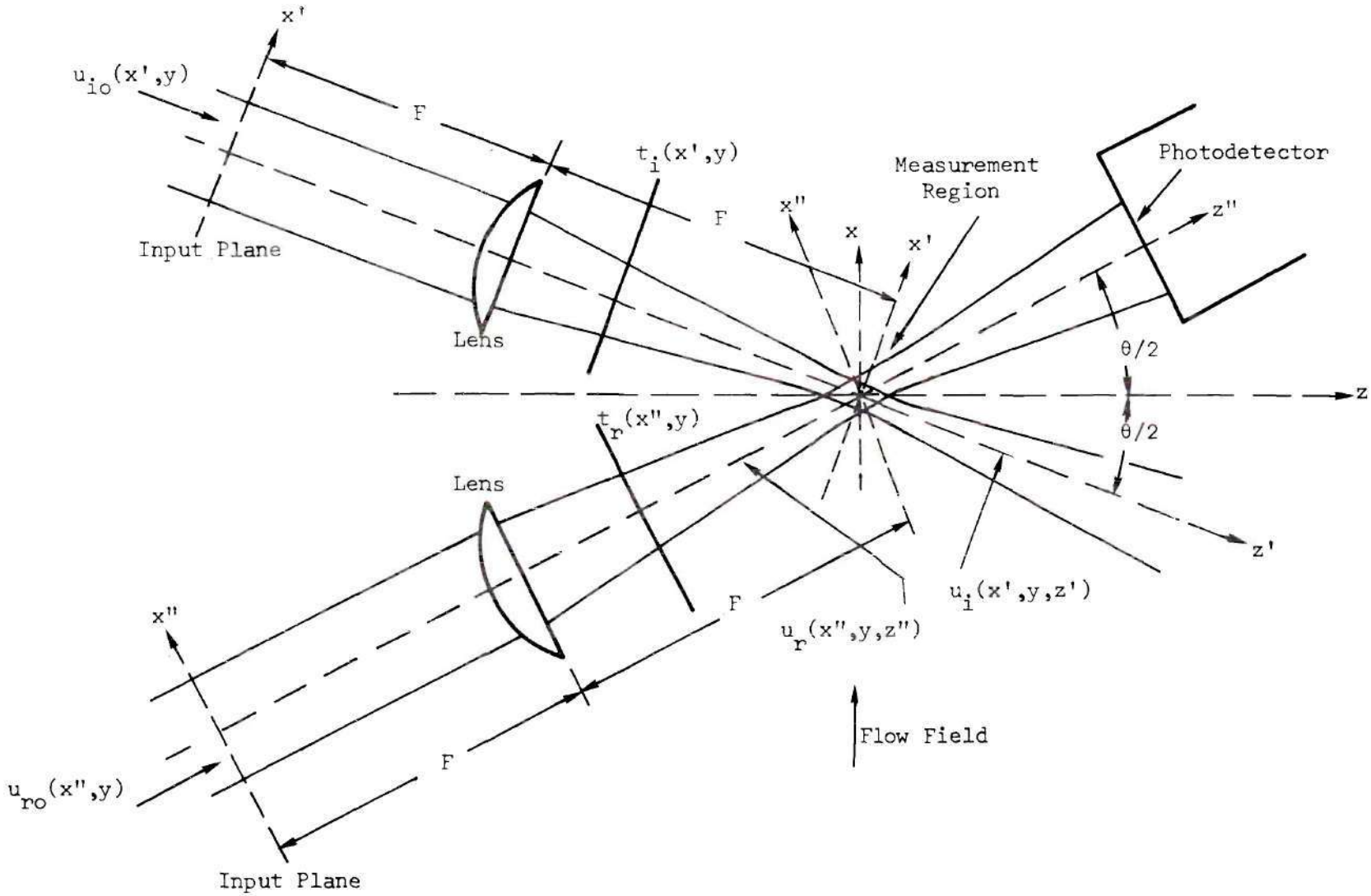

Figure 4. Geometry of Generalized Heterodyne Flowmeter Model

weak[†] incident reference beam has complex amplitude $u_{ro}(x'',y)$ which does not physically overlap $u_{io}(x',y)$. Three coordinate systems are shown: (x',y,z'), associated with the scattering beam; (x'',y,z''), associated with the reference beam; and (x,y,z) with the z axis bisecting the scattering angle θ between the z' and z'' axes. The y axis is common to all three systems. No lenses, apertures, or other spatial filters are shown between the scattering region and the detector, nor is a combining beam splitter used since it is assumed that u_r is the equivalent reference beam for whatever elements might actually be present.

The filters $t_i(x',y)$ and $t_r(x'',y)$ represent any optical elements which may affect the beam upon entering the flow region or within the flow region. Examples are: an air-glass-liquid interface in liquid flow measurements, producing prismatic deflection of beam; a poor window in a wind tunnel, or some other transparent flow retainer with deviations from flatness. As will be seen later, the response of the flowmeter depends on the fields within the flow region and, when expressed in terms of these fields, does not depend explicitly on $t_r(x'',y)$ or $t_i(x',y)$. However, it should be obvious that whatever fields are shown desirable will be impossible to obtain practically if $t_i(x',y)$ and $t_r(x'',y)$ are random phase filters. This will be the case if the windows, of a wind tunnel for example, are not optically flat.

[†]Although the reference beam is quite weak compared with the scattering beam, it is much stronger than the very weak scattered radiation.

It will be assumed henceforth that $t_i(x',y)$ and $t_r(x'',y)$ are equal to 1, i.e. not present. Their presence in the figure is for the purpose of reminding those who would use a flowmeter with a tubular plexiglass flow channel, for example, that any calculations of measurement volume dimensions must be compensated, if possible, for the effects of the flow channel wall.

The spherical lenses and the particular positioning of the input planes shown in Figure 4 are purely arbitrary since an analysis could be made without the lenses and with input planes chosen anywhere on the z' and z'' axes. The input planes are merely planes in which to optimize and discuss the beams $u_r(x'',y,z'')$ and $u_i(x',y,z')$. In most flowmeter applications it is desirable to use focussing lenses, however, so the choice of input planes in front of such lenses allows the results to be more easily relatable to the practical case. No generality is lost; in particular, the "collimated beam" case simply requires *input* distributions of very small extent (focussed). The positions of the lenses one focal length distant from the origin and the positions of the input planes two focal lengths from the origin is a matter of mathematical convenience based on hindsight. Similarly, the choice of equal focal lengths simply avoids mathematical changes of scale. The lenses are assumed larger in diameter than the incident beams, so these diameters are mathematically infinite.

The use of the primed and double-primed co-ordinate systems is necessary to simply describe the paraxial propagation of the two different beams, and the results will be stated sometimes in terms of both

co-ordinate systems simultaneously where the meaning is clear. When it becomes necessary to evaluate an expression in a single co-ordinate system, either the rectangular (x,y,z) system or the non-rectangular, but independent, (x',y,x") system will be used.

As stated in the assumptions, the scatterers are assumed to be dilute point scatterers which affect the transmitted scattering and reference beams only negligibly. Furthermore, the radiation scattered from the reference beam in the direction of the reference beam is relatively weak and not Doppler shifted and is thus not detected as signal. A single scatterer located at the vector point $\bar{p}$ near the origin in the scattering beam produces spherical radiation which reaches the detector plane z_d''. The paraxial approximation of this spherical wave is

$$u_{sp}(x'',y,z_d'') = \tag{31}$$

$$u_i(x_p',y_p,z_p') \frac{C_p e^{jK(z_d''-z_p'') + \frac{jK[(x_p''-x'')^2 + (y_p-y)^2]}{2(z_d''-z_p'')}}}{j\lambda(z_d''-z_p'')}$$

where C_p is a complex constant, proportional to the square root of the scattering cross section,† σ_p^2, given by

$$C_p = \frac{j\lambda}{2} \sqrt{\sigma_p^2/\pi}\, e^{j\phi_p} \tag{32}$$

---

†The total isotropically scattered power is assumed equal to the product of the scattering cross section and the incident intensity.

The phase constant ϕ_p relates the phase of the incident radiation to that of the scattered radiation.

The form of the constant C_p was purposely chosen so that the right-hand part of (31) could be easily identified with the propagation function h(x,y,d) given previously in Equation (11). Thus,

$$u_{sp}(x'',y,z_d'') = C_p u_i(x_p',y_p,z_p')h[(x_p''-x''),(y_p-y),(z_d''-z_p'')] \tag{33}$$

The total scattered field at the detector surface from a collection of scatterers located at positions $\bar{p}_k$, k=1,2,3,... is a linear summation of terms like the right-hand side of (33), i.e.,

$$u_s(x'',y,z_d'') = \sum_k u_{spk}(x'',y,z_d'') \tag{34}$$

The Three-Dimensional System Response

The signal current produced by the generalized flowmeter can now be expressed in terms of the scattering positions $\bar{p}_k$ by using (29) with the sum scattered field as the signal wave.

$$i_s = N \iint \left[\sum_k u_{spk}(x'',y,z_d'')\right] u_r^*(x'',y,z_d'')dx''dy \tag{35}$$

Interchanging the order of integration and summation one obtains the signal current as a linear summation of the signal current produced by each scatterer individually,

$$i_s = \sum_k N \iint u_{spk}(x'',y,z_d'')u_r^*(x'',y,z_d'')dx''dy'' \qquad (36)$$

One term of the summation is thus the system response to a single point scatterer.

Response in Terms of Focal Region Fields

The remainder of this chapter is devoted to an analysis of the flowmeter optical system with respect to the single-scatterer response. One term of (36) may be written out as

$$i_{sp} = NC_p u_i(x_p',y_p,z_p') \cdot \left[\iint h^*[(x_p''-x''),(y_p-y),(z_d''-z_p'')]u_r(x'',y,z_d'')dx''dy\right]^* \qquad (37)$$

The integral is recognized as the inverse propagation convolution, i.e.,

$$i_{sp} = NC_p u_i(x_p',y_p,z_p')\left[h^*[x_p'',y_p,(z_d''-z_p'')] * u_r(x_p'',y_p,z_d'')\right]^* \qquad (38)$$

with the result that

$$i_{sp} = NC_p u_i(x_p',y_p,z_p')u_r^*(x_p'',y_p,z_p'') \qquad (39)$$

Remembering that u_i and u_r are defined in different coordinate systems, Equation (39) is abbreviated with vector notation as

$$i_{sp} = NC_p u_i(\bar{p})u_r^*(\bar{p}) \qquad (40)$$

Equation (40) makes it immediately obvious that *signal current is only obtained from scatterers in the region of intersection of the incident scattering beam and the equivalent reference beam.* An upper bound on the measurement volume dimensions has thus been determined.

The word "equivalent" is stressed again because a user of the Goldstein-type system may be inclined to immediately determine the measurement volume dimensions in terms of the intersection of the *actual* beams present. If small apertures were used in front of the photodetector which blocked part of the reference beam, such a determination would be in error, and improper conclusions might be drawn about the flow field.† It is even possible for the center of the true measurement volume to occur in a slightly different place than the center of intersection of the two actual beams in a Goldstein-type system. If, on the other hand, no restricting apertures are used in front of the detector, the measurement volume is identical with the actual beam intersection region in the Goldstein-type system. Unfortunately, no such simple physical criterion exists in the Foreman configuration since the equivalent reference beam is never physically present and can only be computed.

Response in Terms of Input Plane Distributions

In Equation (40) the response is determined completely independently of the optical input geometry. The response is now to be

---

†This author feels that this particular error is the source of a possibly erroneous conclusion by Morrow[14] concerning the extent of the laminar sublayer near a wall under conditions of turbulent flow.

determined in terms of $u_{io}(x,y)$ and $u_{ro}(x,y)$, the complex amplitudes in the input planes shown in Figure 4. This is accomplished by using Equation (24) to determine $u_i(\bar{p})$ and $u_r^*(\bar{p})$ in terms of integrals involving $u_{io}(x,y)$ and $u_{ro}(x,y)$. Thus,

$$i_{sp} = NC_p e^{jK(z_p'-z_p'')} a(\bar{p}) \tag{41}$$

where $a(\bar{p})$ is given using two co-ordinate systems by

$$a(\bar{p}) = \frac{1}{(\lambda F)^2} \tag{42}$$

$$\cdot \left[\iint u_{io}(a,b) e^{\frac{-jKz_p'}{2F^2}(a^2+b^2)} e^{-j2\pi\left(a\frac{x_p'}{\lambda F} + b\frac{y_p}{\lambda F}\right)} dadb \right]$$

$$\cdot \left[\iint u_{ro}(a,b)\, e^{\frac{-jKz_p''}{2F^2}(a^2+b^2)} e^{-j2\pi\left(a\frac{x_p''}{\lambda F} + b\frac{y_p}{\lambda F}\right)} dadb \right]^*$$

The significance of $a(\bar{p})$ can be determined by examining the exponential term in (41). Converting this exponential to the unprimed (x,y,z) coordinate system gives

$$e^{jK(z_p'-z_p'')} = e^{-j2Kx_p \sin\left(\frac{\theta}{2}\right)} \tag{43}$$

i.e. the exponential depends only on the x co-ordinate of the scatterer

position $\bar{p}$. If one assumed that the scatterer was moving with constant velocity $\bar{v}$ such that

$$\bar{p} = \bar{v}t + \bar{p}_o \tag{44}$$

where $\bar{p}_o$ is a constant vector initial position and

$$\bar{v} = v_x\bar{u}_x + v_y\bar{u}_y + v_z\bar{u}_z \tag{45}$$

then the exponential would become a function of time given by

$$e^{jK(z'_p - z''_p)} = e^{-j2K(v_x t + x_{po})\sin\left(\frac{\theta}{2}\right)} \tag{46}$$

The frequency, f_d, of the sinusoidal variation represented by (46) is

$$f_d = \frac{K}{\pi} v_x \sin\left(\frac{\theta}{2}\right) \tag{47}$$

which is the Doppler frequency predicted by the Doppler formula for a plane wave incident along the z' axis with a plane wave scattered along the z" axis.

The substitution $\bar{p} = \bar{v}t + \bar{p}_o$ has shown that the exponential term alone in (41) gives the desired Doppler signal. Thus the multiplying quantity $a(\bar{v}t + \bar{p}_o)$, which is obtained by the same substitution, is a complex modulation term that can only be detrimental to the desired

signal. A principal task remaining, therefore, is to optimize the input distributions $u_{io}(x',y)$ and $u_{ro}(x'',y)$ so as to reduce the ill effects of $a(\bar{p})$.

An Optimum Class of Input Plane Distributions

The input distributions $u_{io}(x',y)$ and $u_{p}(x'',y)$ have thus far been assumed to be completely general except for the weak constraint that the radiation be directed near the directions of the axes. The objective of this section is to determine specific restrictions on the input plane distributions to make them useful for flowmeter applications. The basis of the restrictions is that $a(\bar{p})$ should be a highly localized function, distributed evenly about the origin. While this localization makes amplitude modulation by $a(\bar{v}t + \bar{p}_o)$ unavoidable, it is assumed desirable to avoid any phase modulation by $a(\bar{v}t + \bar{p}_o)$ so that the instantaneous Doppler frequency[†] will be that given by the plane-wave Doppler formula.

The Phase of the Input Plane Distributions

In order to localize the measurement volume about the chosen origin the requirement will be imposed that $|a(\bar{p})|$ must be maximum at $\bar{p} = 0$. From Equations (40) and (41) one obtains

$$|a(\bar{p})| = |u_i(\bar{p})||u_r(\bar{p})| \tag{48}$$

[†]When the finite duration of the response from a single scatterer is considered, the expression "Doppler frequency" is not meaningful. The "instantaneous Doppler frequency" is defined as the time derivative of the phase of the response divided by 2π.

Thus $|a(\bar{p})|$ can be made maximum at $\bar{p} = 0$ by separately maximizing $|u_i(\bar{p})|$ and $|u_r(\bar{p})|$ at the origin. Since the general expressions for u_i and u_r are of the same form, $u_1(x,y,z)$ will be used to imply either u_i or u_r in their respective co-ordinate systems, with $u_o(x,y)$ being the distribution in the input plane.

The input distribution $u_o(x,y)$ may be written in terms of magnitude and phase as

$$u_o(x,y) = a_o^r(x,y)e^{j\phi_o(x,y)} \tag{49}$$

where $a_o^r(x',y)$ is a non-negative function and $\phi_o(x,y)$ is a real function. The choice

$$\phi_o(x,y) = \phi_o, \tag{50}$$

where ϕ_o is a real constant, will maximize $|u_1(\bar{p}=0)|$ with respect to $\phi_o(x,y)$. To show this, one first determines $|u_1(\bar{p}=0)|$ with the help of (24).

$$|u_1(\bar{p}=0)| = \frac{1}{\lambda F} \left| \iint a_o^r(a,b)e^{j\phi_o(a,b)}\, dadb \right| \tag{51}$$

It is well known that for a complex function $g(x,y)$,

$$\left| \iint g(a,b)dadb \right| \leq \left| \iint |g(a,b)|dadb \right| \tag{52}$$

The stated result follows immediately.

Restricting $u_o(x,y)$ to have constant phase also insures that $|u_1(\bar{p})|$ has an absolute maximum at $\bar{p} = 0$. To see this, one again uses (24) to determine $|u_1(\bar{p})|$ when $u_o(x,y)$ has constant phase; then

$$|u_1(x,y,z)| = \tag{53}$$

$$\frac{1}{\lambda F} \left| \iint a_o^r(a,b)\, e^{\frac{-jKz}{2F^2}(a^2+b^2) - j2\pi\left(a\frac{x}{\lambda F} + b\frac{y}{\lambda F}\right)} \, dadb \right|$$

Using the inequality of (52) again, one obtains

$$|u_1(x,y,z)| \leq |u_1(\bar{p}=0)|. \tag{54}$$

The preceding derivation confirms the well-known fact that a "collimated" beam of light focusses in the back focal plane of a lens. In practice, a light beam propagating in free space can only have one plane with constant phase and thus can never be truly "collimated" like an infinite plane wave. The input plane was chosen to be one focal length in front of the lens by hindsight because this is the one plane from which a constant-phase input distribution always "focusses" to maximum intensity at the back focal point. The word "focusses" is put in quotation marks because the input distribution may be so small in transverse extent that the incident field appears focussed in the input plane while the field beyond the lens appears collimated.

It is enlightening to consider the effects of small departures of the input-plane phase functions from the desired constant phase. To this end one may assume a two-dimensional McClaurin series expansion of the input phase function $\phi_o(x,y)$ about $(x=0,y=0)$. Disregarding higher order terms, the result is[†]

$$\phi_o(x,y) = \phi_o + x \frac{\partial}{\partial x} \phi_o(0,0) + y \frac{\partial}{\partial y} \phi_o(0,0) + \tag{55}$$

$$\frac{x^2}{2} \frac{\partial^2}{\partial x^2} \phi_o(0,0) + xy \frac{\partial^2}{\partial x \partial y} \phi_o(0,0) + \frac{y^2}{2} \frac{\partial^2}{\partial y^2} \phi_o(0,0) + \cdots$$

With reference to Table 1, one observes that the linear terms of (55) represent beam deflections off the axis, as are obtained from prisms. Such a term would cause the beams to intersect elsewhere than at the chosen origin or not at all and thus represents system misalignment. The quadratic terms correspond to phase curvature, such as is introduced in a plane wave transmitted through spherical or cylindrical lenses. Such terms would cause the beam to "focus" at some position on the axis other than $z = 0$ and thus represent another type of misalignment.

The Magnitude of the Input Plane Distributions

Assuming that $u_{io}(x',y)$ and $u_{ro}(x'',y)$ are constant-phase functions and neglecting the phase constant, the focal-plane fields are obtained using (25) as

---

[†]The notation $\frac{\partial}{\partial x} \phi_o(0,0)$ denotes $\frac{\partial}{\partial x} \phi_o(x,y)\Big]_{x=0,y=0}$

$$u_i(x',y,0) = \frac{1}{\lambda F} A_{io}\left(\frac{x'}{\lambda F}, \frac{y}{\lambda F}\right) \tag{56}$$

$$u_r(x'',y,0) = \frac{1}{\lambda F} A_{ro}\left(\frac{x''}{\lambda F}, \frac{y}{\lambda F}\right) \tag{57}$$

where $A_{io}(f_x,f_y)$ and $A_{ro}(f_x,f_y)$ are the Fourier transforms of the non-negative input functions $a^r_{io}(x',y)$ and $a^r_{ro}(x'',y)$. In order that the scattering volume be evenly distributed about the origin, $a^r_{io}(x',y)$ and $a^r_{ro}(x'',y)$ will now be restricted to be even; for example,

$$a^r_{io}(x,y) = a^r_{io}(-x,-y) \tag{58}$$

with the result that $u_i(x',y,0)$ and $u_r(x'',y,0)$ are real and even.

In order to localize the measurement volume, one must constrain $u_i(x',y,0)$ and $u_r(x'',y,0)$ to be non-negligible only for low values of $|\bar{p}|$, i.e., $A_{io}(f_x,f_y)$ and $A_{ro}(f_x,f_y)$ must be "low-pass" spectra. The requirement on $a_{io}(x',y)$ and $a_{ro}(x'',y)$ is analogous to the communications problem of pulse-shaping to conserve bandwidth and is identical to the aperture antenna problem of producing a highly directed antenna pattern. Vast amounts of experience in both these fields reveals that the functions $a_{io}(x',y)$ and $a_{ro}(x'',y)$ should be smoothly varying functions which monotonically decrease along any radial path from the z axis.

The factors which govern the choice of the input-plane distributions are very similar to the pulse communications problem and the aperture antenna problem in that in all three cases one attempts to

simultaneously minimize the extent of the distribution (pulse) in both the space (time) and frequency domains. A subtle difference exists in the reasons for wishing to do so, however. The reason for minimizing physical extent of an antenna aperture distribution is to minimize the physical size and cost of the antenna. In the flowmeter problem it is generally no problem to use lens considerably larger in diameter than the incident beam because the factor which limits the transverse extent of $a_{io}(x',y)$ and $a_{ro}(x'',y)$ is more often the signal bandwidth.

The possible phase modulation of the instantaneous Doppler frequency by $a(\bar{v}t + \bar{p}_o)$ is now considered. Such modulation will be completely avoided if $a(\bar{p})$ has the form

$$a(\bar{p}) = a^r(\bar{p})e^{j\phi_o} \tag{59}$$

where $a^r(\bar{p})$ is a nonnegative real function and $e^{j\phi_o}$ is a constant. It will be shown in the next section that in most cases a good approximation for $a(\bar{p})$, neglecting the phase constant, is the product of the focal plane functions; i.e., throughout the measurement volume.

$$a(\bar{p}) \approx \frac{1}{(\lambda F)^2} A_{io}\left(\frac{x'_p}{\lambda F}, \frac{y_p}{\lambda F}\right) A_{ro}\left(\frac{x''_p}{\lambda F}, \frac{y_p}{\lambda F}\right) . \tag{60}$$

Thus all that is required to avoid phase modulation is that $A_{io}(f_x,f_y)$ and $A_{ro}(f_x,f_y)$ not only be real and even, but also strictly nonnegative. This is equivalent to requiring zero side lobes in the aperture antenna

case where phase reversals are always associated with the zero-crossings of the Fourier transform.

It is impossible to have a nonnegative even function nonzero on a finite (x,y) domain which has a nonnegative, even transform non-zero on a finite (f_x,f_y) domain. An example of a function which does satisfy all requirements but that of having finite extent is the Gaussian exponential function. As is discussed further in Chapter IV a Gaussian input distribution has additional qualities which make it optimum for use with laser flowmeters including the fact that it can be efficiently produced by a gas laser source.

Simplification of the Response Function

An exact evaluation of the expression given in (42) for $a(\bar{p})$ would be so awkward, even for the simplest possible examples, that the result would be difficult to interpret. In Equation (60) of the preceding section an approximation was presented whose justification will be established here. In addition, the variation of the measurement volume dimensions will be considered in terms of the dimensions of the input distributions.

A Fraunhoffer Approximation for the Response

The integral expression given by (24) for the field past a lens is of exactly the same mathematical form as is the propagation integral given in (21). One observes that a Fraunhoffer approximation of (24), which is analogous to the far-field diffraction case, is given by

$$u_1(x,y,z) = \frac{e^{jKz}}{\lambda F} \; U_o\left(\frac{x}{\lambda F} \, , \, \frac{y}{\lambda F}\right) \tag{61}$$

This approximation is obtained when the quadratic exponential is replaced by unity, i.e., when

$$|z| \ll \frac{2}{K}\left(\frac{F}{R_{max}}\right)^2 \tag{62}$$

where R_{max} is the maximum radius for which $u_o(x,y)$ is nonnegligible. If z_p' and z_p'' each satisfy the appropriate equation like (62) for all points in the beam intersection region, then the approximation for $a(\bar{p})$ given by (60) follows directly.

In order to determine a usable inequality with which to replace (62), the distributions $u_{io}(x',y)$ and $u_{ro}(x'',y)$ will be restricted to the class determined as desirable, i.e., constant-phase, with magnitude decreasing monotonically from the center. For this class of functions, a well-established rule of thumb will be borrowed directly from the experience of the aperture antenna field; i.e., the Fraunhoffer field is obtained when the maximum phase error from the omitted quadratic exponential is limited to $2\pi/16$ radians.† The inequality which replaces (62) is thus

$$|z_{max}| \leq \frac{\lambda}{2}\left(\frac{F}{D_{max}}\right)^2 \tag{63}$$

---

†This produces the familiar $2D^2/\lambda$ rule of aperture antenna theory for the boundary of the far field.

where D_{max} is the maximum diameter for which $u_o(x,y)$ is nonnegligible.

If the distribution $u_o(x,y)$ is separable, so that

$$u_o(x,y) = u_{ox}(x)\, u_{oy}(y) \tag{64}$$

then the surface integral is also separable with the result that

$$u_1(x,y,z) \approx \frac{e^{jKz}}{\lambda F} U_{ox}\left(\frac{x}{\lambda F}\right) U_{oy}\left(\frac{y}{\lambda F}\right) \tag{65}$$

In this case one would replace D_{max} in (63) by the larger of the widths of the functions $u_o(x)$, $u_o(y)$. If both $u_{io}(x',y)$ and $u_{ro}(x'',y)$ are separable in the given coordinate systems, then the Fraunhoffer approximation for $a(\bar{p})$ is also separable and given by

$$a(\bar{p}) = \frac{1}{(\lambda F)^2} U_{iox}\left(\frac{x'_p}{\lambda F}\right) U_{ioy}\left(\frac{y_p}{\lambda F}\right) U^*_{roy}\left(\frac{y_p}{\lambda F}\right) U^*_{rox}\left(\frac{x''_p}{\lambda F}\right) \tag{66}$$

The separability of $a(\bar{p})$ in the nonorthogonal coordinate system (x',y,x'') is used for some of the results of Chapter III. This separation cannot be obtained when the Fraunhoffer approximation is not valid.

Measurement Volume Dimensions

One cannot hope to apply Equation (63) to determine the limits of validity of the Fraunhoffer approximation until the extent of the measurement volume is defined. This is a somewhat arbitrary matter since the intersecting beams will never have sharp "edges." In the same way, the input distributions may be defined mathematically over a

large or infinite domain, while having nonnegligible magnitudes over a very small domain. In what follows, arbitrary dimensions for the measurement volume and input distributions are defined and related for the case of separable input functions.

The "widths" and "heights" of the input distributions will be denoted by X'_{io}, X''_{ro}, and Y_{io}, Y_{ro} while the corresponding dimensions of Fraunhoffer fields will be denoted by X'_{i}, X''_{r}, Y_{i}, Y_{r}. The width, height, and length of the measurement volume in the unprimed coordinates will be denoted X, Y, Z.

Now one observes that the "width" of a low-pass time function and the "width" of its Fourier transform are inversely related, usually by a constant near one. For example, a rectangular pulse of duration T has transform whose "bandwidth" B measured between the first zeros of the $\frac{\sin x}{x}$ type transform is given by

$$BT = 2 \tag{67}$$

If the "width" of the function $\exp[-4t^2/T^2]$ is arbitrarily chosen to be T, the separation between the 1/e points, then the "bandwidth" B, measured between the 1/e points of the resulting Gaussian transform is given by

$$BT = \frac{4}{\pi} \tag{68}$$

Leaving the definitions of the widths arbitrary, the well-known Fourier-transform uncertainty principle is given by

$$BT = C_f \tag{69}$$

where C_f depends on the precise definition of the widths.

When the scaling constant λF is included for the case of the Fourier transformation by a lens, one obtains the constant which relates the width (height) of the input distribution to the width (height) of the Fraunhoffer field as $C_f \lambda F$. For example,

$$X_{io} Y_{io} = C_f \lambda F. \tag{70}$$

The height Y of the measurement region is thus bounded by

$$Y = \frac{C_f \lambda F}{\text{Max}(Y_{io}, Y_{ro})} \tag{71}$$

Figure 5 illustrates the computation of bounds on the width and length of the measurement volume. The width, X, as shown in the figure has been arbitrarily taken to be the distance, in the x direction, between the extreme intersection points of the beams at their defined widths. Thus one may show trigonometrically that

$$X = \frac{C_f \lambda F}{2\cos(\theta/2)} \left[\frac{1}{X'_{io}} + \frac{1}{X''_{ro}} \right] \tag{72}$$

A similar bound on the measurement volume length, as shown in the figure, is given by

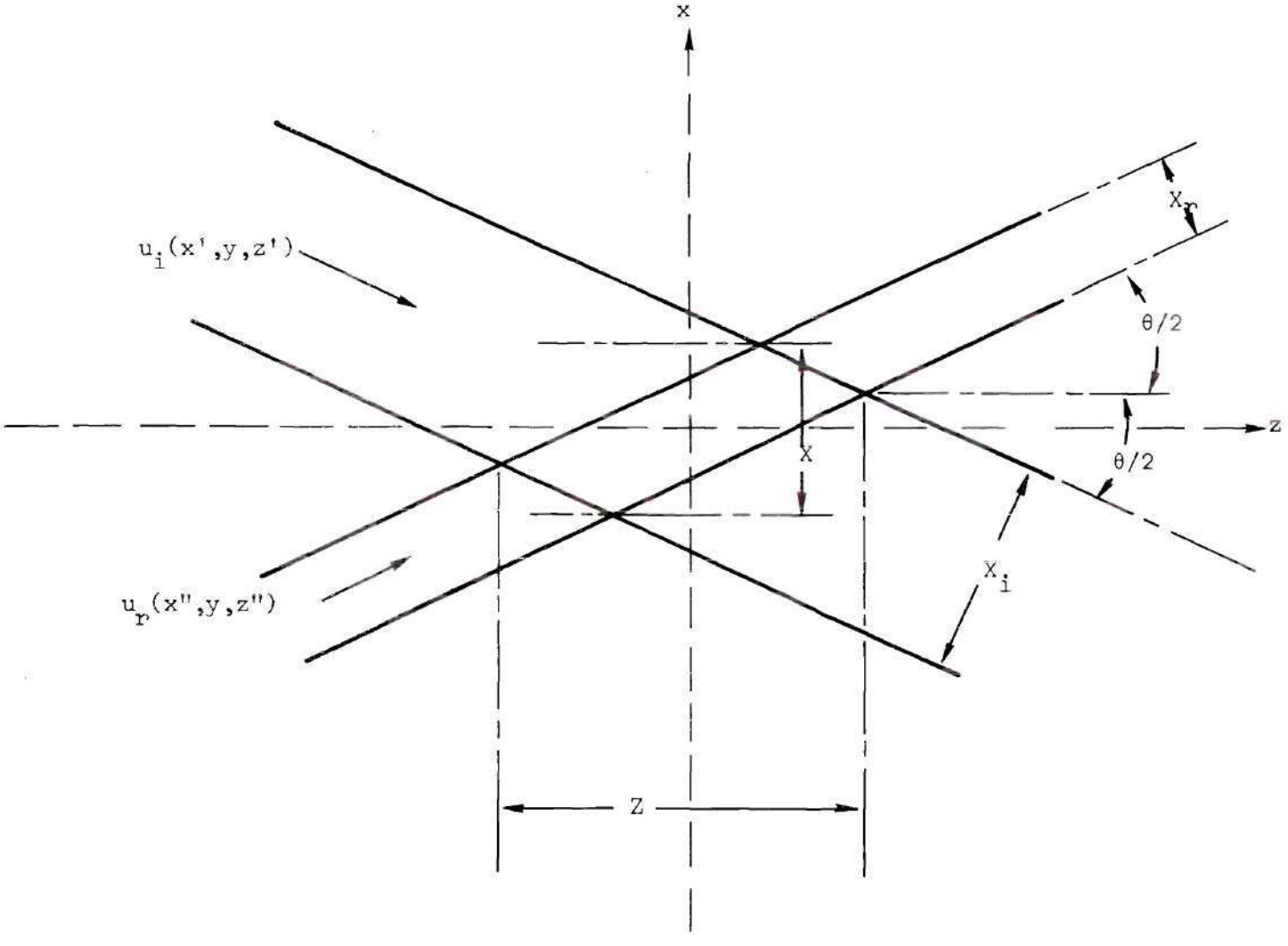

Figure 5. Determination of Measurement Volume Dimensions

$$Z = \frac{C_f \lambda F}{2 \sin(\theta/2)} \left(\frac{1}{X'_{io}} + \frac{1}{X''_{ro}} \right). \tag{73}$$

For the case where $X'_{io} = X''_{ro} = X_o$, Equation (73) becomes

$$Z = \frac{C_f \lambda F}{X_o \sin(\theta/2)} \tag{74}$$

Equation (74) shows a linear dependence of the length of the focal region on an "F/number" of the system defined by

$$F/ = \frac{F}{X_o} \tag{75}$$

where F is the focal length of the focussing lens and X_o is the common width of the beams in the input planes. This criterion does not agree, therefore, with the "depth of focus" criterion[†] used by some investigators, i.e.,

$$Z = 4(f/)^2 \lambda \tag{76}$$

where "f/" is the usual f/ number of a lens defined by

$$f/ = \frac{F}{D_\ell} \tag{77}$$

[†]The "depth of focus" criterion is discussed by Born and Wolf,[25] p. 441, for a uniformly illuminated circular aperture and a spherical lens.

with D_ℓ being the diameter of the focussing lens.

The "depth of focus" criterion might indeed be of value in cases where the Fraunhoffer approximation was not valid throughout the intersection volume if a uniform plane wave were incident at the input plane. As will be shown, however, the Fraunhoffer approximation should almost always be valid for properly aligned flowmeters. It is believed that researchers using (76) as a length criterion would have discovered their error had the formula been used correctly; i.e., if the beam diameter, rather than the lens diameter, had been correctly used in computing f/, the computed length would have been obviously too long.

The following example illustrates the order of magnitude of the dimensions being discussed. The scattering angle is assumed to be 10°. The width and height of the input beams are assumed to be 1 mm, while the diameter of each lens is 1 cm. The lenses focal lengths are 20 cm and the wavelength is 0.5 microns. Thus, with C_f assumed unity, the measurement volume dimensions are approximately given by

$$X \approx 0.1 \text{ mm} \qquad (78)$$
$$Y \approx 0.1 \text{ mm}$$
$$Z \approx 1 \text{ mm}$$

The length calculation based on the "depth of focus" criterion, with f/ = 20 cm/1 cm, gives 0.8 mm which is quite close to the value just determined. Had the "depth of focus" criterion been used correctly, however, with the beam diameter instead of the lens diameter, the f/number would have been f/ = 20 cm/0.1 cm, and the length would have

been determined as Z = 8 cm, a value not possibly correct.

The Limitations of the Fraunhoffer Approximation

For any given choice of input distribution dimensions and lens focal length, a minimum scattering angle θ_{min} must exist such that the Fraunhoffer approximation is not valid for $\theta < \theta_{min}$. This follows from Equation (73) since $1/\sin(\theta/2)$ goes to infinity as θ goes to zero. The value of θ_{min} will be computed here, to show that the Fraunhoffer approximation is valid in a majority of cases.

From Figure 5, the maximum value of $|z''|$ for points in the intersection region may be determined trigonometrically to be[†]

$$|z''_{max}| = \frac{C_f \lambda F}{2} \left(\frac{1}{X'_{io} \sin\theta} + \frac{1}{X''_{ro} \tan\theta} \right) \tag{79}$$

By requiring that $|z''_{max}|$ satisfy the Fraunhoffer boundary restriction given by (63) one obtains the following inequality:

$$\frac{C_f \lambda F}{2} \left(\frac{1}{X'_{io} \sin\theta} + \frac{1}{X''_{ro} \tan\theta} \right) \leq \frac{\lambda}{2} \left(\frac{F}{D} \right)^2 \tag{80}$$

where D is taken to be $\max(X''_{ro}, Y_{ro})$. A solution for the equality in (80) is desired for θ_{min} in the range $(0 < \theta_{min} \leq \pi/2)$. If such a solution exists, then (80) will certainly be satisfied for θ in the range $(\theta_{min} < \theta \leq \pi/2)$. Thus one seeks a solution for θ_{min} in the

---

[†]One must also consider $|z'|$, but only one set of equations is presented.

following equation:

$$C_f\left(\frac{1}{X'_{io}} + \frac{\cos\theta_{min}}{X''_{ro}}\right) = \frac{F\sin\theta_{min}}{D^2} \tag{81}$$

After additional algebraic manipulations, a quadratic equation for $\sin\theta_{min}$ is obtained whose solutions are

$$\sin\theta_{min} = \frac{C_f D^2\left[X''^{\,2}_{ro}F \pm \sqrt{X'^{\,2}_{io}X''^{\,2}_{ro}F^2 + C_f^2D^4\left(X'^{\,2}_{io} - X''^{\,2}_{ro}\right)}\right]}{X'_{io}\left(C_f^2D^4 + X''^{\,2}_{ro}F^2\right)} \tag{82}$$

where one of the solutions is extraneous. A similar equation, with the subscripts interchanged, arises by assuming that $|z'_{max}|$ limits θ instead of $|z''_{max}|$.

For reasons which will become more apparent later, X'_{io} and X''_{ro} should be equal in a well-designed low angle flowmeter optical system.† For this case, the two solutions for $\sin\theta_{min}$ given by Equation (82) become simplified and are given by

$$\sin\theta_{min} = 0 \tag{83}$$

and

---

†One might suspect this just from the form of the single scatterer response given by Equation (40).

$$\sin\theta_{min} = \frac{2C_f D^2 F X_o}{C_f^2 D^4 + X_o^2 F^2} \tag{84}$$

where X_o is the common value of X'_{io} and X''_{ro}. Since (83) does not produce an acceptable solution to the original equation, it is discarded, and (84) represents the desired result. In all practical cases, D will be either equal to X_o or of the same order of magnitude as X_o if $D = Y_o$. On the other hand, $F >> X_o$ in most cases. Thus the $C_f^2 D^4$ term in the denominator of (84) will be negligible in comparison with $X_o^2 F^2$ with the result that

$$\sin\theta_{min} \approx \frac{2C_f D^2}{F X_o} \tag{85}$$

Finally, if $Y_o \geq X_o$, one obtains

$$\sin\theta_{min} \approx \frac{2C_f Y_{ro}^2}{F X_o} \tag{86}$$

or if $X_o \geq Y_o$, then

$$\sin\theta_{min} \approx \frac{2C_f}{F/X_o} \tag{87}$$

In either case, the sine of the minimum angle is given approximately by $2C_f$ divided by a number on the order of magnitude of the F/ number previously defined as F/X_o. In a typical flowmeter, this number would usually exceed 50. The minimum scattering angle would

then be less than two degrees. Since the scattering angle is usually five degrees or larger, the Fraunhoffer approximation will almost always be satisfied.

In the remainder of this presentation, the Fraunhoffer approximation is assumed valid for properly designed and aligned flowmeter optical systems. If one wishes to test a specific set of optical parameters to determine the validity of the approximation for a particular case, Equation (82) may be used approximately, even if the input distributions are not separable, so long as they are constant-phase and monotonically decreasing in magnitude from center.

CHAPTER III

STATISTICAL SIGNAL CHARACTERISTICS OF HETERODYNE FLOWMETERS

Introduction

The signal current produced by a laser flowmeter is a random process from which velocity information is to be extracted in the presence of noise. It is obvious that the signal current produced in the measurement of turbulent flow would be stochastic since a turbulent flow field is itself a random process. One would also expect that Brownian motion of the scatterers would impart randomness to the signal. In this analysis neither of these two causes of randomness are considered. The flow is assumed constant so that the effects being studied may be limited to the optics of the system. The effects of Brownian motion are negligible at all but very low velocities[1] which will be excluded from consideration. The fundamental stochastic nature of the signal arises because of the randomness of the initial positions of the scatterers. The signal consists of a summation of the individual response functions from each scatterer, and the resultant narrow-band signal at the Doppler frequency has randomly time-varying amplitude and phase.

In this chapter, the Poisson volume law is used as a basis for the derivation of a three-dimensional "shot noise" process with which to describe the flowmeter signal current. With the use of results

concerning the white noise produced by optical heterodyne receivers, signal-to-noise expressions are derived from the auto-correlation and power spectrum of the signal process. Finally, a derivation is presented in which the effects of low-frequency laser amplitude fluctuation noise are determined.

The Poisson Law

If the scattering centers were so densely distributed that large numbers of them were always present in the system response volume, then Gaussian statistics might be appropriate. Such was the case in an analysis by Goodman[26] of coherent light scattered by a stationary rough surface. The instantaneous number of signal scatterers in a laser flowmeter may be quite small, less than one in some cases, so that the Gaussian approach is not taken.

The average distance between the scatterers is large compared with their mean diameter in any useful flowmeter system. If this were not true, the optical signals would be attenuated and scattered beyond usefulness, and the flow field would probably be distorted by particle interactions. In addition to being dilutely suspended, the particles are well mixed and randomly diffused throughout the fluid to obtain uniform signal characteristics. These conditions are just those which have been historically used to treat particles as being Poissonly distributed in a fluid volume. Thus, if M is the mean number of particles per unit volume, then in a small sample of fluid of volume V, the probability P(n,V) of n particles being present in V is given by

$$P(n,V) = \frac{(MV)^n}{n!} e^{-MV} \qquad (1)$$

Parzen[†] gives a historical example: W. S. Gosset, writing under the name of "Student" derived the Poisson law as a probability measure for studying the number of minute corpuscles to be found in a sample volume of a liquid under the assumption that the corpuscles were distributed at random throughout the liquid.

The Poisson distribution has long been associated with the "shot noise" random process which occurs, for example, in thermal-emission limited vacuum diodes. In the usual case, the shot noise process is considered to be the response of a linear system to a series of impulses distributed randomly in time. In the flowmeter system, the photocurrent consists of the system response to scattering points which enter the scattering volume randomly in time. However, the flowmeter response is considerably more complex than that of one-dimensional electronic circuit. The response is a function of not only the arrival times but also the magnitude and direction of the velocity v, the positions of entry of the particles into the scattering volume, and the scattering coefficients.

Review of Shot Noise Theory

For purposes of comparison, the results of conventional Poisson shot noise theory will now be briefly reviewed.[††] The impulse response

---

[†] See page 255, Parzen.[27]

[††] See Papoulis[28] for extensive treatment.

of a linear system is assumed to be a real, square-integrable function $h_s(t)$, with Fourier transform $H_s(f)$, such that $h_s(t)$ is non-zero only in the range $0 \leq t \leq t_o$. The system excitation $z(t)$ is a series of unit impulses given by

$$z(t) = \sum_i \delta(t-p_i) \tag{2}$$

where $\delta(t)$ is the unit impulse. The p_i's are the random times of impulse occurrence which obey a Poisson law with constant parameter M', i.e.,

$$P(n,T) = \frac{(M'T)^n e^{-M'T}}{n!} \tag{3}$$

where $P(n,T)$ is the probability of n impulses occurring in any interval of length T. The system response to excitation $z(t)$ is a stationary random process $i(t)$ given by

$$i(t) = \sum_i h_s(t-p_i) \tag{4}$$

The statistics of $i(t)$ are well known. Papoulis[27] gives the mean, m_i, the autocorrelation $R_i(p)$ and the power spectrum $S_i(f)$ as

$$m_i = E[i(t)] = M' \int h_s(a)da \tag{5}$$

$$R_i(p) = E[i(t)i(t+p)] = M' \int h_s(a)h_s(a+p)da + m_i^2 \tag{6}$$

$$S_i(f) = T[R_i(p)] = M'|H_s(f)|^2 + m_i^2\delta(f) \tag{7}$$

where the notation E[ ] indicates statistical expectation.

Formulation of a Three-Dimensional Shot-Noise Process

The Three-Dimensional Signal Process

In Chapter II expressions were derived for the photo-current produced by a scattering particle located at position $\bar{p}$ in the beam intersection volume. Here $h_s(\bar{p})$ will be used to designate the complex response to a single particle with unit scattering constant C_p. Thus

$$h_s(\bar{p}) = Nu_i(\bar{p})u_r^*(\bar{p}) \tag{8}$$

The function $h_s(\bar{p})$ is nonnegligible on a finite domain since the two incident beams are assumed to have finite diameter and to cross, i.e.

$$h_s(\bar{p}) = 0, \quad |\bar{p}| \geq r_{max} \tag{9}$$

where r_{max} is some maximum distance from the origin.

The total complex signal current from a randomly distributed collection of scatterers is

$$i_s = \sum_i C_{pi}h_s(\bar{p}_i) \tag{10}$$

The scattering constants C_{pi} are assumed to be independent random variables, each having the same probability density function $p(C_p)$.

If now the entire collection of scatterers is translated to a position $\bar{r}$ with no relative motion between the scatterers, the signal current is

$$i_s(\bar{r}) = \sum_i C_{pi} h_s(\bar{r}+\bar{p}_i) \tag{11}$$

The desired temporal signal statistics will be obtained by first determining a three-dimensional mean and autocorrelation† for the real random process $i_s^r(\bar{r})$ associated with the complex process $i_s(\bar{r})$.

Determination of the Mean

First the mean value, $m_i^r = E[i_s^r(\bar{r})]$, will be derived. Since

$$m_i^r = m_i + m_i^* = E[i_s(\bar{r})] + E[i_s^*(r)], \tag{12}$$

the complex mean m_i will be determined. For fixed $\bar{r} = \bar{r}_1$, $i_s(\bar{r}_1)$ is a random variable given by

$$i_s(\bar{r}_1) = \sum_{i=1}^{n} C_{pi} h_s(\bar{r}_1+\bar{p}_i) \tag{13}$$

where n, a random variable, is the number of particles initially in a spherical region $R_1(\bar{r}_1)$ of radius r_{max} and centered on position $(-\bar{r}_1)$. Equation (13) follows from (11) since all the scatterers outside of $R_1(\bar{r}_1)$, contribute nothing to $i_s^r(\bar{r}_1)$. The mean value of $i_s(\bar{r}_1)$ may be

---

†Preliminary work with three-dimensional Poisson statistics was performed jointly with C. F. Morris, another Ph.D. student.

evaluated by making use of conditional expectation, i.e.

$$E[i_s(\bar{r}_1)] = \sum_{n=1}^{\infty} E[i_s(\bar{r}_1)|n]P(n) \tag{14}$$

where $E[i_s(\bar{r}_1)|n]$ denotes the conditional expectation of $i_s(\bar{r}_1)$ given n, and where P(n) is the unconditional probability of the exclusive event n particles in $R_1(\bar{r}_1)$. For any fixed number of particles n in the region $R_1(\bar{r}_1)$, the conditional expectation is given by

$$E[i_s(\bar{r}_1)|n] = E\left[\sum_{i=1}^{n} C_{pi} h_s(\bar{r}_1+\bar{p}_i)|n\right] = \sum_{i=1}^{n} E[C_{pi} h_s(\bar{r}_1+\bar{p}_i)|n] \tag{15}$$

The scattering constant C_{pi} has been assumed distributed with independent probability density $p(C_p)$; thus,

$$E[i_s(\bar{r}_1)|n] = E[C_p] \sum_{i=1}^{n} E[h_s(\bar{r}_1+\bar{p}_i)|n] \tag{16}$$

The assumption of the Poisson volume distribution, given by (1), implies that if a scatterer is known to be located in $R_1(\bar{r}_1)$, with total volume V_1 the probability density for its position must be uniform over $R_1(\bar{r}_1)$ and independent of all other scatterer positions. Thus the probability that the particle is located at some position $\bar{b}$ in a volume element $d\bar{b}$ is just $d\bar{b}/V_1$, and hence each term of the summation of (16) gives

$$E[h_s(\bar{r}_1+\bar{p}_i)|h] = \iiint_{R_1(\bar{r}_1)} h_s(\bar{r}_1+\bar{b}) \frac{d\bar{b}}{V_1} \tag{17}$$

Substitution of variables with

$$\bar{a} = \bar{r}_1 + \bar{b} \tag{18}$$

$$d\bar{a} = d\bar{b}$$

gives

$$E[h_s(\bar{r}_1+\bar{p}_i)|n] = \frac{1}{V_1} \iiint_{R_1(o)} h_s(\bar{a})d\bar{a} \tag{19}$$

Since all the terms of the summation in (16) produce identical expressions given by the right-hand side of (19), Equation (16) becomes

$$E[i_s(\bar{r}_1)|n] = E[C_p] \frac{n}{V_1} \iiint_{R_1(o)} h_s(\bar{a})d\bar{a} \tag{20}$$

The unconditional expectation with respect to n may now be obtained by using (1) as indicated in (14)

$$E[i_s(\bar{r}_1)] = \frac{E[C_p]}{V_1} \iiint_{R_1(o)} h_s(a)da \sum_{n=1}^{\infty} n \left[\frac{(MV_1)^n e^{-MV_1}}{n!}\right] \tag{21}$$

The summation is the expected number of particles to be found in volume V_1 and is given by MV_1; thus,

$$E[i_s(\bar{r}_1)] = ME[C_p] \iiint h_s(\bar{a})d\bar{a} \tag{22}$$

The limits of integration in (22) have been extended to infinity since $h_s(\bar{p})$ was assumed to be nonzero only in $R_1(0)$.

Since Equation (22) does not depend on the initial choice of $\bar{r} = \bar{r}_1$, the process $i_s(\bar{r})$ is stationary in the mean. Thus, the mean value of the real process $i_s^r(\bar{r})$ is

$$m_i^r = M\left[E[C_p] \iiint h_s(\bar{a})d\bar{a} + c.c.\right] \tag{23}$$

where "c.c." is used to denote "complex conjugate of the other term in the brackets."

Determination of the Autocorrelation

A three-dimensional autocorrelation function, $R_i^r(\bar{r},\bar{r}+\bar{p}) = E[i_s^r(\bar{r})i_s^r(\bar{r}+\bar{p})]$, is to be determined where $\bar{p}$ is now taken as a vector displacement analogous to the τ usually found in temporal autocorrelations. Expressed in terms of the complex process $i_s(\bar{r})$, $R_i^r(\bar{r},\bar{r}+\bar{p})$ becomes

$$R_i^r(\bar{r},\bar{r}+\bar{p}) = E[i_s(\bar{r})i_s^*(\bar{r}+\bar{p}) + i_s(\bar{r})i_s(\bar{r}+\bar{p}) + c.c.] \tag{24}$$

$$= [R_{i1}(\bar{r},\bar{r}+\bar{p}) + R_{i2}(\bar{r},\bar{r}+\bar{p}) + c.c.]$$

$$= R_i(\bar{r},\bar{r}+\bar{p}) + R_i^*(\bar{r},\bar{r}+\bar{p})$$

where R_{i1} and R_{i2} denote the expectations of the first and second products in (24), and $R_i = R_{i1} + R_{i2}$. Only the derivation for R_{i1} is presented, since R_{i2} follows in a similar manner.

First, two positions $\bar{r}_1$ and $\bar{r}_1 + \bar{p}$ are chosen as constants. Then $i_s(\bar{r}_1)$ and $i_s^*(\bar{r}_1+\bar{p})$ are random variables, and $R_{i1}(\bar{r}_1,\bar{r}_1+\bar{p})$ is given by

$$R_{i1}(\bar{r}_1,\bar{r}_1+\bar{p}) = E\left[\left[\sum_{i=1}^{n} C_{pi} h_s(\bar{r}_1+\bar{p}_i)\right]\left[\sum_{i=1}^{n} C_p^* h_s^*(\bar{r}_1+\bar{p}+\bar{p}_i)\right]\right] \qquad (25)$$

where now n is the random number of scatterers initially in a spherical region $R_2(\bar{r}_1,\bar{p})$, centered at $-\bar{r}_1$, with radius $|\bar{p}| + r_{max}$. There can be no contribution to either $i_s(\bar{r}_1)$ or $i_s^*(\bar{r}_1+\bar{p})$ from any scatterer located outside of $R_2(\bar{r}_1,\bar{p})$. Again, the quantity inside the expectation brackets may be evaluated under the condition that n is given, after which the unconditional expectation with respect to n may be determined. The conditional expectation may be expanded as

$$E[i_s(\bar{r}_1)i_s^*(\bar{r}_1+\bar{p})|n] = \sum_{i=1}^{n} E[|C_{pi}|^2 h_s(\bar{r}_1+\bar{p}_i)h_s^*(\bar{r}_1+\bar{p}+\bar{p}_i)|n] \qquad (26)$$

$$+ \sum_{\substack{i=1 \\ l\neq j}}^{n}\sum_{j=1}^{n} E[C_{pi}C_{pj}^* h_s(\bar{r}_1+\bar{p}_i)h_s^*(\bar{r}_1+\bar{p}+p_j)|n]$$

Equation (26) was obtained from (25) by replacing the product of summations with a double summation and then separating this into a summation of terms for which i = j and a summation of terms for which $i \neq j$.

The first summation in (26) has the same form as that obtained in (15) while determining the complex mean m_i. By steps similar to those following (15), one obtains one term of $R_{i1}(\bar{r}_1,\bar{r}_1+\bar{p})$ as

$$E[|C_p|^2] \iiint h_s(\bar{a})h_s^*(\bar{a}+\bar{p})d\bar{a} \tag{27}$$

Now since C_{pi}, C_{pj}^*, $h_s(\bar{r}_1+\bar{p}_i)$ and $h_s^*(\bar{r}_1+\bar{p}+\bar{p}_j)$ are all independent random variables if $i \neq j$, the conditional expectations in the second summation of (26) are each evaluated as

$$E[C_{pi}C_{pj}^*h_s(\bar{r}_1+\bar{p}_i)h_s^*(\bar{r}_1+\bar{p}+\bar{p}_j)|n\ ] = \tag{28}$$

$$= E[C_p]E[C_p^*]E[h_s(\bar{r}_1+\bar{p}_i)]E[h_s^*(\bar{r}_1+\bar{p}+p_j)]$$

$$= |E[C_p]|^2 \frac{1}{V_2^2} \left|\iiint h_s(\bar{a})d\bar{a}\right|^2$$

where V_2 is the volume of $R_2(\bar{r}_1,\bar{p})$. There are $n^2 - n$ such identical terms in (26). Thus one evaluates the unconditional expectation as[†]

$$\frac{|E[C_p]|^2}{V_2^2} \left|\iiint h_s(\bar{a})d\bar{a}\right|^2 \sum_{n=1}^{\infty} (n^2-n) \frac{(MV_2)^n e^{-MV_2}}{h!} \tag{29}$$

$$= M^2|E[C_p]|^2 \left|\iiint h_s(\bar{a})da\right|^2 = |m_i|^2$$

Combining the results of (27) and (29), one obtains the evaluation of (25) as

---

[†]The first and second moments of the Poisson distribution are $E[n] = MV_2$, $E[n^2] = (MV_2)^2 + MV_2$. Thus, $E[n^2] - E[n] = (MV_2)^2$.

$$R_{il}(\bar{p}) = ME[|C_p|^2] \iiint h_s(\bar{a})h_s^*(\bar{a}+\bar{p})d\bar{a} + |m_i|^2 \qquad (30)$$

where the $\bar{r}_1$ notation has dropped from $R_{il}(\bar{r}_2,\bar{r}_1+\bar{p})$ since (30) shows that R_{il} depends only on $\bar{p}$. The processes $i_s(\bar{r})$ and $i_s^r(\bar{r})$ are thus wide-sense stationary[†] since R_{i2} is given by

$$R_{i2}(\bar{p}) = ME[C_p^2] \iiint h_s(\bar{a})h_s(\bar{a}+\bar{p})d\bar{a} + m_i^2 \qquad (31)$$

N-Dimensional Shot Noise

One recalls that the autocorrelation R_i^r of the real process $i_s^r(\bar{r})$ is the sum of R_{il}, R_{i2} and their complex conjugates. For the special case in which the scattering constants C_{pi} are *real*, then

$$m_i^r = ME[C_p] \iiint h_s^r(\bar{a})d\bar{a} \qquad (32)$$

and

$$R_i^r(\bar{p}) = E[C_p^2]M\iiint h_s^r(\bar{a})h_s^r(\bar{a}+\bar{p})d\bar{a} + m_i^{r\,2} \qquad (33)$$

where $h_s^r(\bar{r})$ is the real impulse[††] response of the system given by

$$h_s^r(\bar{r}) = h_s(\bar{r}) + h_s^*(\bar{r}) \qquad (34)$$

[†]First and second order statistics independent of the origin of $\bar{r}$.

[††]This is an impulse of scattering material at the location of the point scatterer. Of course, the system model would be invalid for a continuous distribution of scattering material, but this is of no consequence here.

For completeness, it is observed that if the three-dimensional Fourier transform of $h_s^r(\bar{r})$ is given by $H_s(\bar{f})$ where

$$\bar{f} = (f_x, f_y, f_z), \tag{35}$$

then a three-dimensional "power spectrum" defined as the three-dimensional Fourier transform of the autocorrelation will be given by[†]

$$S_i(\bar{f}) = ME[C_p^2]\left|H_s(\bar{f})\right|^2 + m_i^2\delta(\bar{f}) \tag{36}$$

where $\delta(\bar{f})$ is a three-dimensional impulse function.

Equations (32), (33), and (36) are seen to be of exactly the same form, except for the mean and mean-square scattering constants, as the one-dimensional shot noise expressions given by way of review in Equations (5), (6), and (7). There appears to be nothing in the derivation which would be essentially altered in an N-dimensional analysis, and it is assumed that the extension is immediate. It is probable that these results will be applicable to other N-dimensional systems in which the initial positions of the impulse excitation are randomly distributed in an N-dimensional volume.

[†]The integral in (33) is a three-dimensional correlation integral. The Fourier transform theorem given by Equation (2-7) applies in determining the three-dimensional Fourier transform.

Application to a System of Translating Scatterers

The Temporal Process

The results concerning three-dimensional shot noise will now be applied to the flowmeter analysis under the constraint of constant flow velocity. Thus if $\bar{r}(t) = \bar{v}t$, the entire collection of scatterers translates with velocity $\bar{v}$. The real signal current i_s^r is a function of time and the vector parameter $\bar{v}$, such that

$$i_s^r(t;\bar{v}) = i_s^r[\bar{r}(t)] \tag{37}$$

At any time t_1, $i_s^r(t;\bar{v})$ is a random variable and $\bar{r}$ is a fixed vector $\bar{r}_1 = \bar{v}t_1$. Thus from Equation (23)

$$E[i_s^r(t_1;\bar{v})] = E[i_s^r(\bar{r}_1)] = m_i^r \tag{38}$$

independently of the choice of t_1. The mean value of $i_s^r(t;\bar{v})$ is thus a constant in time.

The autocorrelation, $R_i^r(t,t+\tau;\bar{v})$, of the signal current is determined by choosing $t = t_1$ and then evaluating

$$R_i^r(t_1,t_1+\tau;\bar{v}) = E[i_s^r(t_1;\bar{v})i_s^r(t_1+\tau;\bar{v})] = E\left[i_s^r[\bar{r}(t_1)]i_s^r[\bar{r}(t_1+\tau)]\right] \tag{39}$$

But for constant velocity

$$\bar{r}(t_1+\tau) = \bar{r}(t_1) + \bar{v}\tau \tag{40}$$

so

$$R_i^r(t_1,t_1+\tau;\bar{v}) = E[i_s^r(\bar{r}_1)i_s^r(\bar{r}_1+\bar{p})] \tag{41}$$

where $\bar{r}_1 = \bar{r}(t_1)$ and $\bar{p} = \bar{v}\tau$. Thus

$$R_i^r(t_1,t_1+\tau;\bar{v}) = R_i^r(\bar{v}\tau) \tag{42}$$

and hence the signal current is wide sense stationary. One observes that if the velocity of translation were time varying, the mean value of the signal current would be unaffected, but the autocorrelation would become a function of t as well as τ since (40) would no longer hold. Thus stationary second order statistics of the temporal response would not be obtained for the unsteady flow case.

Neglecting the mean value of the signal current,[†] the important result of the statistical derivation is the autocorrelation of the signal current, which is given by

$$R_i^r(\tau;\bar{v}) = R_i(\tau;\bar{v}) + R_i^*(\tau;\bar{v}) = R_{i1}(\tau;\bar{v}) + R_{i2}(\tau,\bar{v}) + \text{c.c.} \tag{43}$$

$$= ME[|C_p|^2] \iiint h_s(\bar{a})h_s^*(\bar{a}+\bar{v}\tau)d\bar{a}$$

$$+ ME[C_p^2] \iiint h_s(\bar{a})h_s(\bar{a}+\bar{v}\tau)d\bar{a} + \text{c.c.}$$

[†]The mean value of the signal current is not necessarily zero, but it is entirely negligible in comparison with the mean photocurrent produced by the reference beam and will henceforth be omitted.

The Autocorrelation in Terms of the Optical Fields

The result given by (43) can now be stated in terms of the fields incident on the flowmeter measurement volume. Thus using Equation (8)

$$R_i(\tau;\bar{v}) = N^2 ME[|C_p|^2] \iiint u_i(\bar{a})u_r^*(\bar{a})u_i^*(\bar{a}+\bar{v}\tau)u_r(\bar{a}+\bar{v}\tau)d\bar{a} \qquad (44)$$

$$+ N^2 ME[C_p^2] \iiint u_i(\bar{a})u_r^*(\bar{a})u_i(\bar{a}+\bar{v}\tau)u_r^*(\bar{a}+\bar{v}\tau)d\bar{a}$$

The autocorrelation may also be expressed in terms of the input plane distributions. Using the Fraunhoffer approximation, one has

$$h_s(\bar{r}) = \frac{Ne^{jK(z'-z'')}}{(\lambda F)^2} U_{io}\left(\frac{x'}{\lambda F}, \frac{y}{\lambda F}\right)U_{ro}^*\left(\frac{x''}{\lambda F}, \frac{y}{\lambda F}\right) \qquad (45)$$

where the z' and z" variables may be eliminated since

$$e^{jK(z'-z'')} = e^{-jK(x'+x'')\tan(\theta/2)} \qquad (46)$$

Also one has

$$-K(v_x'+v_x'')\tan(\theta/2) = -2Kv_x\sin(\theta/2)\tau = -2\pi f_d\tau. \qquad (47)$$

Thus, when (45) is substituted in (43) one obtains

$$R_{il}(\tau;\bar{v}) = M \frac{N^2}{(\lambda F)^4} E[|C_p|^2]e^{j2\pi f_d\tau} \qquad (48)$$

$$\cdot \iiint U_{io}\left(\frac{x'}{\lambda F}, \frac{y}{\lambda F}\right) U^{*}_{ro}\left(\frac{x''}{\lambda F}, \frac{y}{\lambda F}\right) U^{*}_{io}\left(\frac{x'+v_{x'}\tau}{\lambda F}, \frac{y+v_{y}\tau}{\lambda F}\right)$$

$$\cdot U_{ro}\left(\frac{x''+v_{x''}\tau}{\lambda F}, \frac{y+v_{y}\tau}{\lambda F}\right) d\bar{r}$$

and

$$R_{i2}(\tau;\bar{v}) = M \frac{N^2}{(\lambda F)^4} E[C_p^2] e^{-j2\pi f_d \tau} \iiint \left[e^{-j2K(x'+x'')\tan(\theta/2)} \right. \quad (49)$$

$$\cdot U_{io}\left(\frac{x'}{\lambda F}, \frac{y}{\lambda F}\right) U^{*}_{ro}\left(\frac{x''}{\lambda F}, \frac{y}{\lambda F}\right) U_{io}\left(\frac{x'+v_{x'}\tau}{\lambda F}, \frac{y+v_{y}\tau}{\lambda F}\right)$$

$$\left. U^{*}_{ro}\left(\frac{x''+v_{x''}\tau}{\lambda F}, \frac{y+v_{y}\tau}{\lambda F}\right) \right] d\bar{r}$$

One observes that (48) and (49) have been reduced to the single nonorthogonal coordinate system (x',y,x''). The volume differential $d\bar{r}$ may be expressed in this coordinate system as

$$d\bar{r} = |J(x',y,x'')| dx' \, dy \, dx'' = \frac{dx' \, dy \, dx''}{|\sin\theta|} \quad (50)$$

where $J(x',y,x'') = -1/\sin\theta$ is the Jacobian of the transformation from (x,y,z) coordinates to (x',y,x'') coordinates.

The total signal power delivered to a unity resistor is the mean-square signal current which is obtained by setting $\tau = 0$ in the autocorrelation function $R_i^r(\tau;\bar{v})$.

The Signal Power Spectrum

The distribution of the signal power in the temporal frequency domain is the Fourier transform of $R_i^r(\tau;\bar{v})$ with respect to τ. Thus, the *power spectrum*, $S_i^r(f;\bar{v})$ is

$$S_i^r(f;\bar{v}) = T[R_i^r(\tau;\bar{v})] \tag{51}$$

where, because of the properties of autocorrelation functions and Fourier transforms, $S_i^r(f;\bar{v})$ is a real, nonnegative, even function of frequency.

It is only necessary to consider the terms of $S_i^r(f;\bar{v})$ associated with the function $R_i(\tau,\bar{v})$. Recalling that

$$R_i^r(\tau;\bar{v}) = R_i(\tau;\bar{v}) + R_i^*(\tau;\bar{v}) \tag{52}$$

one defines a *complex power spectrum*, $S_i(f,\bar{v})$ given by

$$S_i(f;\bar{v}) = T[R_i(\tau;\bar{v})] \tag{53}$$

where the real power spectrum may be recovered as

$$S_i^r(f;\bar{v}) = S_i(f;\bar{v}) + S_i^*(-f;\bar{v}) \tag{54}$$

Evaluation of the flowmeter power spectrum is somewhat difficult. The goal is to determine the power spectrum in terms of the input

distributions $u_{io}(x',y)$ and $u_{ro}(x'',y)$. In what follows, the input distributions will be restricted to be separable. The more involved case of nonseparable input functions is left as a recommendation for future work. The procedure is simplified for the separable case by the fact that the integral expressions given in (48) and (49), for the components of the autocorrelation function, become separable in the(x',y,x") coordinate system. Thus with

$$U_{io}(f_{x'},f_y) = U_{iox}(f_{x'})U_{ioy}(f_y) \tag{55}$$

$$U_{ro}(f_{x''},f_y) = U_{rox}(f_{x''})U_{roy}(f_y) \tag{56}$$

where $x'/\lambda F = f_{x'}$, $y/\lambda F = f_y$, $x''/\lambda F = f_{x''}$, one obtains from (48)

$$R_{il}(\tau;\bar{v}) = \frac{MN^2E[|C_p|^2]}{\lambda F|\sin\theta|}\, e^{j2\pi f_d\tau} \tag{57}$$

$$\cdot \left[\int U_{ioy}(f_y)U^*_{roy}(f_y)U^*_{ioy}(f_y+C_y\tau)U_{roy}(f_y+C_y\tau)df_y\right]$$

$$\cdot \left[\int U_{iox}(f_{x'})U^*_{iox}(f_{x'}+C_{x'}\tau)df_{x'}\right]$$

$$\cdot \left[\int U^*_{rox}(f_{x''})U_{rox}(f_{x''}+C_{x''}\tau)df_{x''}\right]$$

where $C_{x'} = v_{x''}/\lambda F$, $C_y = v_y/\lambda F$, $C_{x''} = v_{x''}/\lambda F$.

In Appendix B it is shown R_{i2} is identically zero if the incident distribution $u_{ro}(x',y) = 0$ for $x'' \geq F \tan(\theta/2)$ or if $u_{io}(x',y) = 0$ for $x' \leq -F \tan(\theta/2)$. Since both of these conditions will always be satisfied in a practical flowmeter experiment, R_{i2} will henceforth be neglected, and R_{i1} will be denoted by R_i.

Since the complex power spectrum $S_i(f,\bar{v})$ is the Fourier transform of the *product* of four functions of τ in (57), the desired result is the *convolution* of the transforms of each factor. The first factor transforms simply as

$$T[e^{j2\pi f_d \tau}] = \delta(f-f_d) \tag{58}$$

Thus in the final convolution this term shifts the spectrum to the Doppler frequency center. The remaining three spectral functions should therefore convolve to give a low-pass function evenly distributed about, and peaked at, the zero frequency axis.

Of the three integral expressions, the first presents the most complexity so it will be discussed in detail. The results for the other two expressions follow from a similar, but simpler, use of Fourier transform theorems. The integral expression in (57) which involves f_y will be denoted $q(C_y\tau)$. Now it is known that if

$$T[q(\tau)] = Q(f) \tag{59}$$

then

$$T[q(C_y\tau)] = \frac{1}{|C_y|} \; Q\left(\frac{f}{C_y}\right) \tag{60}$$

Thus one considers

$$Q(f) = T\left[\int [U_{ioy}(f_y)U^*_{roy}(f_y)][U_{ioy}(f_y+\tau)U^*_{roy}(f_y+\tau)]^* df_y\right] \tag{61}$$

The following Fourier transform theorems apply: If $T[g(\tau)] = G(f)$, then $T[g(\tau) \oplus g^*(\tau)] = |G(-f)|^2$; but $G(-f) = IT[g(\tau)]$, so $T[g(\tau) \oplus g^*(\tau)] = |IT[g(\tau)]|^2$, and thus

$$Q(f) = |IT[U_{ioy}(\tau)U^*_{roy}(\tau)]|^2 \tag{62}$$

Using Equation (2-7) one has

$$IT[U_{ioy}(\tau)U^*_{roy}(\tau)] = u^*_{roy}(f) \oplus u_{ioy}(f), \tag{63}$$

so

$$Q(f) = \left|\int u^*_{roy}(b)u_{ioy}(b+f)db\right|^2 \tag{64}$$

or

$$T[q(C_y\tau)] = \frac{1}{|C_y|} \left|\int u^*_{roy}(b)u_{ioy}(b + \frac{f}{C_y})db\right|^2 \tag{65}$$

The power spectrum obtained as the Fourier transform of (57) is thus[†]

$$S_i(f;\bar{v}) = \frac{MN^2E[|C_p|^2](\lambda F)^2}{|\sin\theta||v_{x'}\ v_y\ v_{x''}|}\ \delta(f-f_d) * \tag{66}$$

$$\left|\int u^*_{roy}(b)u_{ioy}\left(b + \frac{\lambda Ff}{v_y}\right)db\right|^2 * \left|u_{iox}\left(\frac{\lambda Ff}{v_{x'}}\right)\right|^2 * \left|u_{rox}\left(\frac{\lambda Ff}{v_{x''}}\right)\right|^2$$

where the convolutions are with respect to f.

Equation (66) expresses the power spectrum directly in terms of the separable input-plane distributions. One sees immediately that if $u_{io}(x',y)$ and $u_{ro}(x'',y)$ are even, low-pass functions, the spectrum shape determined by the last three terms of (66) will be even and peaked at zero frequency as desired. Furthermore one sees that the complex power spectrum $S_i(f;\bar{v})$ is, in fact, real and nonnegative. Thus

$$S^r_i(f;\bar{v}) = S_i(f;\bar{v}) + S_i(-f;\bar{v}) \tag{67}$$

Assuming that the spectrum is band-pass, one has

$$S^r_i(f;\bar{v}) = S_i(f;\bar{v}), \quad f > 0 \tag{68}$$

[†]A negative sign has been omitted from the argument of u_{rox} under the assumption that u_{rox} is even.

$$= S_i(-f;\bar{v}), \quad f < 0$$

Further implications of (66) will be discussed at the close of this chapter, and the power spectrum will be calculated for a specific example in Chapter IV.

Signal-to-Noise Ratios (SNR)

Review of Optical Heterodyne SNR Theory

Optical heterodyne SNR theory is well established.[16-19] The random arrival of photons gives rise to white Poisson shot noise (quantum noise) in the output current of a photodetector. The real mean-square quantum noise current produced at a photocathode by the incident radiation is

$$E[i_{nq}^2] = 2eB_n i_{dc} \tag{69}$$

where B_n is the electronic bandwidth and i_{dc} is the mean photocurrent. This is equivalent to a two-sided white-noise power spectrum of spectral density N_q given by

$$N_q = ei_{dc} \tag{70}$$

It has been shown that the maximum optical heterodyne SNR is obtained when the reference beam power is made sufficiently large that contributions to i_{dc} from the signal wave and any background light sources are made negligible. This is the basis for the assumption in

Chapter II that the reference beam power greatly exceeded the scattered wave power.

As with any electronic system, thermal noise is produced by the load resistance across which signal voltage is developed. This thermal noise, and all the noise sources of the electronic amplifiers which may be required, will be negligible if the quantum noise can be made to predominate without loss of signal-to-quantum-noise ratio. Such a condition is achieved in two ways: first by increasing the reference beam power, in which case the signal and quantum-noise powers increase at the same rate; second by using a low-noise preamplifier, such as an electron multiplier, which produces no thermal noise. A photomultiplier tube, for example, may be used to obtain nearly the same output signal-to-noise ratio as was present at the photocathode. It is usually a simple matter to obtain amplified quantum noise far in excess of the thermal noise with little degradation of the signal-to-noise ratio.

Since all other noise sources can be rendered negligible, the system signal power to noise power ratio is essentially that obtained at the photocathode and is given by

$$SNR = \frac{E[i_s^{r\,2}]}{2B_n N_q} = \frac{E[i_s^{r\,2}]}{2B_n e i_{dc}} \tag{71}$$

where i_{dc} is now attributed to the reference beam alone.

SNR for Heterodyne Flowmeters

The mean square signal current is

$$E[i_s^{r^2}] = R_i^r(\tau=0;\bar{v}) = 2R_{i1}(\tau=0;\bar{v}) \tag{72}$$

where $R_{i1}(\tau=0,\bar{v})$ is obtained from (48) and is real. The DC photocurrent is obtained from (2-28), with the plane of integration taken to be the input plane,† as

$$i_{dc} = N \iint |u_{ro}(x'',y)|^2 dx'' \, dy \tag{73}$$

or using Parseval's theorem,

$$i_{dc} = N \iint |U_{ro}(f_{x'},f_y)|^2 df_{x'} df_y \tag{74}$$

Thus the signal power to noise power ratio is given by

$$SNR = \frac{M\eta E[|C_p|^2]}{hf_o B_n (\lambda F)|\sin\theta|} \cdot \frac{\iiint |U_{io}(f_{x'},f_y)|^2 |U_{ro}(f_{x''},f_y)|^2 df_{x'} df_y df_{x''}}{\iint |U_{ro}(f_{x''},f_y)|^2 df_{x''} df_y} \tag{75}$$

where the spatial frequency arguments have been replaced in (48) to simplify notation, and the definition of N as

---

†Any z plane gives the same result for total reference beam power.

$$N = \frac{ne}{hf_o} \tag{76}$$

has been recalled.

Equation (75) may be useful when considering a specific electronic detection system, but it is desirable now to restate the signal-to-noise ratio in a form independent of the bandwidth B_n. It is thus assumed that the optimum detection electronics will have a variable detection bandwidth matched to the signal bandwidth at all times. The commonly used "noise bandwidth" criterion will be adopted here which states that the bandwidth B_n is that bandwidth required to pass all the signal power if the one sided signal power spectrum were white with constant density given by the true power spectrum at the center signal frequency. The total positive-frequency signal power is given by

$$\frac{1}{2} E[i_s^{r\,2}] = \int_o^\infty S_i^r(f;\bar{v})df \tag{77}$$

$$= \int S_i(f;\bar{v})df$$

Thus

$$B_n = \frac{\int S_i(f;\bar{v})df}{S_i(f_d;\bar{v})} \tag{78}$$

With the noise bandwidth defined by (78) and the signal power expressed by (77), the SNR given by (71) may be rewritten independently of the detection bandwidth as

$$SNR = \frac{S_i(f_d;\bar{v})}{N_q} = \frac{S_i(f_d;\bar{v})}{ei_{dc}} \tag{79}$$

i.e., as the peak signal power spectral density divided by the white noise power spectral density. This form of the signal-to-noise ratio expression was used as a basis for experimental work reported in Chapter VII.

A Modification of Optical Heterodyne SNR Theory

In all treatments of optical heterodyne SNR theory known to this author, it has been indicated that increasing the reference beam power increases the SNR until the SNR asymptotically becomes independent of the reference beam power when quantum noise predominates. Use of this was made in the previous sections.

During the experimental work reported in Chapter VII, it was unfortunately discovered that increasing the reference beam power drastically *reduced* the SNR until the signal became completely lost in noise. The excess noise contributed by the increased reference beam power was of a low-pass nature, in the 0-100 KHz region of the spectrum, and the signal fell within this range. The excess noise was caused by intensity fluctuations[†] of the laser beam and was quite appreciable in spite of the fact that such intensity fluctuations were less than 1 per cent according to the laser specifications.

[†]Laser intensity fluctuation noise is produced by mode intermodulation and gas plasma effects--private communication with Dr. Fred Shoffner, University of Tennessee Space Institute, Tullahoma, Tennessee.

A theoretical analysis of the effect of laser intensity fluctuation noise on optimum optical heterodyne SNR is presented in Appendix C. The analysis shows that if the signal modulation lies in the same low-pass frequency range as the intensity fluctuation noise, the signal to noise ratio is *reduced* by increasing the reference beam power. This is true, even if the signal wave is frequency modulated instead of amplitude modulated, because the intensity fluctuation noise of the reference beam is *additive* rather than multiplicative when the reference beam power greatly exceeds the signal beam power (as is usually the case).

Assuming that the total laser power is given by

$$P(t) = P_{\ell}[1 + n(t)], \tag{80}$$

where n(t) is an independent stationary wideband intensity fluctuation process with power spectrum $S_n(f)$ given by

$$S_n(f) = T\left[E[n(t)n(t+\tau)]\right], \tag{81}$$

Appendix C indicates that the heterodyne SNR given by (79) should be modified as

$$SNR = \frac{S_i(f_d;\bar{v})}{ei_{dc} + i_{dc}^2 S_n(f_d)} . \tag{82}$$

The intensity fluctuation noise term is seen to vary as the square of the DC current (or average reference beam power) while the variation of the quantum noise component is linear.

Discussion of Results

The Power Spectrum

While the results of the three-dimensional Poisson shot noise analysis will most likely be applicable to other multi-dimensional linear systems, the analysis was primarily motivated by the necessity of obtaining the power spectrum of the signal current from a generalized laser flowmeter. This power spectrum has been obtained for the case of separable, constant-phase, input aperture distributions as

$$S_i^r(f;\bar{v}) = S_i(f;\bar{v}) + S_i(-f;\bar{v}) \tag{83}$$

where $S_i(f;\bar{v})$ is given by Equation (66).

It is useful to note that the assumption of constant-phase input distributions was required only to assure the validity of the Fraunhoffer approximation which was used. Thus the effects of small input phase deviations on the power spectrum may be obtained from (66) with the assumption that the deviations are sufficiently small that the Fraunhoffer approximation is not violated. One observes directly that small phase deviations of u_{iox} or u_{rox} have no effect whatsoever on $S_i(f;\bar{v})$. This means, for example, that very small angular misalignment of one or both beams in the x direction has no effect on the signal power spectrum. It should be observed, however, that the Fraunhoffer

approximation would quickly be violated by such angular misalignments since the intersection region would move away from the lens focal planes.

Small variations of the phase of u_{ioy} and u_{roy} are more significant since the result of the autocorrelation integral involving the dummy variable b in Equation (66) does depend on phase. While the limitations on the effects of focus (phase curvature) misalignment cannot be established without further work, the effects of angular misalignment (linear phase error) can be completely determined. This is true since deflection of one or both beams in the y direction can only improve the Fraunhoffer approximation by reducing the region of overlap which remains centered in the intersection of the focal planes. The effects of y-dependent linear phase errors are calculated for a special case in the next chapter.

The power spectrum expression reveals that, for a perfectly aligned system with constant-phase input distributions, the spectral width depends on the heights and widths of the input distributions and the velocity components parallel to these dimensions. These relationships will be further clarified in the next chapter, but a few observations can be made in general here. First, the nature of convolutions of low-pass functions is such that several convolutions always result in a function approaching Gaussian in shape. This is a result of the central limit theorem of statistics. The degree to which this happens when the number of convolutions is only three is a strong function of the shapes of the initial functions, but for the type of input plane

distributions previously shown desirable the resulting spectrum will always be approximately Gaussian shaped.

The "width" of the spectrum, defined in some broad sense, will generally exceed the width of the widest component term of the multiple convolution. It does little good, therefore, to try to greatly reduce the spectral width by reducing the width of u_{iox}, say, at the exclusion of u_{rox} if $v_{x'} \approx v_{x''}$. A particularly interesting result, not reported in the literature, is the fact that if $v_y >> v_x$, then the spectral width is determined principally by v_y and the dimensions Y_{io}, Y_{ro} rather than by the dimensions parallel to the v_x component of velocity which is being measured.

Signal-to-Noise Ratios

The modification of optical heterodyne SNR theory will be temporarily disregarded since the signal spectrum will generally not fall within the frequency range of intensity fluctuation noise for velocities greater than a few feet per second.

First one observes in Equation (75) that the SNR is proportional to η/hf_oB as is expected from other heterodyne SNR treatments. The dependence of the SNR on $ME[|C_p|^2]$ indicates that the signal power obtained from each scatterer adds linearly in the total average and that the phase of the scattering constant C_{pi} is of no consequence. Recalling that

$$|C_p|^2 = \frac{\lambda^2}{4\pi} \sigma_p^2, \tag{84}$$

where σ_p^2 is the scattering cross section, possibly adjusted to account for nonisotropic scattering, one sees that the signal-to-noise ratio is proportional to the mean scattering cross section. The presence of the $|\sin\theta|$ term in the denominator of (75) reflects the fact that the scattering volume is enlarged to include more scatterers as the beam intersection angle decreases. This is in addition to whatever increase in $E[\sigma_p^2]$ may be obtained by decreasing θ in cases where scattering is not isotropic.

The ratio of the two integrals in (75) is also revealing. One sees that changing the reference beam power by replacing $|u_{ro}|^2$ by $C|u_{ro}|^2$ has no effect on SNR while the SNR is directly proportional to similar changes in the scattering beam power. This is in agreement with less complex expressions which have been obtained by others studying optical heterodyne SNR theory. A second point concerns the fact that the numerator, proportional to signal power, does not depend on the velocity $\bar{v}$. Equation (75) is misleading in this respect since in all cases the required bandwidth B_n is linear function of the magnitude of the velocity.

The dependence of the SNR on the input distributions and on the velocity components can be determined from Equation (79) with $S_i(f_d;\bar{v})$ obtained from (66). In Equation (79) an equivalent noise bandwidth has been assumed so that the effects of velocity change are incorporated. From (66) it would appear, however, that the SNR is inversely proportional to the cube of the magnitude of the velocity because of the $|v_{x'}v_y v_{x''}|$ term in the denominator. This is an erroneous conclusion

since the true effects are disguised in the convolution and correlation integrals. The linear dependence of SNR on $1/|\bar{v}|$ is demonstrated for a specific example in the next chapter.

Equation (79) gives the SNR in a form which is useful for purposes of measurement with a power spectrum analyzer. This may be done by measuring the white noise spectral density, N_q, in a region where the bandpass signal spectrum is negligible and then subtracting this value from the peak signal-plus-noise value to obtain $S_i(f_d;\bar{v})$, each to within the same multiplicative gain constant which cancels in the SNR. One should observe, however, that the current i_{dc} in (79) is the *photo-cathode* current. For an electron multiplier current gain of G_e the anode power spectrum $S_{ia}(f;\bar{v})$ would be given by

$$S_{ia}(f;\bar{v}) = G_e^2 S_i(f;\bar{v}) \tag{85}$$

while the anode DC current would be

$$i_{dca} = G_e i_{dc} \tag{86}$$

Thus, it is *not* an acceptable procedure to measure the signal power spectrum and the *DC current* at the anode and use Equation (79) to determine the SNR since the result would be too large by a factor of G_e.

The Effects of Laser Intensity Fluctuation Noise

Laser intensity fluctuation noise is produced by mode intermodulation and gas plasma effects. It is generally of a low-pass

nature, less than a few hundred KHz in bandwidth, although discrete frequency oscillations sometimes occur. This type of noise will not be a problem in most wind tunnel measurements because typical signal frequencies will be in the tens of megaherz range. The problem will arise in the measurement of boundary layer flow near a wall or in liquid flow studies where velocities are small.

The reason why the intensity fluctuation noise can become a problem is that large amounts of scattered light are produced by scatterers not in the measurement volume. This background light produces unnecessary quantum noise which may be suppressed by increasing the reference beam power until it greatly exceeds *all* the scattered light from the regions near the measurement volume. In the process, however, the reference beam power becomes so great that even minute (1 per cent or less) intensity fluctuations become significant.

The alternatives for overcoming the problem of intensity fluctuation noise are either to use a highly stabilized laser or to use critically aligned spatial filters to remove as much background light as possible so that the reference beam need not serve this purpose. Decreasing the reference beam power decreases i_{dc} in proportion. Thus the fluctuation noise component decreases by i_{dc}^2 while the signal and quantum noise decrease by i_{dc}.

One way to obtain the required spatial filtering is to image the measurement volume with a lens slightly larger than the reference beam onto an aperture slightly larger than the image of the measurement volume. This is exactly the type of spatial filtering action which a

stable, more powerful reference beam can automatically perform in effect. Most experienced flowmeter investigators have found it desirable experimentally to use some type of lens-aperture filter for the scattered radiation prior to detection. Other reasons, such as ease of alignment or decreased spectral broadening, are usually given, but it is entirely possible that part of their improved success may be attributed to decreased intensity fluctuation noise in some cases.

CHAPTER IV

MEASUREMENT VOLUME, BANDWIDTH, AND SNR VARIATIONS FOR A SPECIALIZED CLASS OF OPTIMUM FLOWMETERS

The purpose of this chapter is to clarify the meaning of some of the general expressions which have been deduced by analytically evaluating the expressions for a certain optimum class of flowmeters employing Gaussian beams. In particular, variations of the following quantities are considered in terms of the scattering angle, the input beam parameters, the optics, and the velocity: the measurement volume dimensions, the signal spectrum bandwidth, and the signal-to-noise ratio.

An elliptical Gaussian laser beam is discussed first as the source of optimum input-plane distributions. The quantities mentioned above are then analytically evaluated for elliptical Gaussian input distributions, and the effects of small misalignments are considered. The interpretation and use of the analytical results depend on a variety of factors associated with specific applications. Therefore the results are considered in greater detail for the specific application of high-velocity two-dimensional flow as a useful example.

The Elliptical Gaussian Beam

Motivation

The specialized optimum input-plane distributions which will be assumed in this chapter are separable Gaussian functions of the following form

$$u_o(x,y) = \frac{\sqrt{P}\, e^{-\left[\frac{x^2}{w_{ox}^2} + \frac{y^2}{w_{oy}^2}\right]}}{\sqrt{\frac{\pi}{2} w_{ox} w_{oy}}} \qquad (1)$$

where P is the total beam power, and w_{ox}, w_{oy} are the "beam waist" radii along the x and y axes, respectively, at which the field magnitude is reduced by 1/e from the value at the optical axis. The propagating beam arising from the distribution of (1) will be called the elliptical Gaussian beam.

There are several reasons for choosing the class of input distributions given by (1). The first is that this distribution satisfies all the requirements set forth in Chapter II for an optimum choice, except that of finite transverse extent. This is of little consequence practically since the Gaussian beam contains 91 per cent of its total power within the ellipse defined by the minor and major axes w_{ox} and w_{oy} and virtually all of the power within a slightly larger region. There is therefore no reason why lens diameters cannot be large enough to be essentially infinite in most applications.

A second reason for choosing the elliptical Gaussian function is based on the desire to simultaneously minimize the measurement volume dimensions and the signal spectral width. Papoulis† gives the solution to a problem which heuristically applies here. The problem is that of simultaneously minimizing the duration and bandwidth of a temporal

---

†See Papoulis,[22] page 193.

pulse, with "duration" and "bandwidth" being defined as a normalized second moment of the pulse and its Fourier transform, respectively. The resulting pulse shape is a Gaussian pulse. Now the signal spectrum and the measurement volume do not form a Fourier transform pair. However, the functions $u_{iox}(x)$ and $u_{ix}(x)$, for example, *are* scaled transform pairs. The spectrum $S_i(f;\bar{v})$ is exactly Gaussian *only* if all the input plane functions are Gaussian. These facts suggest strongly that some type of two-dimensional Gaussian input distribution will best minimize both the signal bandwidth B and the measurement volume dimensions X,Y,Z.

Still another reason for choosing the class of functions given by (1) is based on power efficiency. The only uniphase mode of oscillation of a laser cavity is the TEM_{oo} Gaussian (circular) beam[29] which at its plane of minimum diameter has the distribution

$$u_{oo}(x,y) = \frac{\sqrt{P}}{\sqrt{\frac{\pi}{2}}\, w_o} e^{-\left[\frac{x^2 + y^2}{w_o^2}\right]}$$

As will be shown below, an elliptical Gaussian beam can be generated almost losslessly from the TEM_{oo} laser mode, but any other constant-phase distribution would require attenuation of part of the available

laser power.[†] From an efficiency standpoint, then, the elliptical Gaussian beam is optimum in terms of practical sources.

The use of the elliptical Gaussian beam, rather than the TEM_{∞} beam, has been postulated because it is more general and it will allow improvements of the flowmeter operation not possible with circular symmetric input distributions. The choice of the elliptical axes, however, has been made arbitrarily to restrict the function to the class for which the power spectrum has been analyzed, i.e., separable in x and y coordinates.

Propagation of an Elliptical Gaussian Beam

The propagating mode of the TEM_{∞} Gaussian beam given by (2) is well known. The TEM_{∞} beam is a special case of the elliptical Gaussian beam, whose propagating mode is derived in Appendix D. The derivation is based on the fact that, with (1) as the input distribution in the front focal plane of a lens, the field beyond the lens is another elliptical Gaussian beam whose minimum dimensions occur in the back focal plane of the lens, i.e.

$$u(x,y,z=0) = U_o\left[\frac{x}{\lambda F}, \frac{y}{\lambda F}\right] = \frac{\sqrt{P}}{\sqrt{\frac{\pi}{2} w_x w_y}} e^{-\left[\frac{x^2}{w_x^2} + \frac{y^2}{w_y^2}\right]} \qquad (3)$$

[†]For example, a uniformly illuminated aperture can be approximately obtained by placing a small aperture in a large TEM_{∞} beam, but this is inefficient and unnecessary.

where w_x and w_y are the beam waist constants of the beam beyond the lens. In terms of the input beam waist constants one has,

$$w_x = \frac{\lambda F}{\pi w_{ox}}, \qquad w_y = \frac{\lambda F}{\pi w_{oy}} \tag{4}$$

It is observed that if one arbitrarily adopts the convention that $X_{io} = 2\, w_{ox}$, $X_i = 2\, w_x$, etc., then the factor C_f, previously defined, is given by $C_f = 4/\pi$.

Since the evaluations of this chapter are based on the Fraunhoffer approximation, the complete propagating mode of the elliptical Gaussian beam is not required here. It is presented in Appendix D because the derivation might be useful in other applications.

Generation of an Elliptical Gaussian Beam

Two methods of generating an elliptical Gaussian beam from a TEM_{oo} mode beam are briefly considered. The first is somewhat hypothetical and impractical, but the concept will be needed later. In the first method one would place a one-dimensional Gaussian attenuation filter $t(x,y)$ in a TEM_{oo} mode beam at the beam waist. Thus to obtain a shortened x radius, the filter could be of the form

$$t(x,y) = e^{-\frac{x^2}{w_f^2}} \tag{5}$$

With the incident beam radius being w_o, the radii after filtering would be

$$w_{oy} = w_o, \quad w_{ox} = \frac{w_o w_f}{\sqrt{w_o^2 + w_f^2}} \tag{6}$$

and the transmitted beam power would be reduced by a factor ξ given by

$$\xi = \frac{w_f}{\sqrt{w_o^2 + w_f^2}} \tag{7}$$

The attenuation method poses two difficulties. The first is that it is not efficient, just as using apertures is not efficient. The second is that such a filter would be difficult to fabricate. A suitably exposed piece of film, for example, would produce grain noise and phase variations which would be undesirable.

Figure 6 illustrates an efficient way to produce an elliptical Gaussian beam which involves the use of good cylindrical lenses. An ideal thin cylindrical lens is a transmission phase filter of the form given by Table 1 as

$$t(x,y) = e^{-\frac{jK}{2F_x} x^2} \tag{8}$$

Such a lens affects the phase distribution in one dimension only. Using two such lenses with focal lengths F_1, F_2, spaced a distance $F_1 + F_2$ apart one can image the x dependent factor of a separable input plane distribution in the back focal plane of the second lens. The magnification ratio is F_2/F_1. If another pair of cylindrical lenses with focal

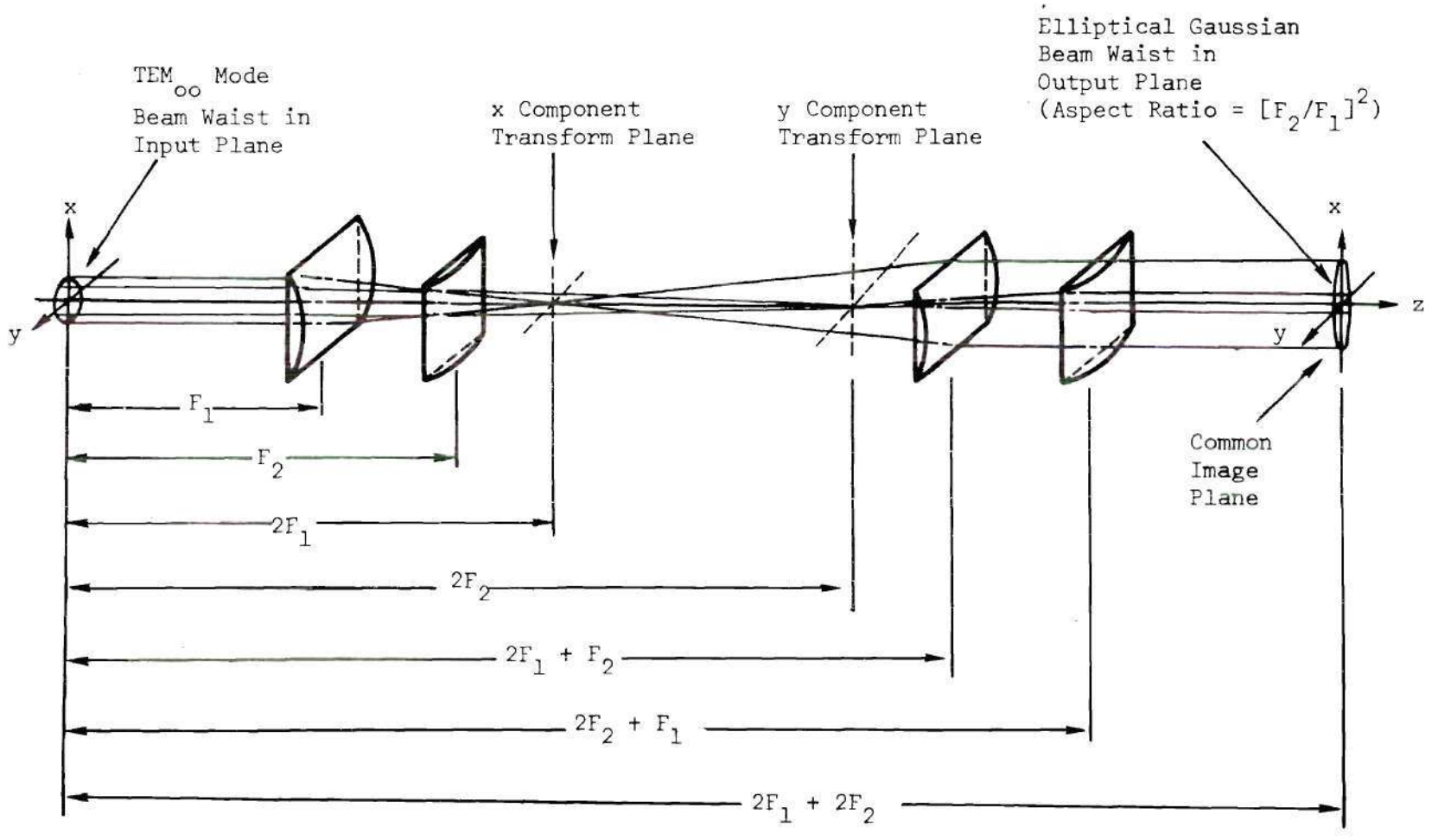

Figure 6. An Arrangement of Cylindrical Lenses to Produce an Elliptical Gaussian Beam

lengths F_2 and F_1 are inserted at right angles to the first pair, then the y dependent factor will be imaged with demagnification ratio F_1/F_2.

In Figure 6 a TEM_{oo} beam waist in the input plane will be imaged as an elliptical Gaussian beam with its waist in the output plane with aspect ratio

$$\frac{w_x}{w_y} = (F_2/F_1)^2 \tag{9}$$

Other optical arrangements which require fewer lenses and less physical space are also possible.

Evaluation of General Expressions

Definition of Terms

The definitions of the X,Y,Z, the width, height, and length of the measurement volume, were given in Chapter II in terms of the input widths and heights X'_{io}, Y_{io}, X''_{ro}, Y_{ro}. The arbitrary convention mentioned above, that $C_f = 4/\pi$, and, for example, that $X'_i = 2w'_x$ and $X'_{io} = 2w'_{ox}$ will be maintained.

The form of the SNR which will be considered is that given by Equation (3-79) as the ratio of the peak signal power spectral density to the white quantum noise spectral density. The use of this form of the SNR implies optimum detection electronics whose bandwidth adjusts as the center Doppler frequency is changed. The effects of intensity fluctuation noise are omitted since they can be avoided in most flowmeter applications by careful system design.

The bandwidth of the signal power spectrum, $S_i(f;\bar{v})$ rather than the entire power spectrum itself, will be of principal interest here since the power spectrum will always be exactly Gaussian shaped. The signal bandwidth B will be arbitrarily defined as that bandwidth between the 1/e points of the spectrum. This definition differs by about 11 per cent from the "noise bandwidth" B_n previously defined, but it simplifies notation slightly. The relationship between B and B_n is

$$\frac{B_n}{B} = \frac{\sqrt{\pi}}{2} \tag{10}$$

Insofar as the optical system design affects the design of the detection electronics, the fractional bandwidth of the signal, B/, given by

$$B/ = \frac{B}{f_d} \tag{11}$$

is important. This is true since one desires a narrow-band signal with B/ much less than unity. Therefore this quantity will also be evaluated.

The Measurement Volume Dimensions

From Equation (2-72) and the preceding definitions, one obtains the width of the measurement volume as

$$X = \frac{\lambda F}{\pi \cos(\theta/2)} \left[\frac{1}{w'_{ox}} \quad \frac{1}{w''_{ox}} \right] \tag{12}$$

where w'_{ox} and w''_{ox} are the x directed Gaussian beam radii of the scattering beam and reference beam input distributions, respectively. Similarly, the height is obtained using Equation (2-71) as

$$Y = \frac{2\lambda F}{\pi} \frac{1}{\max(w'_{oy}, w''_{oy})} \tag{13}$$

where w'_{oy} and w''_{oy} are the y directed radii of the input distributions.

The length of the measurement volume is obtained from Equation (2-73) as

$$Z = \frac{\lambda F}{\pi \sin(\theta/2)} \left[\frac{1}{w'_{ox}} + \frac{1}{w''_{ox}}\right] \tag{14}$$

Evaluation of the Power Spectrum

To obtain the bandwidth and SNR, the integral expression for the power spectrum given by Equation (3-66) must be evaluated with $u_{io}(x',y)$ and $u_{ro}(x'',y)$ being of the elliptical Gaussian form given by (1). Hence with

$$C_1 = \frac{M\eta^2 e^2 \lambda^2 E[\sigma_p^2] P_i P_r}{4\pi h^2 f_o^2 |\sin\theta|} \tag{15}$$

Equation (3-66) becomes

$$S_i(f;\bar{v}) = \frac{(\lambda F)^2 C_1}{|v'_x v_y v''_x|} \delta(f-f_d) * \tag{16}$$

$$\left[\frac{1}{\sqrt{\frac{\pi}{2}\, w'_{oy} w''_{oy}}} \int e^{-\frac{b^2}{w''^2_{oy}}} e^{-\frac{\left(b + \frac{\lambda F f}{v_y}\right)^2}{w'^2_{oy}}} db\right]^2 *$$

$$\left[\frac{1}{w'_{ox}\sqrt{\frac{\pi}{2}}} e^{-2\left(\frac{\lambda F f}{v' x' ox}\right)^2}\right] * \left[\frac{1}{w''_{ox}\sqrt{\frac{\pi}{2}}} e^{-2\left(\frac{\lambda F f}{v'' x'' ox}\right)^2}\right]$$

To evaluate (16) one may make use of the following property of the zero-mean Gaussian probability density function, $p(x,\sigma^2)$.

$$p(x,\sigma_1^2) * p(x,\sigma_2^2) = p(x,\sigma_1^2) \oplus p(x,\sigma_2^2) = p(x,\sigma_1^2 + \sigma_2^2) \qquad (17)$$

where

$$p(x,\sigma^2) = \frac{1}{\sqrt{2\pi}\,\sigma} e^{-\frac{x^2}{2\sigma^2}} \qquad (18)$$

The correlation integral in (16) which depends on the dummy variable b thus becomes

$$\int e^{-\frac{b^2}{w''^2_{oy}}} e^{-\frac{\left[b + \frac{\lambda F f}{v_y}\right]^2}{w'^2_{oy}}} db = \qquad (19)$$

$$\pi w'_{oy} w''_{oy} p\left[\frac{\lambda F f}{v_y}, \frac{w'^2_{oy}}{2}\right] \oplus p\left[\frac{\lambda F f}{v_y}, \frac{w''^2_{oy}}{2}\right]$$

$$= \pi w'_{oy} w''_{oy} p\left[\frac{\lambda F f}{v_y}, \frac{w'^2_{oy} + w''^2_{oy}}{2}\right]$$

$$= \frac{\sqrt{\pi}\, w'_{oy} w''_{oy}}{\sqrt{w'^2_{oy} + w''^2_{oy}}} \; e^{-\frac{(\lambda F f / v_y)^2}{w'^2_{oy} + w''^2_{oy}}}$$

The three terms in brackets in (16) may now be algebraically rearranged as

$$\left[\frac{2\, w'_{oy} w''_{oy}}{w'^2_{oy} + w''^2_{oy}} \; e^{-\frac{f^2}{2\frac{v_y^2}{(2\lambda F)^2}(w'^2_{oy} + w''^2_{oy})}}\right] * \tag{20}$$

$$\left[\sqrt{\frac{2}{\pi}}\, \frac{1}{w'_{ox}}\, e^{-\frac{f^2}{2\frac{v'^2_x}{(2\lambda F)^2} w'^2_{ox}}}\right] * \left[\sqrt{\frac{2}{\pi}}\, \frac{1}{w''_{ox}}\, e^{-\frac{f^2}{2\frac{v''^2_x}{(2\lambda F)^2} w''^2_{ox}}}\right]$$

$$= \frac{\sqrt{2\pi}\ |v_x', v_y v_x''|\, w'_{oy} w''_{oy}}{(\lambda F)^3 \sqrt{w'^2_{oy} + w''^2_{oy}}}\ p\left[f,\ \frac{v_y^2 (w'^2_{oy} + w''^2_{oy})}{(2\lambda F)^2}\right] *$$

$$p\left[f,\ \frac{v'^2_x\ w'^2_{ox}}{(2\lambda F)^2}\right] * p\left[f,\ \frac{v''^2_x\ w''^2_{ox}}{(2\lambda F)^2}\right]$$

The convolution relation given by (17) may now be applied twice so that the quantity described by (20) becomes

$$\frac{\sqrt{2\pi}\ |v_x', v_y v_x''|\, w'_{oy} w''_{oy}}{(\lambda F)^3 \sqrt{w'^2_{oy} + w''^2_{oy}}}\ p\left[f,\ \frac{v_y^2 (w'^2_{oy} + w''^2_{oy}) + v'^2_x w'^2_{ox} + v''^2_x w''^2_{ox})}{(2\lambda F)^2}\right] \qquad (21)$$

Expression (21) is the evaluation of the three terms in brackets in Equation (16) for the power spectrum. The convolution with the delta function in (16) replaces f by $f - f_d$. Several of the premultiplying constants in (21) and (16) cancel, leaving as a result

$$S_i(f;\bar{v}) = \frac{2C_1 w'_{oy} w''_{oy}}{\sqrt{w'^2_{oy} + w''^2_{oy}}}\ \frac{e^{-\frac{2(\lambda F)^2 (f-f_d)^2}{\left[v_y^2 (w'^2_{oy} + w''^2_{oy}) + v'^2_x w'^2_{ox} + v''^2_x w''^2_{ox}\right]}}}{\sqrt{v_y^2 (w'^2_{oy} + w''^2_{oy}) + v'^2_x w'^2_{ox} + v''^2_x w''^2_{ox}}} \qquad (22)$$

The negative frequency portion of the complete power spectrum $S_i^r(f;\bar{v})$ is obtained by replacing f by -f in (22).

The Signal Bandwidth and the SNR

All the information given by (22) is contained in the value $S_i(f_d,\bar{v})$, the bandwidth B, and the exponential form. In other words

$$S_i(f;\bar{v}) = S_i(f_d;\bar{v})\, e^{-\frac{(f-f_d)^2}{(B/2)^2}} \tag{23}$$

where

$$S_i(f_d;\bar{v}) = \frac{2C_1 w'_{oy} w''_{oy}}{\sqrt{w'^2_{oy} + w''^2_{oy}}} \frac{1}{\gamma} \tag{24}$$

and

$$B = \frac{\sqrt{2}\,\gamma}{\lambda F} \tag{25}$$

with

$$\gamma = \sqrt{v_y^2(w'^2_{oy} + w''^2_{oy}) + v_{x'}^2 w'^2_{ox} + v_{x''}^2 w''^2_{ox}} \tag{26}$$

One observes that γ is proportional to the velocity magnitude. Thus the bandwidth, B, is proportional to the velocity magnitude, and the value $S_i(f_d;\bar{v})$ is inversely proportional to the velocity magnitude.

The fractional bandwidth B/ is obtained, after recalling that

$$f_d = \frac{K}{\pi} v_x \sin(\theta/2) = \frac{2v_x}{\lambda} \sin(\theta/2), \tag{27}$$

as

$$B/ = \frac{\gamma}{\sqrt{2}\, F\, v_x \sin(\theta/2)} \tag{28}$$

The SNR was obtained in Equation (3-79) as

$$SNR = \frac{S_i(f_d;\bar{v})}{e\, i_{dc}} \tag{29}$$

where for the elliptical Gaussian reference beam with power P_r,

$$i_{dc} = \frac{\eta e}{h f_o} P_r \tag{30}$$

Thus from Equations (14), (23), and (29)

$$SNR = \frac{2M\eta\lambda^2 E[\sigma_p^2] P_i}{4\pi h f_o |\sin\theta|} \cdot \frac{w'_{oy} w''_{oy}}{\sqrt{w'^2_{oy} + w''^2_{oy}}} \cdot \frac{1}{\gamma} \tag{31}$$

A Condition for SNR Improvement

The four input beam-waist parameters have been left arbitrary. Although it is not true for the x-dependent parameters because of the $v_{x'}$ and $v_{x''}$ factors in γ, there is complete symmetry in all the

expressions which have been evaluated with regard to w'_{oy} and w''_{oy}. This fact suggests the possibility that one should choose w'_{oy} and w''_{oy} equal. This choice maximizes the SNR as will now be shown.

It is assumed that some value has been chosen as the desired Y dimension of the measurement volume. By Equation (13), this choice establishes the value of $\mathrm{Max}(w'_{oy}, w''_{oy})$. Let it be supposed that w''_{oy} is the larger value. Then

$$w'_{oy} = \varepsilon\, w''_{oy} \tag{32}$$

where ε is some value in the range

$$0 \leq \varepsilon \leq 1 \tag{33}$$

The SNR, omitting constant multipliers, is

$$\mathrm{SNR} = \frac{w''^{2}_{oy}\,\varepsilon}{\sqrt{w''^{2}_{oy} + \varepsilon^{2} w''^{2}_{oy}}} \cdot \frac{1}{\sqrt{v_y^2 (w''^{2}_{oy} + w''^{2}_{oy}\varepsilon^{2}) + v_{x'}^{2} w'^{2}_{ox} + v_{x''}^{2} w''^{2}_{ox}}} \tag{34}$$

The SNR is thus proportional to

$$\frac{\varepsilon}{\sqrt{1 + \varepsilon^{2}}} \cdot \frac{1}{\sqrt{(1 + \varepsilon^{2}) + C_2}} \tag{35}$$

where C_2 is a positive constant. The first derivative of Expression (35) is positive on the range $0 \leq \varepsilon \leq 1$. Thus the SNR is maximized at

$\varepsilon = 1$, or $w'_{oy} = w''_{oy}$. The same result is obtained if w'_{oy} is initially assumed larger than w''_{oy}.

Discussion

The results of this section are now briefly summarized and discussed. It has been shown that the input-plane parameters w'_{oy} and w''_{oy} should be equal, with common value w_{oy}. For this case, the width and length of the measurement volume are given by (12) and (14) and the height is given by

$$Y = \frac{2\lambda F}{\pi w_{oy}} \tag{36}$$

The center signal frequency is given by

$$f_d = \frac{K}{\pi} v_x \sin(\theta/2) \tag{37}$$

and the bandwidth between the 1/e values of the signal power spectrum is given by

$$B = \frac{\sqrt{2}\,\gamma}{\lambda F} \tag{38}$$

where γ is reduced to

$$\gamma = \sqrt{2v_y^2 w_{oy}^2 + v_{x'}^2 w_{ox}'^2 + v_{x''}^2 w_{ox}''^2} \tag{39}$$

The fractional bandwidth is given by

$$B/ = \frac{\gamma}{\sqrt{2}\ F\ v_x \sin(\theta/2)} \tag{40}$$

and the SNR is given by

$$SNR = \frac{M\eta\lambda^2 E[\sigma_p^2]P_i}{2\sqrt{2}\ \pi\ hf_o|\sin\theta|}\ \frac{w_{oy}}{\gamma} \tag{41}$$

The implications of the factor γ are somewhat obscured by the fact that the velocity components have been expressed in a non-orthogonal coordinate system for the sake of analysis. When the velocity is expressed in the rectangular (x,y,z) coordinate system, γ assumes the form

$$\gamma = \sqrt{2w_{oy}^2 v_y^2 + [w'^2_{ox}+w''^2_{ox}][v_x^2\cos^2(\theta/2) + v_z^2\sin^2(\theta/2)] + [w'^2_{ox}-w''^2_{ox}]v_x v_z \sin\theta} \tag{42}$$

Even when expressed in a conventional coordinate system, the effect of γ on the signal characteristics remains somewhat obscured in complexity unless a specific application is considered for which desired measurement volume dimensions are known as well as the general direction and magnitude of the velocity. It is evident, as stated previously, however, that γ is proportional to the magnitude of the velocity. Thus the SNR is inversely proportional to, and the signal bandwidth is proportional to, the velocity magnitude while the fractional bandwidth is not affected by the velocity magnitude.

Equation (41) reveals that the SNR is not a function of the focal length of the focussing lenses. This result occurs since an increase of focal length decreases the magnitude of the response current for each individual scatterer but increases the scattering volume to include more scatterers. The net result is that no change occurs in the SNR.

Different aspects of the results which have been obtained assume more or less importance in different applications of laser flowmeters. For example, in the study of boundary layer flow in a liquid the velocities incurred would be small and a very small measurement volume would be desired. In such a case a large scattering angle would reduce the measurement volume length and fractional bandwidth and increase the Doppler sensitivity. The SNR would be decreased, but this would be a minor problem at very low velocities. On the other hand, at very high wind-tunnel velocities one desires as little Doppler sensitivity as possible so that photodetector bandwidths will not be exceeded, and the SNR may be a critical factor.

In order to further illustrate the use of the results which have been obtained, the application of measuring high-velocity two-dimensional flow in a wind tunnel will be considered in more detail after the next section. The next section is devoted to the effect of a small angular misalignment of the beams incident at the input-planes.

The Effect of Angular Misalignment of the Incident Beams

In Chapter II it was pointed out that small phase errors in the assumed constant-phase input-plane distributions were equivalent to small misalignments of the flowmeter optical system. In Chapter III it

was observed that, within the Fraunhoffer approximation, x dependent phase errors have no effect on the signal power spectrum and hence the SNR. The effect of a small y dependent linear phase error may be determined analytically for the elliptical Gaussian input distributions assumed in this chapter. This is done below for the case where $w'_{oy} = w''_{oy} = w_{oy}$.

It will be assumed that the reference beam is deflected slightly off the z" axis in the y direction by a small angle ψ.[†] Thus the input distribution $u_{ro}(x'',y)$ is modified by a small linear phase shift, $\exp[jK\psi y]$, while the scattering beam distribution remains unchanged. In the signal power spectrum expression given by (3-66), the correlation integral involving the dummy variable b is modified from the form evaluated in (19) to become

$$\int e^{-\frac{b^2}{w_{oy}^2} - jK\psi b} e^{-\frac{\left(b + \frac{\lambda Ff}{v_y}\right)^2}{w_{oy}^2}} db \tag{43}$$

$$= e^{-\frac{1}{2}\left(\frac{\lambda Ff}{v_y w_{oy}}\right)^2} \int e^{-\frac{(b + \lambda Ff/2v_y)^2}{2(w_{oy}/2)^2}} e^{-j2\pi \frac{\psi}{\lambda} b} db$$

where the right-hand side is obtained by completing the square in the exponent. The integral on the right-hand side of (43) is a Fourier

---

[†]The result is the same if ψ is considered to be the difference between a small error in each of the two beams.

transform of a Gaussian exponential function of the form

$$T\left[e^{-\frac{(x+m)^2}{2\sigma^2}}\right] = \sqrt{2\pi}\,\sigma\, e^{-\frac{(2\pi f_x)^2(\sigma^2)}{2} + j2\pi f_x m} \tag{44}$$

Thus, the right-hand side of (43) becomes

$$\sqrt{\frac{\pi}{2}}\, w_{oy}\, e^{-\frac{(\lambda F f)^2}{2v_y^2 w_{oy}^2}}\, e^{-\frac{\pi^2\psi^2 w_{oy}^2}{2\lambda^2}} \tag{45}$$

where the imaginary part of the exponent has been dropped since it will not appear in the squared magnitude of the integral.

Expression (45) agrees with the result of Equation (19) for the case where $w'_{oy} = w''_{oy}$, except for the exponential term involving ψ. Since this term is not a function of f, it may be squared and taken outside the convolutions in (3-66). The result is that the entire power spectrum is reduced by the constant value

$$e^{-\frac{\pi^2\psi^2 w_{oy}^2}{\lambda^2}} \tag{46}$$

Hence $S_i(f_d;\bar{v})$ is reduced by this factor and so is the SNR.

Expression (46) indicates that the sensitivity to vertical misalignment increases as w_{oy} increases. This is as it should be since

the measurement volume dimension Y simultaneously decreases and complete beam intersection becomes more difficult to obtain without alignment error.

An Example Application: High-Velocity, Two-Dimensional Flow

In this section one type of laser flowmeter application is considered in more detail to illustrate the use of the equations which have been derived. The application is that of measuring two-dimensional† high-speed flow in a wind tunnel. Thus only the x and y components are nonzero and the length of the measurement volume in the z direction is not of great concern. The scattering angle must be kept small to provide better SNR and low Doppler sensitivity.

Optimization with Respect to w'_{ox} and w''_{ox}

Under the conditions described above, an optimum relation between w'_{ox} and w''_{ox} is to be determined. The quantity γ given in Equation (42) simplifies considerably since $\cos^2(\theta/2) \approx 1$ and $v_z = 0$. Thus

$$\gamma = \sqrt{2\, w_{oy}^2 v_y^2 + [w_{ox}'^2 + w_{ox}''^2] v_x^2} \tag{47}$$

Now for this specific case, the SNR and the bandwidth are symmetrically related to w'_{ox} and w''_{ox}. One wishes to maximize the SNR and minimize the measurement volume width given by

---

†Two-dimensional flow refers to situations in which a model of constant cross section is tested with the model axis normal to the undisturbed free stream velocity. An example is the testing of an airplane wing section.

$$X = \frac{\lambda F}{\pi}\left[\frac{1}{w'_{ox}} + \frac{1}{w''_{ox}}\right] \tag{48}$$

where the $\cos(\theta/2)$ term in the denominator has been neglected.

In order to determine an optimum relation between w'_{ox} and w''_{ox}, it is assumed that some desired value of the measurement volume width has been established and is held constant and that

$$w''_{ox} = \varepsilon w'_{ox} \tag{49}$$

where ε has a positive real value. Then from Equation (48) one has

$$\frac{1}{w'_{ox}} + \frac{1}{w''_{ox}} = \frac{1}{w'_{ox}}\left(1 + \frac{1}{\varepsilon}\right) = C_3 \tag{50}$$

where $C_3 = X\,\pi/\lambda F$. Now γ is to be minimized with respect to ε, subject to (49) and (50). From Equation (47) one sees that γ may be minimized with respect to w'_{ox} and w''_{ox} by minimizing the quantity, $w'^2_{ox} + w''^2_{ox}$, which will be designated by γ'. Using Equations (49) and (50), γ' is reduced to a function of ε alone as

$$\gamma' = \frac{1}{C_3^2}\left(\varepsilon^2 + 1\right)\left(1 + \frac{1}{\varepsilon}\right)^2 \tag{51}$$

When one sets the first derivative of γ' equal to zero to obtain minimum γ', only one positive real solution results, i.e., $\varepsilon = 1$. Thus the choice, $w'_{ox} = w''_{ox} = w_{ox}$ assures minimum γ for fixed measurement

volume width. The same result is obtained by fixing γ' and minimizing the dimension X.

Summary of Optimized Results

For the case of high-velocity two-dimensional flow with $w'_{ox} = w''_{ox}$ and $\cos(\theta/2) \approx 1$ the previous results reduce to the following form:

$$X = \frac{2\lambda F}{\pi w_{ox}} , \quad Y = \frac{2\lambda F}{\pi w_{oy}} , \quad Z = \frac{2\lambda F}{\pi w_{ox} \sin(\theta/2)} \tag{52}$$

$$B = \frac{2\sqrt{w_{oy}^2 v_y^2 + w_{ox}^2 v_x^2}}{\lambda F} \qquad B/ = \frac{\sqrt{w_{oy}^2 \frac{v_y^2}{v_x^2} + w_{ox}^2}}{F \sin(\theta/2)} \tag{53}$$

$$SNR = \frac{M\eta\lambda^2 E[\sigma_p^2] P_i}{4\pi h f_o |\sin\theta|} \quad \frac{w_{oy}}{\sqrt{w_{oy}^2 v_y^2 + w_{ox}^2 v_x^2}} \tag{54}$$

The minimum angle θ_{min} for which these results are valid is very pertinent for the low-angle case. From Equations (2-86) and (2-87) one obtains

$$\sin\theta_{min} = \frac{16}{\pi F} \frac{w_{oy}^2}{w_{ox}}, \quad w_{oy} \geq w_{ox} \tag{55}$$

$$= \frac{16\, w_{ox}}{\pi F}, \quad w_{ox} \geq w_{oy}$$

These results will now be applied to obtain further insight concerning their meaning.

The Relation of w_{ox} and w_{oy} to the Velocity Direction

In this section, the effects of velocity direction in the xy plane and variations of w_{ox} and w_{oy} are considered. The results show the value of allowing the input distributions to be elliptical Gaussian beams rather than being restricted to the circular TEM_{oo} Gaussian distribution. Three cases will be considered: $w_{ox} = w_{oy}$, which is the TEM_{oo} case; $w_{ox} > w_{oy}$, the horizontal distributions; and $w_{ox} < w_{oy}$, the vertical distributions.

The TEM_{oo} Case. In the first case, $w_{ox} = w_{oy} = w_o$. Thus all three of the measurement volume dimensions vary inversely with the input beam radius w_o, and the total volume is inversely proportional to w_o^3. The SNR is not affected by changes of w_o, provided the total incident power is unchanged. If, however, w_o were reduced by a factor ξ with a Gaussian attenuation filter, the SNR would decrease by ξ^2 due to loss of scattering beam power. The bandwidth and fractional bandwidth are directly proportional to w_o.

If the velocity vector $\bar{v}$ is considered as a function of direction by assuming

$$\bar{v} = v \cos\psi_v \, \bar{u}_x + v \sin\psi_v \, \bar{u}_y \tag{56}$$

then one observes that the bandwidth B, in (53), is not a function of ψ_v since $\sin^2\psi_v + \cos^2\psi_v = 1$. The fractional bandwidth, however, is given by

$$B/ = \frac{w_o}{F \sin(\theta/2)} \sqrt{1 + \tan^2(\psi_v)} \qquad (57)$$

Thus if one attempts to measure a small v_x component in the presence of a large v_y component, $\tan^2(\psi_v)$ will be very large and the signal will cease to be a useful bandpass function.

Even if B/ is sufficiently small in a given instance, the SNR will be determined by the vector velocity magnitude. This means that a system with SNR just sufficient to measure a small velocity $\bar{v} = v_x \bar{u}_x$ will be inadequate for measuring the same v_x component in the presence of a large v_y component.

The minimum scattering angle for which the results are valid in the TEM_{oo} case is given approximately by

$$2 \sin(\theta_{min}/2) \approx \sin\theta_{min} = \frac{16 w_o}{\pi F} \qquad (58)$$

This corresponds to a fractional bandwidth B/ given by (57) as

$$B/ = \frac{\pi}{8} \sqrt{1 + \tan^2(\psi_v)} \qquad (59)$$

It would be very difficult to construct a useful electronic detection subsystem with B/ as large as is indicated by (59), so it is safe to say the minimum angle criterion will not be violated.

$w_{ox} > w_{oy}$. Inspection of the results given by (52) through (55) indicates that an advantage can be obtained, when v_x is much less than v_y, by reducing w_{oy} to a value less than w_{ox}. This creates a

horizontal input distribution which results in a vertical distribution in the measurement region. The improvement occurs because the fractional bandwidth is reduced without increasing the measurement volume width or length. Thus, improvement in B/ is accompanied only by a linear increase in the total measurement volume, as opposed to the cubic increase with the TEM_{oo} case.

So long as $w_{oy}^2 v_y^2$ remains much greater than $w_{ox}^2 v_x^2$, the SNR is little affected by decreasing w_{oy} if the incident scattering beam power remains unchanged. Even if a Gaussian attenuation filter were used to reduce w_{oy} by a factor ξ, the SNR would only decrease linearly, instead of by the square of ξ as was the case with the TEM_{oo} case. If v_y is not much greater than v_x, it is not advantageous to reduce w_{oy} to a value less than w_{ox}.

The minimum θ criterion is not likely to be violated for the case where v_y is much larger than v_x. To see this, one expresses the fractional bandwidth as

$$B/ = \frac{w_{ox}\sqrt{\left[\frac{w_{oy}}{w_{ox}}\right]^2\left[\frac{v_y}{v_x}\right]^2 + 1}}{F \sin(\theta/2)} \qquad (60)$$

Assuming $w_{oy}^2 v_y^2$ is greater than $w_{ox}^2 v_x^2$, the fractional bandwidth obtained with θ_{min} determined by

$$2 \sin(\theta_{min}/2) = \frac{16\, w_{ox}}{\pi F} \qquad (61)$$

is

$$B/ = \frac{\pi}{8}\sqrt{\left[\frac{w_{oy}}{w_{ox}}\right]^2\left[\frac{v_y}{v_x}\right]^2 + 1} \qquad (62)$$

As with the TEM_{oo} case, this value is too large to be practical, so θ will have to be larger than θ_{min}.

$\underline{w_{ox} < w_{oy}}$. For cases where the component being measured is the principal component, i.e., when v_x is much larger than v_y, significant advantages are obtained by choosing w_{ox} less than w_{oy}. This creates a vertical input distribution which results in a horizontal distribution in the scattering region. One improvement which occurs is that the fractional bandwidth may be reduced without increasing the measurement volume height. Thus the total measurement volume increases only as the square of the inverse bandwidth reduction. This is an improvement over the TEM_{oo} case in which the total volume increased as the cube of the inverse of the bandwidth reduction.

In the TEM_{oo} case, reducing the input radius w_o to decrease bandwidth resulted in no change of the SNR. For the case of large v_x, however, the SNR is inversely proportional to w_{ox}, and thus *increases* as w_{ox} is made smaller to reduce the fractional bandwidth. Even if w_{ox} is decreased by a factor ξ with a Gaussian attenuation filter, there is no decrease in SNR, since the loss of scattering power in the numerator is cancelled by the same decreasing factor in the denominator.

Unfortunately, it is quite possible to violate the minimum scattering angle criterion, which is required for the validity of the

results, when v_x is much larger than v_y. To see this one may consider the case when $v_y = 0$. Then

$$B/ = \frac{w_{ox}}{F \sin(\theta/2)} \tag{63}$$

The minimum angle θ_{min} is given by

$$\sin(\theta_{min}/2) \approx \frac{8}{\pi F} \frac{w_{oy}^2}{w_{ox}} \tag{64}$$

Thus at θ_{min}, the fractional bandwidth is

$$B/ = \frac{\pi}{8} \frac{w_{ox}^2}{w_{oy}^2} \tag{65}$$

which may be quite acceptable if $w_{ox} < w_{oy}$. One cannot then continue to decrease the bandwidth and increase the SNR by decreasing w_{ox} without eventually violating the minimum θ criterion.

An Important Implication for Measurement of Two-Dimensional Flow

It has been shown that, for measurement of a small v_x velocity component in the presence of a large v_y component, it is most effective to use identical elliptical Gaussian input plane distributions with w_{oy} less than w_{ox}. Similarly for velocity fields in which v_x is the principal component, one should choose w_{ox} less than w_{oy}. In each of these instances, better trade-off relations between the measurement volume dimensions, the bandwidth, and the SNR have been obtained than is possible if the input distributions are restricted to be circularly

symmetric as is the case with an unmodified TEM_{oo} Gaussian beam.

The implication is that the optimum choices for the input-plane distributions are identical elliptical Gaussian distributions, *rotated about the z' and z" axes so that their smallest beam radius parameters are essentially parallel to the principal direction of flow.* In order to verify this statement and to establish optimum ratios of w_{ox} to w_{oy} one would have to evaluate the signal power spectrum expression for nonseparable input-plane distributions. This task has not yet been undertaken.

Discussion and Summary

In this chapter, the general theoretical results of Chapters II and III have been applied for the optimum case of elliptical Gaussian input-plane distributions, whose propagating form and methods of generation were first discussed. Algebraic expressions for the measurement volume dimensions, the signal bandwidth, the fractional bandwidth, the minimum scattering angle, and the SNR were obtained for a perfectly aligned system. It was shown that the input distribution heights in the y direction should be equal if one is to obtain the best trade-off between SNR and the measurement volume height.

It was shown in this chapter that a y-dependent linear phase error, or angular misalignment, results in an exponential decrease in SNR. The decrease in SNR with misalignment angle is a function of the height of the input distributions.

Further interpretation and simplification of the algebraic results of this chapter have been obtained for the specific practical

application of measuring high-velocity two-dimensional flow. For this case it was shown that the best trade-off between SNR and measurement volume width is obtained by having the input distribution widths be equal. As a result of having studied the effects of choosing the input beam heights less than the input beam widths when v_y greatly exceeds v_x and vice versa, it has been concluded that the minor axis of the elliptical Gaussian input-plane distributions should be approximately parallel to the principal direction of flow.

CHAPTER V

A SIMPLIFIED OPTICAL SYSTEM FOR LOW-ANGLE HETERODYNE FLOWMETERS

The preceding chapters have been devoted to the analysis of a theoretical model of a laser flowmeter optical system. This chapter concerns an improved practical implementation which is useful for measurements in which the distances involved and the scattering angle are both relatively small. The optical system described is useful, for example, for measurements of two-dimensional flow in a wind-tunnel.

In what follows, the simplified optical system is presented first from a ray-optics point of view and then discussed analytically to show its relationship to the generalized theoretical optical model treated in Chapter II. The chapter is concluded with a discussion of the practical advantages and disadvantages of the system.

Description of Simplified System

The easiest way to insure that the *equivalent* reference beam for a heterodyne flowmeter is known and controllable is to cause it to be identical with the *actual* reference beam. This may be accomplished by designing a system like the Goldstein system, with the scattering and reference beams physically intersecting in the measurement region, which has no apertures beyond the scattering region that block any appreciable portion of the reference beam. In other words, all control of the

detected signal radiation characteristics and all system alignment should be done on the input side of the system by controlling the incident scattering and reference beams.

Figure 7 illustrates, by the use of two ray-optics concepts, a method of insuring proper alignment of the system. The first, as illustrated in (a) is that *two parallel, collimated beams incident on a spherical lens will focus to a point and cross in the back focal plane of the lens.* This is exactly the condition required for perfect system alignment if one beam is a relatively weak reference beam and the other is a strong scattering beam coherent with the first.

In the (b) part of Figure 7 a simple and efficient method for obtaining the two required beams is shown. *An optically flat piece of glass with accurately parallel sides generates a second beam of low intensity by internal reflection which is accurately parallel to the transmitted portion of the original beam.* Coatings on the surface which reduce power loss are also shown. The intensity and separation of the reference beam can be controlled by the coatings, the angle of rotation and the thickness of the optical flat. An additional flexibility lies in the possibility of using multiple internal reflections as indicated by the dashed lines. *This method of generating two parallel beams from one automatically produces beams with equal transverse dimensions, i.e., the optimum case.*

A complete optical system using the concepts just described is shown schematically in Figure 8. The input window to the flow test region must be optically flat so that one or both beams will not be

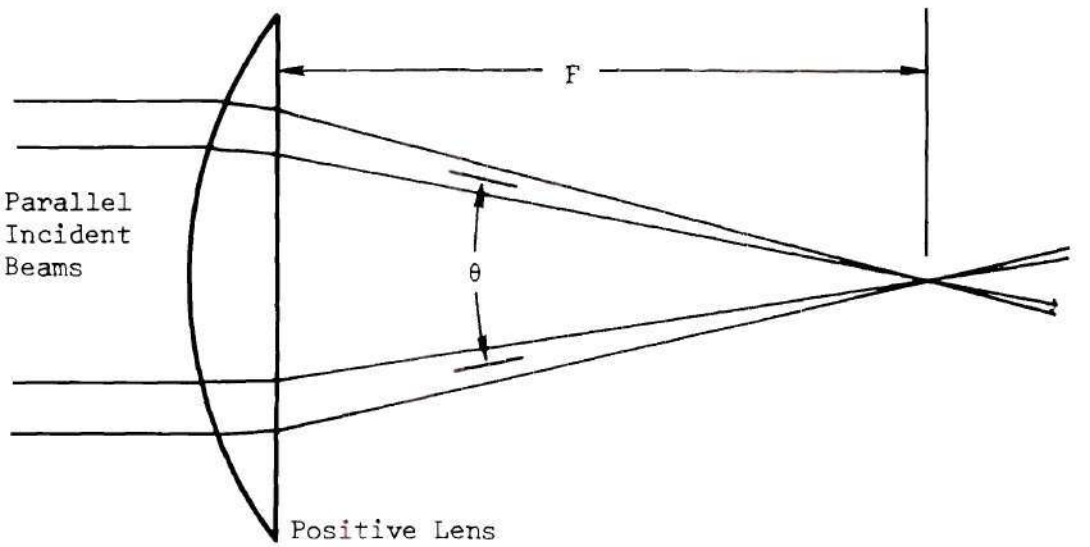

(a) Heterodyne Alignment Achieved by Single Lens

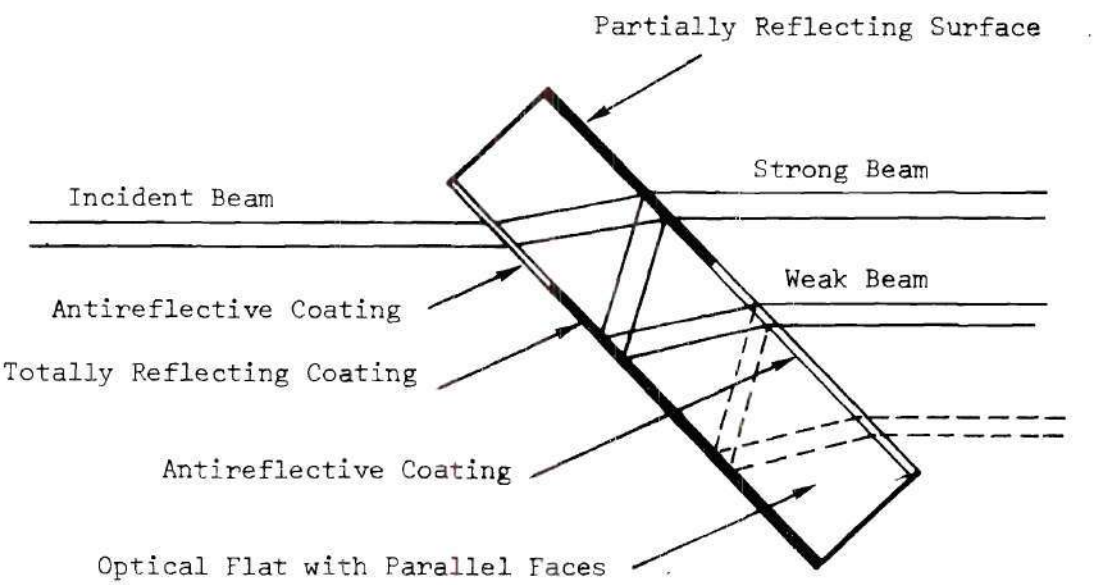

(b) Element Which Produces Parallel Beams with Correct Intensity Ratio

Figure 7. Concepts for Simplified Optical System

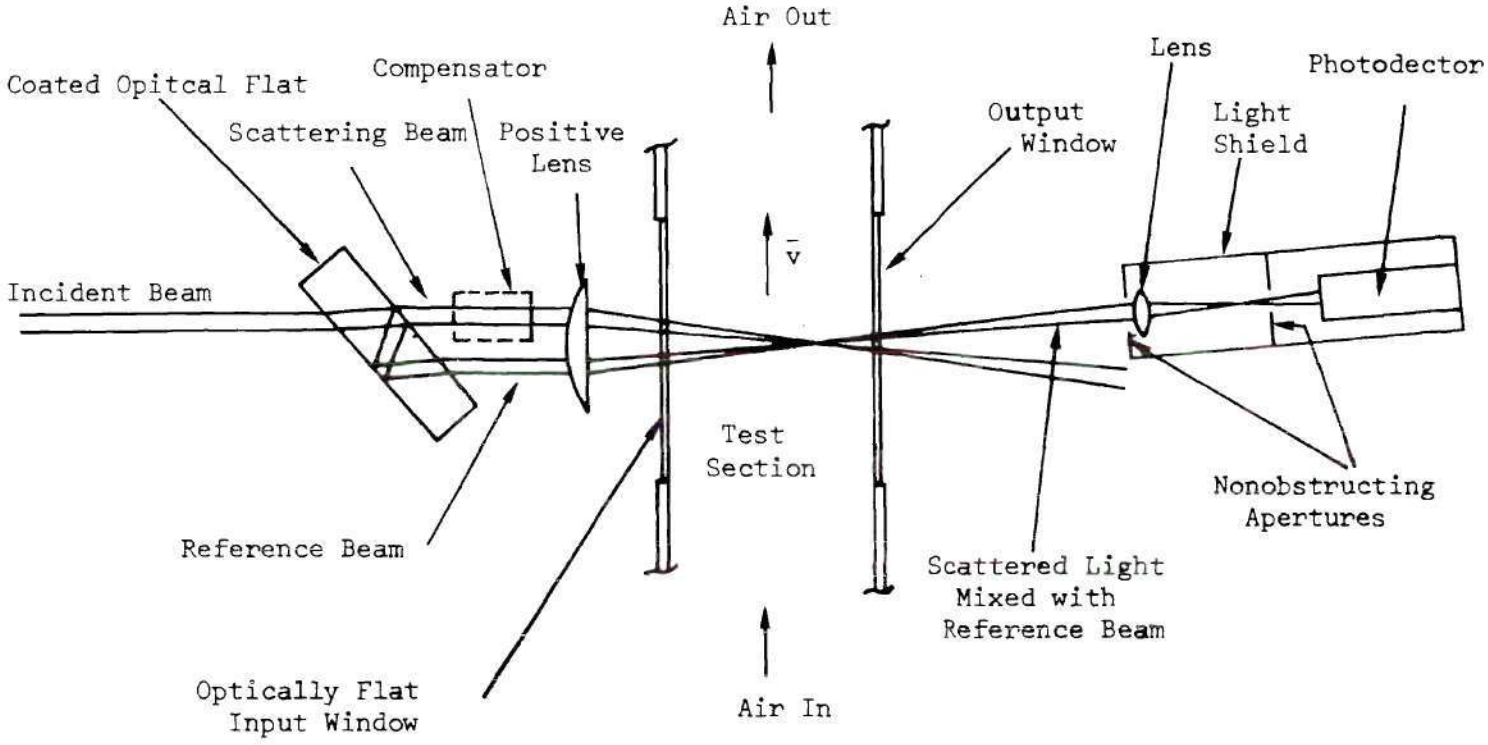

Figure 8. A Simplified Low-Angle Heterodyne Flowmeter Optical System

deflected by local prismatic refraction. The window on the far side of the test section, however, need only be transparent since one recalls from Chapter II that phase filters will not affect the signal current once the radiation is mixed. A path length compensator which is not always necessary is shown in the scattering beam. This element is discussed later.

The specific set of collection optics has arbitrarily been shown as one which will prevent most of the background light produced by the environment, the optical surfaces, and scatterers not in the measurement volume from reaching the photodetector. The only requirements, however, are that some shielding is provided for the photodetector with apertures which do *not* obstruct appreciable reference beam power. These apertures can be appreciably larger than the reference beam diameter so alignment of the collection optics need not be critical.

Equivalence of System with Generalized System

The optical system of Figure 8 is essentially equivalent to the generalized flowmeter system illustrated in Figure 4 of Chapter II. This equivalence is now demonstrated analytically for one of the incident beams as illustrated in Figure 9.

It is assumed that at the single focussing lens the complex amplitude $\bar{u}(x,y)$ of the incident beam in the plane of the lens is

$$\bar{u}(x,y) - u_{\ell}(x-x_{o},y) \tag{1}$$

where $u_{\ell}(x,y)$ is an even function and where x_{o} is the distance between

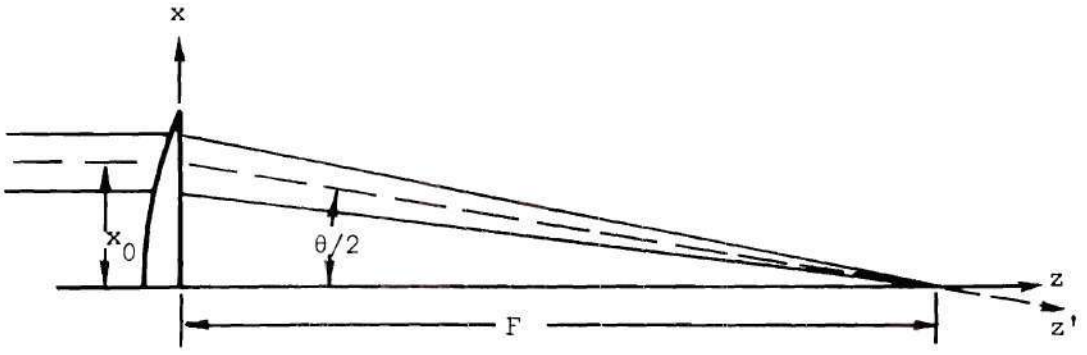

(a) Offset Beam Incident on Lens

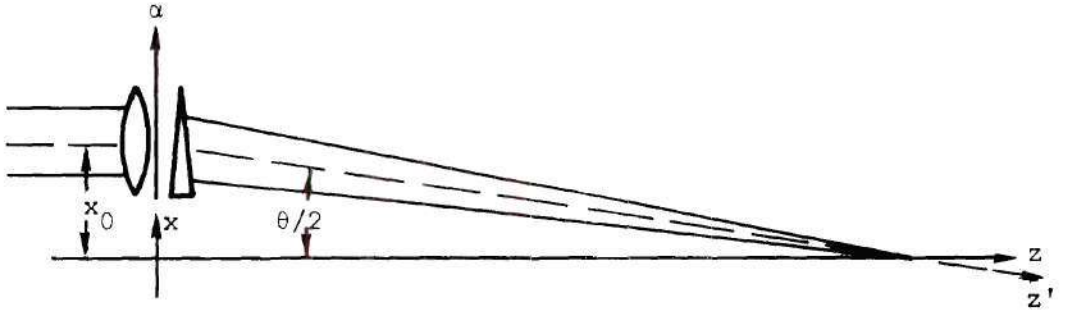

(b) Equivalent Lens and Prism Centered at α = 0

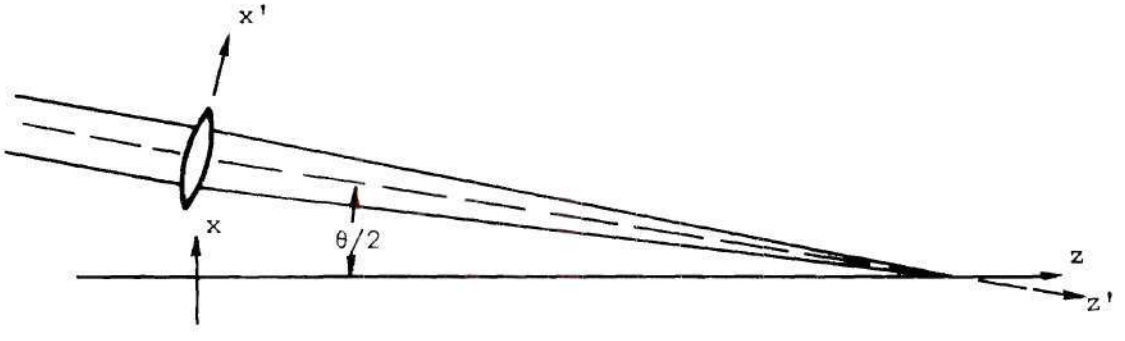

(c) Equivalent Rotation of Incident Beam and Lens with Prism Removed

Figure 9. Equivalence of Single Lens System and Generalized System.

the axis of the incident beam and the axis of the lens. One recalls that the transmission function for an ideal spherical lens is $\exp[-jK(x^2+y^2)/2F]$; just beyond the lens one obtains

$$u^+(x,y) = u_\ell^-(x-x_o,y)e^{-\frac{jK}{2F}(x^2+y^2)} \tag{2}$$

or with the substitution of variables

$$\alpha = x - x_o \tag{4}$$

$$u^+(\alpha+x_o,y) = u_\ell^-(\alpha,y)e^{-\frac{jK}{2F}[(\alpha+x_o)^2 + y^2]} \tag{5}$$

$$= u_\ell^-(\alpha,y)e^{-\frac{K}{2F}[\alpha^2+y^2]}\ e^{-\frac{jKx_o}{F}\alpha}$$

where a phase constant has been dropped in the last expression of (5).

The factors of the last expression of (5) represent an incident distribution, a spherical lens centered at $\alpha = 0$, $y = 0$, and a prism with deflection angle $\theta/2$ given by[†]

$$\frac{\theta}{2} \approx \sin\frac{\theta}{2} \approx \tan\frac{\theta}{2} = \frac{x_o}{F} \tag{6}$$

Since the effect of a small-angle prism is just a rotation of the axis of propagation, the prism is effectively removed by assuming that the

---

[†]Small angles are implied by the use of scalar diffraction theory to describe the effect of a lens.

incident beam and the lens at $\alpha = 0$ are rotated into the z' axis, i.e., $u_\ell^-(\alpha,y)$ is replaced by $u_\ell^-(x',y)$. The result is that considerations for the input-plane distributions of the generalized flowmeter now apply to input distributions translated a distance of plus or minus x_o in the xy plane one focal length in front of the single focussing lens. Thus the single input distribution $u_o(x,y)$ is

$$u_o(x,y) = u_{io}(x-x_o,y) + u_{ro}(x+x_o,y) \tag{7}$$

where $u_{io}(x,y)$ and $u_{ro}(x,y)$ should be of the form determined for $u_{io}(x',y)$ and $u_{ro}(x'',y)$ in Chapter II. If the conclusions of Chapter IV concerning the relationship between $u_{io}(x',y)$ and $u_{ro}(x'',y)$ apply in general, it is desirable that u_{io} and u_{ro} be constant-phase with

$$u_{ro}(x,y) = \sqrt{P_r/P_i}\, u_{io}(x,y) \tag{8}$$

i.e., that the input plane distributions differ in form only by a constant factor.

Path Length Difference Effects

Unfortunately, it is not possible for the two input distributions, produced by an element such as the optical flat shown in 7(b), to both be constant-phase and equal unless path-length compensation is used.† If, for example, $u_i(x,y)$ were a constant phase function in the

†A path-length compensator could be just another optical flat, coated to reduce reflection losses.

input plane, then $u_r(x,y)$ would be given by

$$u_r(x,y) = \sqrt{P_r/P_i}\, h(x,y,L) \ast u_i(x,y) \tag{8}$$

where L is the extra distance the reference beam propagates† due to internal reflections in the optical flat. Depending on the transverse dimensions of $u_i(x,y)$, the extra propagation distance may or may not have negligible consequences.

The only effect of the path length difference L is to produce a quadratic phase factor on the reference beam distribution in the back focal plain of the lens, i.e., using the Fraunhoffer approximation one obtains

$$u_r(x'',y,z'') = e^{jKz''} U_{ro}\left(\frac{x''}{\lambda F}, \frac{y}{\lambda F}\right) = \tag{9}$$

$$\sqrt{P_r/P_i}\, U_{io}\left(\frac{x''}{\lambda F}, \frac{y}{\lambda F}\right) H\left(\frac{x''}{\lambda F}, \frac{y}{\lambda F}, L\right) e^{jKz''}$$

$$= \sqrt{P_r/P_i}\, e^{jKz''} U_{io}\left(\frac{x''}{\lambda F}, \frac{y}{\lambda F}\right) e^{-\pi\lambda L\left[\left(\frac{x''}{\lambda F}\right)^2 + \left(\frac{y}{\lambda F}\right)^2\right]} \tag{10}$$

From Equation (10) it may be seen that the tolerable path length difference, for which the quadratic exponential is negligible, increases as the transverse dimensions of $U_{io}(f_x,f_y)$ decrease. In other words,

---

†This path length difference is assumed to be much less than the temporal coherence length of the laser source.

the tolerable value of L decreases as the dimensions of $u_{io}(x,y)$ decrease.

In many flowmeter applications no path length compensation will be required. To see this without additinal analysis, one need only consider the problem heuristically. If the incident beam *appears* "collimated," it means that it is of sufficiently large transverse extent that propagation over a short distance does not appreciably alter it by diffraction; thus in (6) the effect of the convolution with h(x,y,L) is negligible. If, on the other hand, the input distribution is so small that it *appears* "focussed," this means that propagation over short distances does appreciably change the form of the complex amplitude, and path length compensation is required. The latter will be the case in applications where very small bandwidths are to be obtained at the expense of very large measurement volumes by "focussing" the incident beam in the input plane to obtain "collimated" beams in the intersection region.

Advantages and Disadvantages

When the distance from the optics to the measurement region is small enough that it is practical to use a single focussing lens, the system just described has significant advantages over other systems reported in the literature. As already mentioned, the system automatically insures that the transverse dimensions of the reference and scattering beams will be identical as is desirable. In addition, a minimum number of optical elements is required, no neutral density

filters are necessary, and all the incident power is used efficiently.

The simplified system is especially convenient for low scattering angle applications since the two incident beams can be made as close together as desired simply by reducing the thickness of the optical flat or by rotating it more towards normal to the incident beam. Very small scattering angles are difficult to achieve in most of the other systems which have been reported since the mechanical holders for the various optical elements occupy space and can get in the way of one or more of the beams.

The most outstanding advantage of the simplified optical system is that if the optical flat and focussing lens are of high quality, virtually no heterodyne alignment is required. The optical flat is a rigid body; if it moves the alignment is unaffected. If the lens moves transversely, the position of the measurement region moves, but heterodyne alignment is maintained.

Since the apertures in the photodetector shield are not used for heterodyne alignment, they may be made large enough so that the positions of the elements on the far side of the test section are not critical. This greatly reduces the requirements on the rigidity of the support structure which must extend around to the other side of the test section to hold the detection optics.

The disadvantages of the simplified system are few. The system is restricted to be short range, due to the practical limitations on size for high quality lenses and optical flats. At the limits of practical sizes for good lenses and optical flats, these elements become

relatively expensive, but the cost should be made up in reduced man-hours of effort expended in adjusting micrometers to achieve and maintain system operation.

CHAPTER VI

A NEW CONCEPT FOR FLOW MEASUREMENT-- THE INTERFERENCE FLOWMETER

When two coherent light beams intersect in space at a small angle, an interference pattern may be observed on an opaque screen inserted in the region of beam intersection. The mathematical expression for the intensity incident on the screen includes cross-product terms of the same mathematical form as the expression which has been obtained in Chapter II for the single-scatterer response function of a heterodyne flowmeter. This similarity of mathematical expression has led to the concept of the "interference flowmeter" which is presented in this chapter.

The concept of the interference flowmeter is as follows: if two coherent plane waves intersect at a small angle, the intensity pattern which results is sinusoidally varying in space in one direction. If a small scatterer is allowed to translate through the region at a constant velocity, *the light scattered in all directions* will be sinusoidally modulated in intensity and the frequency of modulation will be proportional to one component of the scatterer velocity.

There is an alternate point of view for the concept just stated: the electromagnetic field scattered from one incident plane wave in a particular direction is Doppler shifted. The field scattered from the other incident plane wave in the same scattering direction is Doppler

shifted by a different amount due to the difference in direction of the incident field. The two scattered fields are perfectly aligned for square-law detection of one by the other at a photodetector, so *the difference in Doppler frequency shifts is detected.* This difference frequency can be shown to depend only on the directions of the incident plane waves and not on the particular direction of scattering.

The two heuristic points of view of the concept just described both give the same result for the frequency of the detected signal; however, it seems more instructive in the context of quasi-static fields to use the expression "interference flowmeter" rather than "differential Doppler heterodyne flowmeter."[†] Furthermore it is well to divorce this system from the concept of optical heterodyne detection since the signal-to-noise ratio considerations are quite different from those of optical heterodyne communications theory. In the remainder of this chapter an introductory theory for the characteristics of an interference flowmeter is developed analytically. At the end of the chapter some of the unique potential applications of the system are presented.

Principles of an Interference Flowmeter

Figure 10 illustrates the discussion which follows. A point scatterer is located at position $\bar{p}$ in the vicinity of the intersection

---

[†]At the time of final writing of this dissertation a recent restricted government report[31] was discovered which describes an experimental system much like that developed in this chapter. The authors refer to the system as a "type II symmetric heterodyne system."

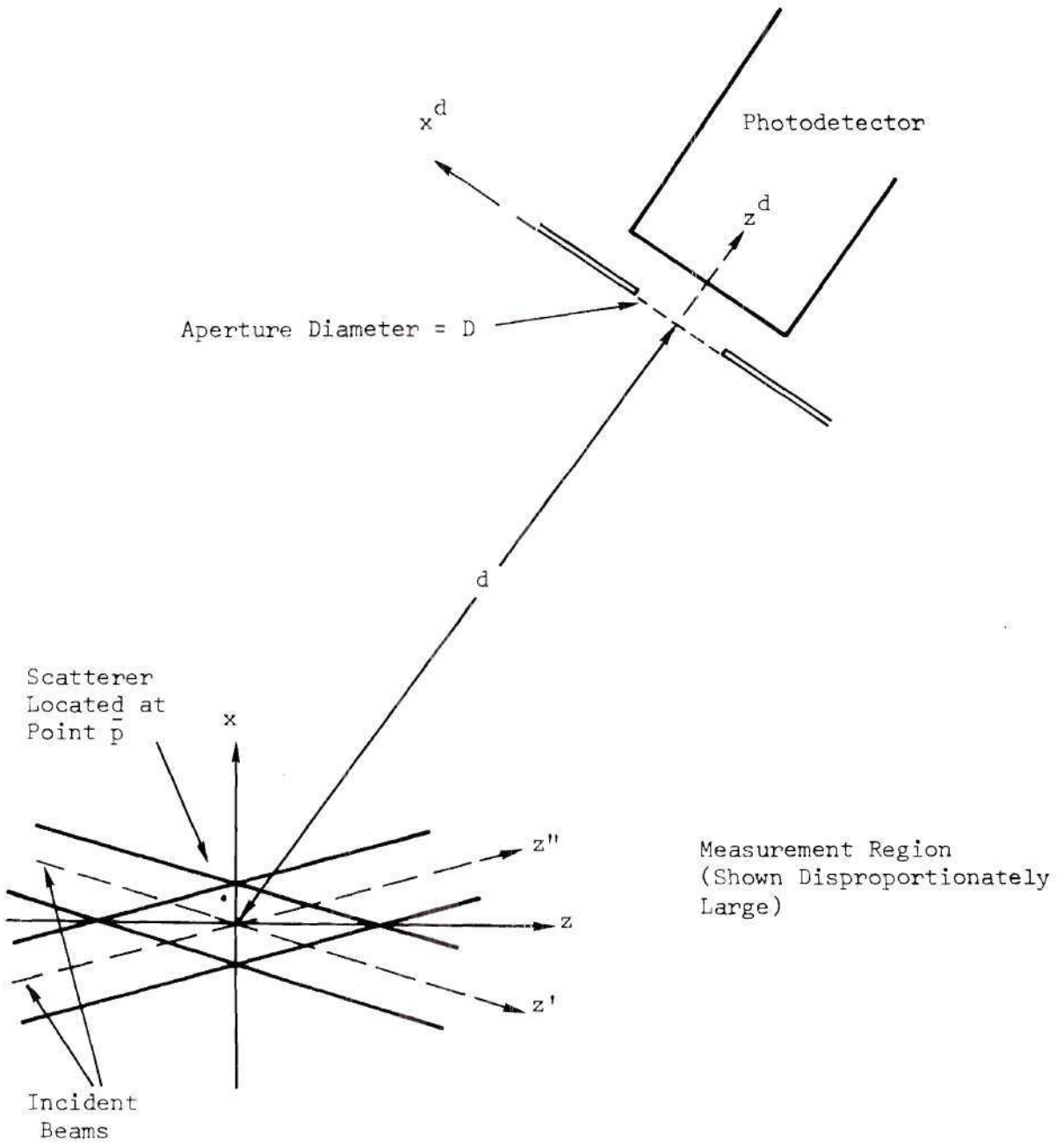

Figure 10. An Interference Flowmeter System

of two paraxial, monochromatic beams which will be designated by $u_i(x',y,z')$ and $u_r(x'',y,z'')$ as was done in the similar case of the preceding chapters. In this chapter, however, the assumption that u_i is much greater in total power than u_r is *not* made. A photodetector is placed behind a circular aperture of diameter D, located at distance d from the origin, where d is much greater than either D or the dimensions of the beam intersection region.

If the intersection angle θ is small, it is meaningful to consider the total intensity, $I_t(\bar{p})$, incident along the z axis on a scattering point $\bar{p}$ located in the vicinity of the beam intersection region.† At the photodetection aperture, the intensity I_s of the scattered radiation is given approximately by a constant value of

$$I_s = I_t(\bar{p})\ \sigma_p^2\ \frac{1}{4\pi d^2} \tag{1}$$

where σ_p^2 is the scattering cross section. The total power collected through the aperture of diameter D is $\frac{\pi D^2}{4} I_s$, so the photocurrent, i, produced by the scatterer is

$$i = \frac{N\sigma_p^2 D^2}{16\ d^2} I_t(\bar{p}) \tag{2}$$

where as before

---

†If θ is not small, Equations (1) through (4) still give useful results but a vector electromagnetic theory analysis would be required for preciseness.

$$N = \frac{\eta e}{h f_o} \tag{3}$$

The intensity incident in the xy plane located at $z = z_p$, i.e. in the plane of the scatterer, is

$$I_t(x,y,z_p) = \left|[u_i(x',y,z') + u_r(x'',y,z'')]_{z=z_p}\right|^2 \tag{4}$$

Thus with $x = x_p$ and $y = y_p$, Equation (4) may be substituted in (2) to obtain the photocurrent as

$$i = \frac{N\sigma_p^2 D^2}{16\, d^2}\left[|u_i(\bar{p})|^2 + |u_r(\bar{p})|^2 + u_i(\bar{p})u_r^*(\bar{p}) + u_i^*(\bar{p})u_r(\bar{p})\right] \tag{5}$$

One immediately recognizes that the cross product terms, $u_i(\bar{p})u_r^*(\bar{p})$ and its complex conjugate in (5), are of exactly the same form as those obtained in the analysis of the generalized heterodyne flowmeter as the signal terms. The results of Chapter II are thus directly applicable: the measurement region is the region of intersection of the beams; the input geometry of the optics and the optimum input-plane distributions are the same as for the heterodyne flowmeter; the form of the single-scatterer *signal current* is the same except for constant multipliers; and the expected value of the signal current is near zero because of its oscillatory nature.

The thing which is strikingly different between (5) and the results of Chapter II is the presence of the terms $|u_i(\bar{p})|^2$ and $|u_r(\bar{p})|^2$ instead of the constant DC current proportional to the total

reference beam power. Assuming that the fields $u_i(x',y,z')$ and $u_r(x'',y,z'')$ are of an optimum form, as determined in Chapter II, then the square magnitude terms will give rise to low-pass time functions when particle motion is considered. The power spectrum of such terms will be negligible in the frequency range of the signal, but a non-negligible DC current will result which will be the principal cause of photon shot noise.

Figure 11 illustrates typical terms of i as a function of x_p for two different z planes. Graphs with the same relative shapes describe i as a function of time if the velocity of the scatterer is constant in the x direction. The (a) and (b) parts of the figure depict the photo current produced by scatterers in the z = 0 plane and a z plane beyond the beam intersection region, respectively. *One observes that scatterers outside the measurement region produce no useful signal but do contribute to the total DC current and thus the photon shot noise.* As will be discussed later, the light scattered outside the beam intersection region should not be allowed to reach the photodetector.

The low-pass terms illustrated in Figure 11(a) which are associated with signal terms cannot be removed. Given a fixed total power in these low-pass terms one wishes to obtain the maximum possible amplitude for the signal terms. It can be demonstrated for the case of uniform plane waves incident that maximum signal current for fixed detected DC current would occur if the magnitudes of the two incident beams were equal, i.e. one divides up the incident beam power equally

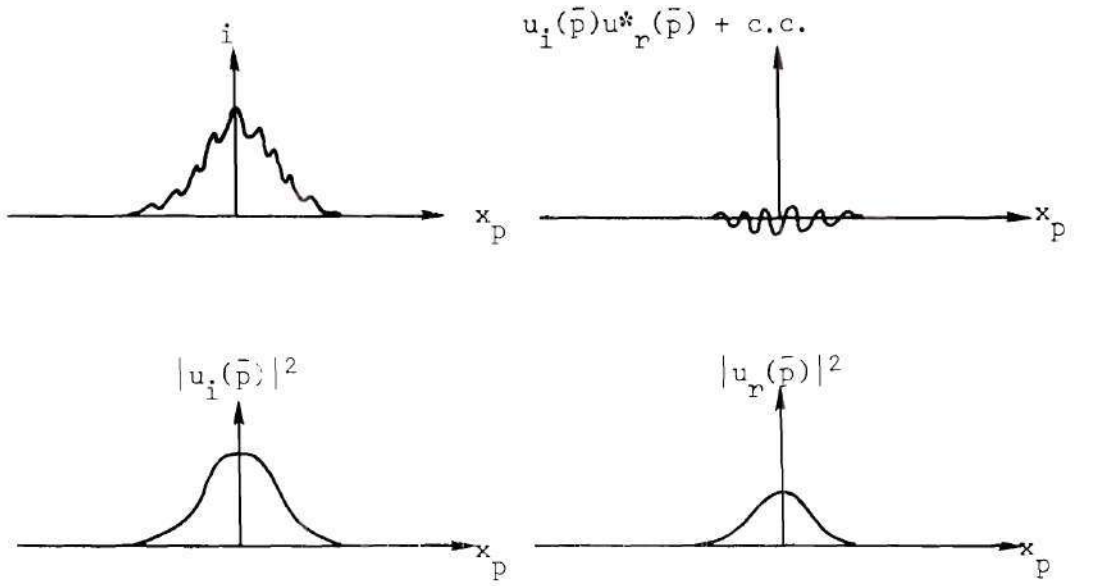

(a) Scatterer in z = 0 Plane

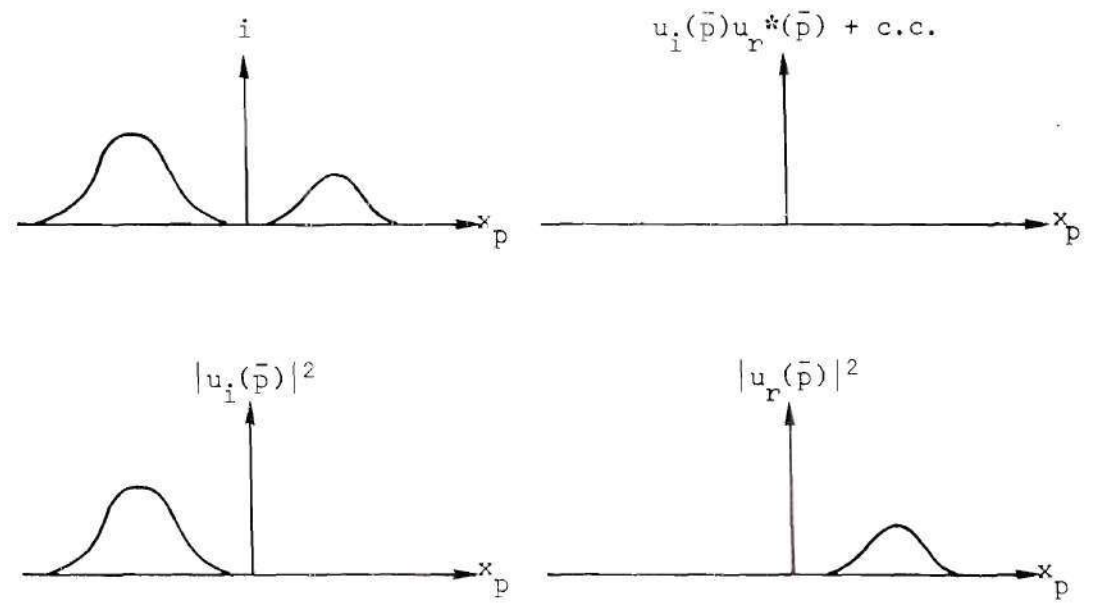

(b) Scatterer in z Plane Beyond Intersection Volume

Figure 11. Photocurrent Components Produced by a Single Scatterer.

to obtain maximum "fringe visibility"[†] in the interference pattern. This criterion implies that maximum signal-to-noise ratio in the output signal is obtained when the two electromagnetic fields reaching the photodetector surface by way of scattering are of equal magnitude, a condition quite unlike the optimum SNR criterion for optical heterodyne communications in which one magnitude greatly exceeds the other.

Response from a Collection of Scatterers

Unlike the heterodyne flowmeter which employs a strong reference beam, the response of an interference flowmeter to a *collection* of scatterers is generally nonlinear since the square magnitude of the total scattered field is detected. The response for a collection of scatterers consists of a single summation of expressions like that of (5), which is the linear part, plus a double summation of surface integrals, which is the nonlinear part. A complete analysis of the general nonlinear response, including statistical signal properties, would make a good subject for research in itself. Such an analysis has not yet been undertaken, but it will be demonstrated heuristically here that in many useful cases where the scatterer number density is sufficiently low the effects of the nonlinear response will be negligible. On the other hand, one intuitively suspects that at high scatterer number densities the nonlinear terms will dominate.

[†]A commonly used measure of contrast in interference patterns.

Linearization of Response

The total power collected by the aperture with diameter D in Figure 10 is unchanged if a lossless spherical lens of focal length d/2 is placed in the aperture. The scatterers are then imaged in the plane at distance d behind the lens but are not resolved. Thus, if no other scatterers were present, each scatterer would be imaged as an Airy disc† of diameter 2.44 $\lambda d/D$ which contained 84 per cent of the collected power for that scatterer. If the lens diameter D is made sufficiently large and the density of scatterers sufficiently small, then the light collected by the lens from each scatterer is imaged to a different nonoverlapping location on the image plane. In this case there can be essentially no effect on the detected current from interference between the images of the separate scatterers, and the photocurrent is given by the summation of expressions like that of Equation (5). If, on the other hand, the Airy discs were so large and the density of scatterers was so great that considerable overlap occurred in the image, then an analysis of the nonlinear response would be required.

As an example, it will be assumed that the beam intersection region has dimensions of 0.1 mm x 0.1 mm x 1 mm. The collecting lens is assumed to have focal length, F = 20 cm, and diameter, D = 5 cm,

---

†The intensity pattern for the image of a point scatterer illuminated by monochromatic light and imaged by a spherical lens with circular aperture is a central circular disk surrounded by concentric rings. The pattern is of the same form as the Fraunhoffer diffraction pattern of a circular aperture. See Goodman[21] and Born and Wolf.[25]

and be located at d = 40 cm. The Airy disc diameter is thus approximately 0.01 mm and the disc area is approximately $10^{-4}(\text{mm})^2$. If the collecting lens were viewing the measurement region from the side, the area of the image of the region would be approximately $0.1(\text{mm})^2$. Allowing an area in the image of $4 \times 10^{-4}(\text{mm})^2$ per scatterer should insure little overlap of the Airy discs in an average random pattern. Thus up to 250 scatterers could be present in the $0.01(\text{mm})^3$ measurement volume without affecting the linearity of the response appreciably. If the measurement volume were smaller, the collecting lens were smaller, or the viewing angle of the collecting lens were different, the permissible number of scatterers in the measurement volume would be reduced.

The heuristic result which has been obtained is that it is quite possible to have many scatterers in the measurement volume simultaneously and still obtain linear response if the collecting lens is of sufficiently large aperture.[†] In such cases the photocurrent may be written directly from (5) as the sum of the low-pass terms plus the sum of the signal terms as

$$i = i_{\ell p} + i_s + i_s^* \tag{6}$$

where

[†]This is a fortunate coincidence since increased collecting lens diameter implies more collected light power.

$$i_{\ell p} = \frac{ND^2}{16d^2} \sum_k \sigma_{pk}^2 [|u_i(\bar{p}_k)|^2 + |u_r(\bar{p}_k)|^2] \tag{7}$$

$$i_s = \frac{ND^2}{16d^2} \sum_k \sigma_{pk}^2 u_i(\bar{p}_k) u_r^*(\bar{p}_k) \tag{8}$$

Spatial Filtering of the Scattered Radiation

Unlike the heterodyne flowmeter, the interference flowmeter has no spatial filtering of the scattered radiation inherent in the detection process. It is emphasized again, therefore, that without special precautions there will be many more scatterers contributing to $i_{\ell p}$ in (7) than to i_s in (8). Although a theoretical imaging lens was previously discussed only as part of a heuristic argument, a physical lens in the same position offers the means by which the unnecessary terms of (7) may be eliminated. If a small aperture the size of the image of the beam intersection volume is accurately placed in the image plane, then only the terms of $i_{\ell p}$ associated with signal-producing scatterers will be detected. This requires that the collecting lens be of sufficient quality and aperture to resolve the dimensions of the measurement volume. It is not necessary, however, for the lens to be "diffraction limited," i.e. the physical lens need not actually produce the theoretical Airy disc for each scatterer, so long as the image of a point scatterer remains appreciably smaller than the aperture in the image plane.

With the lens-aperture filter in place, the signal current given by (8) would not be modified unless the aperture were deliberately made

smaller than the image of the measurement region. On the other hand, the low-pass current given by (7) would be modified by a function $|t(\bar{p})|^2$ which is the projected intensity image of the filter aperture back onto the measurement region boundaries. Thus $i_{\ell p}$ is given by

$$i_{\ell p} = \frac{ND^2}{16d^2} \sum_k \sigma_{pk}^2 [|u_i(\bar{p}_k)|^2 + |u_r(\bar{p}_k)|^2] |t(\bar{p}_k)|^2 \qquad (9)$$

The function $|t(\bar{p})|^2$ is easily expressible only in the (x^d, y^d, z^d) coordinate system; this makes (9) a very difficult expression to evaluate since u_i and u_r are conveniently expressed only in the separate (x',y,z') and (x",y,z") coordinate systems.

A spatial filter consisting, for example, of a lens and an aperture is absolutely necessary if the best possible signal-to-noise ratios are to be obtained using the interference flowmeter. This requirement imposes additional complexity of system alignment but also provides increased system flexibility as discussed at the end of this chapter.

Signal Power Spectrum and Signal-to-Noise Ratio

The Power Spectrum

Neglecting the phase of the scattering constant which later proved inconsequential, the single-scatterer complex signal response of the heterodyne flowmeter was given by

$$i_{sp} = \frac{N\lambda}{2} \sqrt{\sigma_p^2 / \pi}\, u_i(\bar{p}) u_r^*(\bar{p}) \qquad (10)$$

The single-scatterer complex signal response of the interference flowmeter is

$$i_{sp} = \frac{ND^2\sigma_p^2}{16d^2} u_i(\bar{p})\, u_r^*(\bar{p}) \tag{11}$$

The signal power spectrum, $S_i(f)$, may thus be calculated in exactly the same manner as was done in Chapter III for the heterodyne flowmeter system. The result differs only in the multiplicative constants and is given by Equation (3-66) with the constant

$$E[|C_p|^2] = \frac{\lambda^2}{4\pi} E[\sigma_p^2] \tag{12}$$

replaced by

$$\left(\frac{D^2}{16d^2}\right)^2 E[(\sigma_p^2)^2] \tag{13}$$

One observes that the detected signal power depends on the *fourth power* of the ratio D/d.

The Signal-to-Noise Ratio

In the case of the heterodyne flowmeter, it was assumed that the reference beam power would be large enough so that photon shot noise dominated all other receiver noise sources. This assumption cannot be made for the interference flowmeter system. It will be assumed, however, that a low-noise electron multiplier tube is used to insure that either photon noise *or* dark current noise dominates the thermal noise

of the load resistor and all following amplifier noise sources. The small noise produced by the electron multiplier chain is neglected, and background light is assumed to be removed by spatial and spectral filtering.

If the SNR is limited by the photo-multiplier dark current noise, assumed constant with variations of the incident radiation, then a linear increase in laser source power will effect a square increase in SNR: the signal power is proportional to the square of the optical power as can be determined from (3-66) with the modification indicated by (12) and (13). In addition, with constant photodetector-produced noise power, the SNR may be increased as the *fourth power* of the collecting lens diameter as shown by (13). Neither of these two powerful means of increasing the SNR is available in the heterodyne flowmeter system where only a linear increase in SNR accompanies an increase in laser power.

It is now assumed that the laser power, collecting aperture, scattering coefficient, and photodetector noise level are such that photon shot noise predominates over the constant photodetector noise. In this case the SNR becomes difficult to determine because *the noise is no longer independent of the signal*. As an example, one considers the situation in which the scatterer number density is very low so that less than one scatterer is present on the average in the measurement volume. During the presence of a scatterer, photon noise is produced by the low-pass component of the scattered light, but in the absence of a scatterer, the noise level reverts to the constant mean value produced

by the phototube itself. The case where photon shot noise predominates will not be discussed further.

Several conclusions concerning the signal power and SNR of the interference flowmeter can be drawn. A comparison of expressions (12) and (13) reveals that if the scattering cross section is on the order of a square wavelength in size and if the mean-square scattering cross section is on the order of λ^4, then the signal-current power for the interference flowmeter will be much less than that of the heterodyne flowmeter since D^2/d^2 will usually be much less than one. The DC current produced in the interference flowmeter will also be considerably less than that which would be produced by a strong reference beam; the SNR could thus be better for the interference flowmeter than for the heterodyne flowmeter in some applications in spite of the conversion gain associated with heterodyne detection. In cases where the SNR is limited by the sensitivity of the photodetector, it can be improved as the fourth power of the increase in diameter of the collecting aperture. Since the complexity of the nonlinear response for the general case and the lack of independence of the signal and photon shot noise has prevented a direct application of the results of Chapter III to the general interference flowmeter, it is finally concluded that further research should be directed to this area.

Applications of the Interference Flowmeter

Implementation

The interference flowmeter is well-suited for implementation using an optical arrangement similar to that of the simplified

heterodyne flowmeter optics since it will probably be most useful at short ranges due to the dependence of the SNR on the ratio D/d. Figure 12(a) illustrates how a properly coated optical flat with parallel faces can be used to produce two equal, parallel incident beams which are focussed by a single lens. The collection optics would then consist of a shielded photomultiplier tube with a small aperture located in the image plane of a positive collecting lens as shown in 12(b). A spectral filter may be required in some instances when high ambient light is present. The collecting optics may be placed anywhere that is convenient to view the beam intersection region, but if the SNR is low, it would be improved in many cases by detecting forward scattered radiation (excluding the incident beams). Unlike the simplified heterodyne system, critical alignment *is* required for the collection optics since the spatial filter aperture will be quite small in most cases.

Unique Potential

Four possibilities for use of the interference flowmeter have been conceived for situations where the heterodyne flowmeter is impractical. The first and most obvious is for measurements where some opaque body would obstruct the forward scattered radiation which must be detected in the heterodyne system. For example, in a high-speed wind tunnel the scattering angle must be small for the heterodyne system. The model being tested would get in the way of the signal radiation in many cases. Even with a two-dimensional model and a window on the far side of the tunnel, one could not get the beam intersection

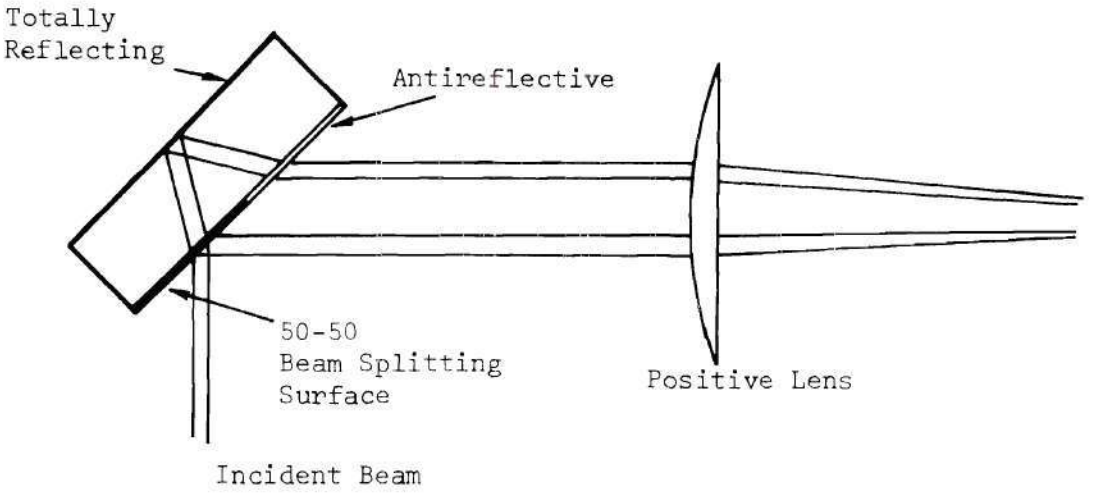

(a) An Efficient Input Geometry

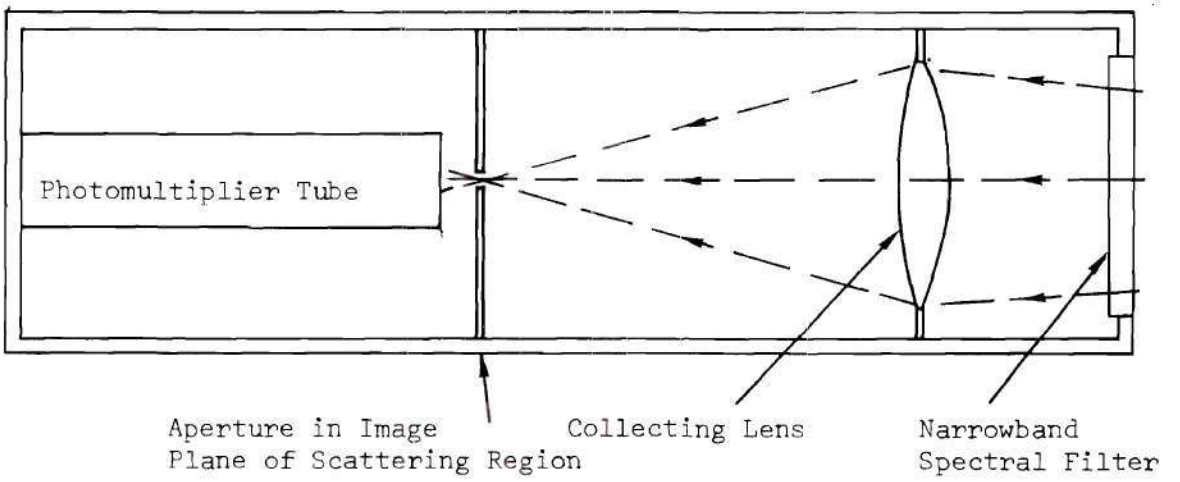

(b) Conceptual Photomultiplier Tube Housing Providing Spectral and Spatial Filtering

Figure 12. Conceptual Elements of an Interference Flowmeter

region exceedingly close to the model as would be required in a boundary layer study. The interference flowmeter solves this problem since the same low angle between the incident beams can be used to produce the same detected frequency while the back scattered light is detected. Furthermore, using the back scattered light allows one to construct the entire optical assembly on a single rigid plate which eliminates the necessity of having a support member around the measurement region to hold the collection optics.

Because of the backscatter detection possibility, the interference flowmeter will be able to measure the *transverse* velocity of a rough surface. In this application the roughness of the surface will no doubt affect the choice of optics used since for very smooth surfaces the effective scatterer number density will be quite high and the nonlinear response terms will probably become significant.

The third unique possibility provided by the interference flowmeter is the reduction of the measurement volume length without affecting the spectral width of the signal. When the scattering angle is small, the length of the measurement volume will always be much greater than the width in a heterodyne system because of the $1/\sin\theta$ multiplier in the length expression. When the velocity being measured is essentially transverse to the z axis, the spectral width is determined by the width and height of the measurement region, but the length is determined by the same parameters of the input distributions which determine the width. By using an interference flowmeter, however, the length of the measurement region can be independently shortened by

placing the collection optics to collect side-scattered radiation; the aperture in the image plane would then be chosen to not restrict the transverse dimensions of the image but to only pass a small portion of the length of the image. Such a system would be of great value in measuring flow where large velocity gradients exist along the z direction.

The last unique application to be discussed for an interference flowmeter concerns the measurement of cross-correlation functions or cross-spectra in turbulent flow. For these applications one wishes to measure simultaneously the velocity at two nearby points. Using a small scattering angle and producing a beam intersection region much longer than it is wide, the side scatter could again be detected as above but with *two* small apertures in the image plane, each passing light to a separate photodetector. In such an application the back of the apertures might have to be imaged with a microscope objective with considerable magnification to allow separation of the two signals physically to two separate detectors.

In summary, the interference flowmeter concept is similar to, but different in many ways from, the optical heterodyne Doppler flowmeter concept. The center signal frequency is determined in terms of the angle between the two incident beams by the same formula used for the heterodyne flowmeter, the functional form of the input plane distributions should be of the same class as that determined for the heterodyne flowmeter, and the linear portion of the signal will have the same spectral characteristics if the effective measurement volume

is not reduced by the image-plane aperture; but the general signal characteristics of the interference flowmeter are nonlinear, the SNR behavior is different, the requirements of the collection optics are more severe, and the distribution of incident power in the input beams should be equal instead of very unequal. The superior flexibility for applications of the interference flowmeter over the heterodyne flowmeter for many short-range applications should insure that it has a useful future.

CHAPTER VII

EXPERIMENTAL INVESTIGATION OF LASER FLOWMETERS

The purpose of this chapter is to present the results of experimental work which was performed to verify some of the theoretical results which have been obtained.† The major objectives of the experiments were to study the behavior of the heterodyne flowmeter signal-to-noise ratio and signal bandwidth for comparison with the specific results of Chapter IV and to verify the feasibility of the simplified heterodyne optical system and the interference flowmeter system.

Experimental Verification of Heterodyne Flowmeter Theory

The results of Chapter IV apply specifically to the case where the input-plane distributions of a generalized heterodyne flowmeter are constant-phase Gaussian distributions. These results were specialized further for the case of low-angle scattering and transverse velocity fields, the same case for which the simplified heterodyne optical system was theoretically shown to be useful in Chapter V. All of the experiments reported in this section were performed using the

---

†Preliminary experiments were performed in the spring of 1968 in the School of Electrical Engineering, Georgia Institute of Technology. The author expresses gratitude to the Lockheed Georgia Company for financial support and use of the facilities of the Systems Sciences Research Laboratory in which the major portion of the experimental work was performed during the summer of 1968.

simplified heterodyne optical system. The feasibility of the system was thus immediately demonstrated by the fact that the system was easy to set up and performed quite well. It has been assumed that the equivalence of the simplified system with the generalized system employing two input lenses is valid; therefore the experimental results should agree with the predictions for the specialized low-angle case in Chapter IV.

The results desired from the heterodyne experiments were the changes of the signal-to-noise ratio and the signal bandwidth produced by changes of the optical system or velocity parameters.

Experimental Apparatus

Verification of theory based on the assumption of steady flow required the use of a wind tunnel capable of producing constant-velocity flow in a test section. Obtaining constant velocity air flow is not a trivial problem as was discovered in several attempts to construct a small low-velocity recirculating tunnel according to advice from aeronautical engineers. The sensitivity of the laser flowmeter was such that it was easy to observe velocity jitter and spectral broadening produced by unwanted turbulence in these tunnels. The tunnel finally used for the experiments was a non-recirculating smoke tunnel with a velocity range of one to two feet per second which was borrowed from the Aerospace Laboratory.† No observable velocity jitter was detectable with this tunnel, but it was difficult to obtain good mixing of the

---

†Lockheed Georgia Research Laboratories.

smoke which was introduced as a smoke stream at the intake end of the tunnel. The smoke was produced by heating electric train smoke oil, the method usually used with the smoke tunnel.

Figure 13 illustrates the arrangement of the input beam optics and the smoke tunnel. Additional elements used in controlling the input beam distribution are not shown since they varied between experiments as described later. The incident laser beam was produced by a Spectra-Physics model 125 He-Ne laser nominally rated at 50 mw at a wavelength of 6328Å. The laser's measured power output in the TEM_{oo} mode was 40 mw. The laser was located approximately 25 feet from the experiment in another room and produced a beam whose diameter[†] at the input plane was between 5/16 and 3/8 inches.

The optical flat shown in Figure 13 was a high-quality 2 in. diameter, 0.5 in. thick optical window made by Perkin Elmer. The optical flat was anti-reflection coated on one side for normal incidence, but when used at 45°, as shown, the coating acted as an angle-sensitive partial reflector. The other side of the flat was uncoated; the flat was thus not coated in the optimum manner described in Chapter V and a small amount of optical power was lost in reflections. The lens used for focussing was a doublet binocular objective with focal length F = 8 inches. The optical window in the wind tunnel was an optical flat acquired from Edmund Scientific, presumed to be originally part of a gun sight or other surplus device.

[†]The diameter of the Gaussian beam was measured by eye, and the value is thus a subjective judgment.

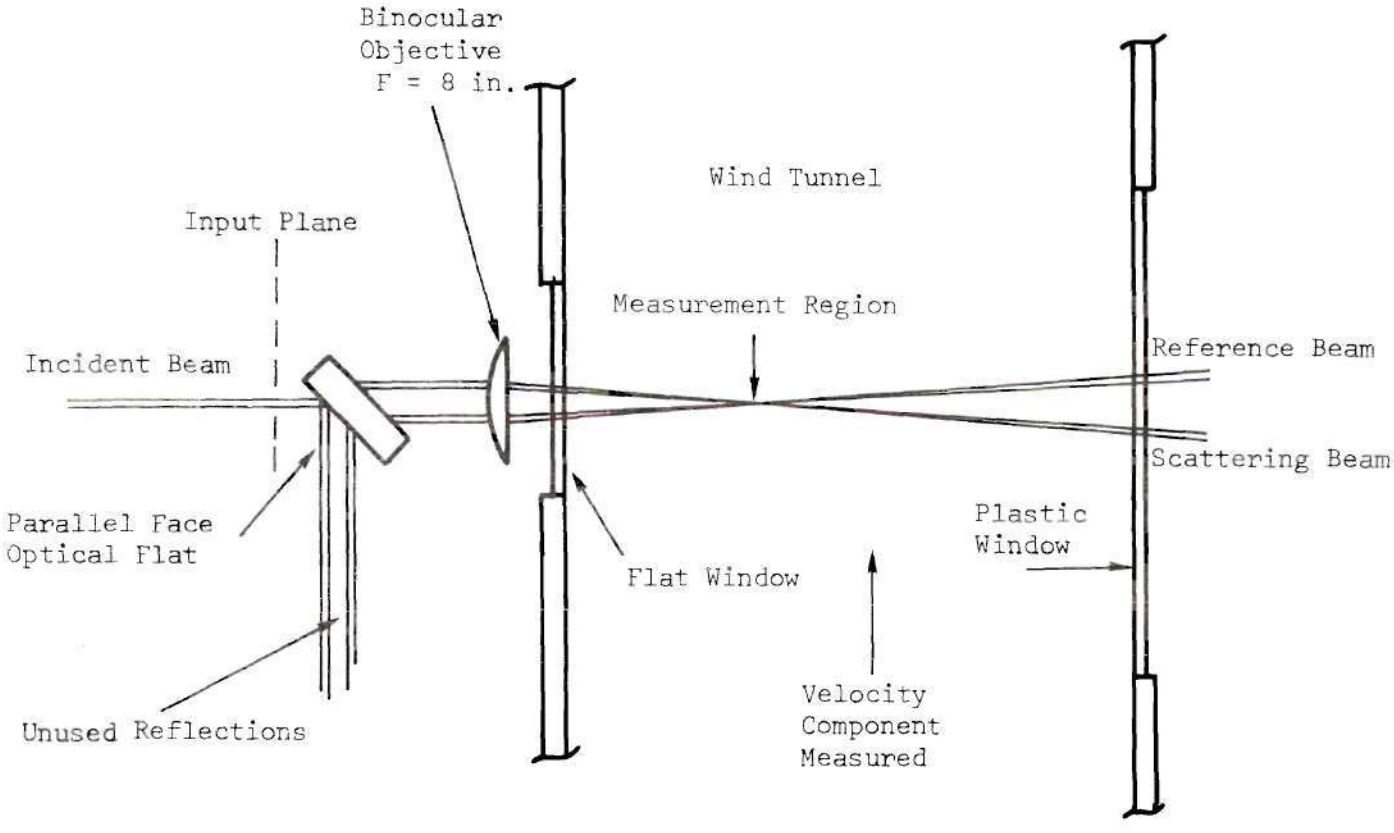

Figure 13. Input Optics for Experimental Heterodyne System

The Perkin Elmer flat produced parallel incident beams separated by approximately 3/8 in. This separation was measured by first reducing the incident beam diameter to approximately 0.6 mm with a lens pair and then using a ruled scale to visually measure the separation between the small diameter beams. Since the focal length of the lens was 8 inches, the scattering angle θ was

$$\theta = 2 \tan^{-1}\left(\frac{3/16}{8}\right) = 0.047 \text{ radians} = 2.7^{\circ} \qquad (1)$$

with the corresponding Doppler sensitivity of

$$f_d = \frac{K}{\pi} \sin(\theta/2) v_x = 74 \text{ KHz } v_x(\text{m/sec}) = 22 \text{ KHz } v_x(\text{ft/sec}) \qquad (2)$$

Figure 14 illustrates the collection optics and the RCA 7102 photomultiplier used. A large iris diaphragm was placed to block the scattering beam and some of the unnecessary scattered light, but the reference beam power was not obstructed. An inexpensive long focal length lens was used to converge the reference beam and the mixed scattered radiation through another pair of 3/8-inch apertures in the photomultiplier shield. The photomultiplier shield was adequate to eliminate any effects of room light at the operating voltages used for the heterodyne experiments. The apertures in the photomultiplier shield did not obscure any appreciable portion of the reference beam.

A block diagram of the electronics used for detection of the signal is shown in Figure 15. An RC cross-over circuit in the

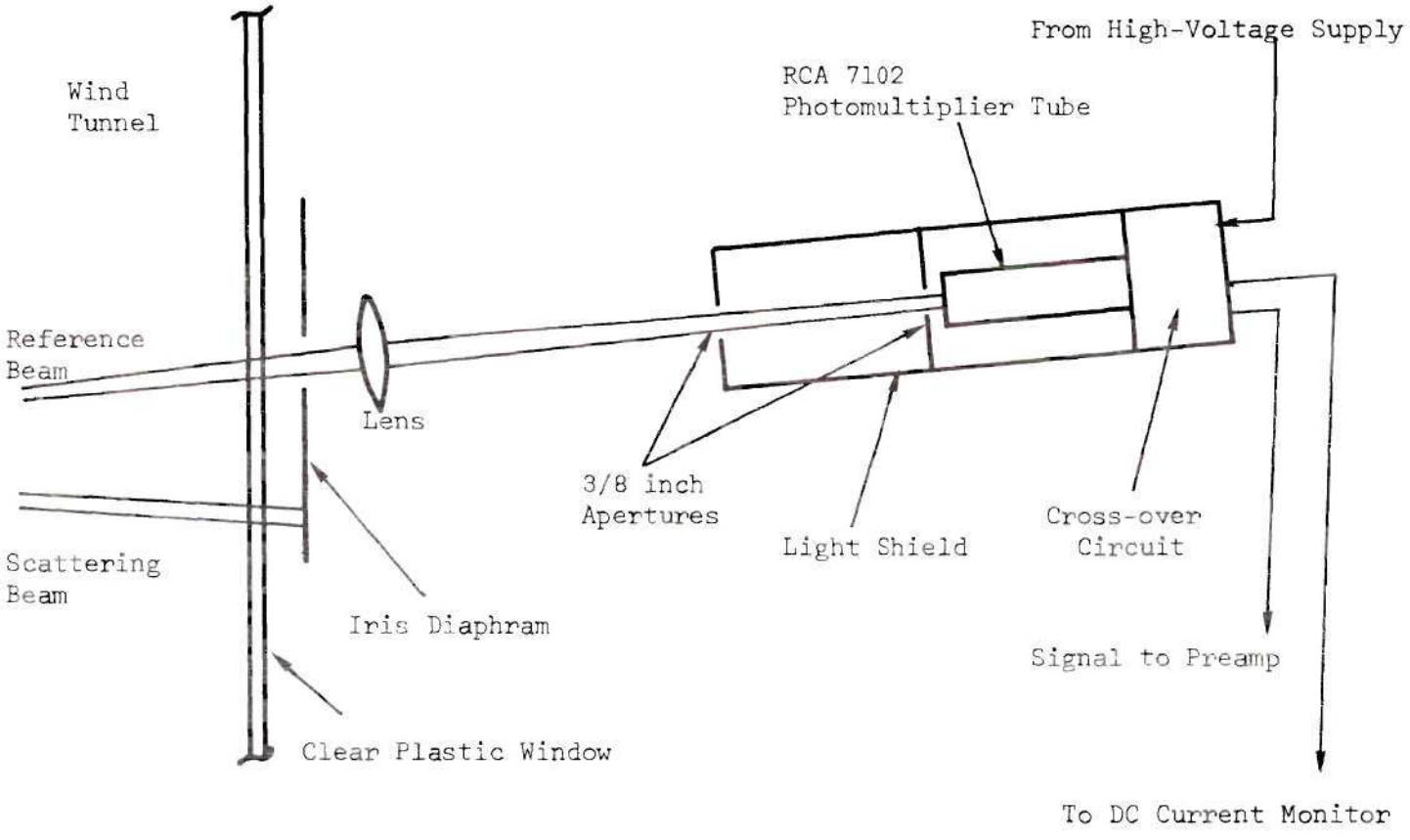

Figure 14. Collection Optics for Heterodyne System.

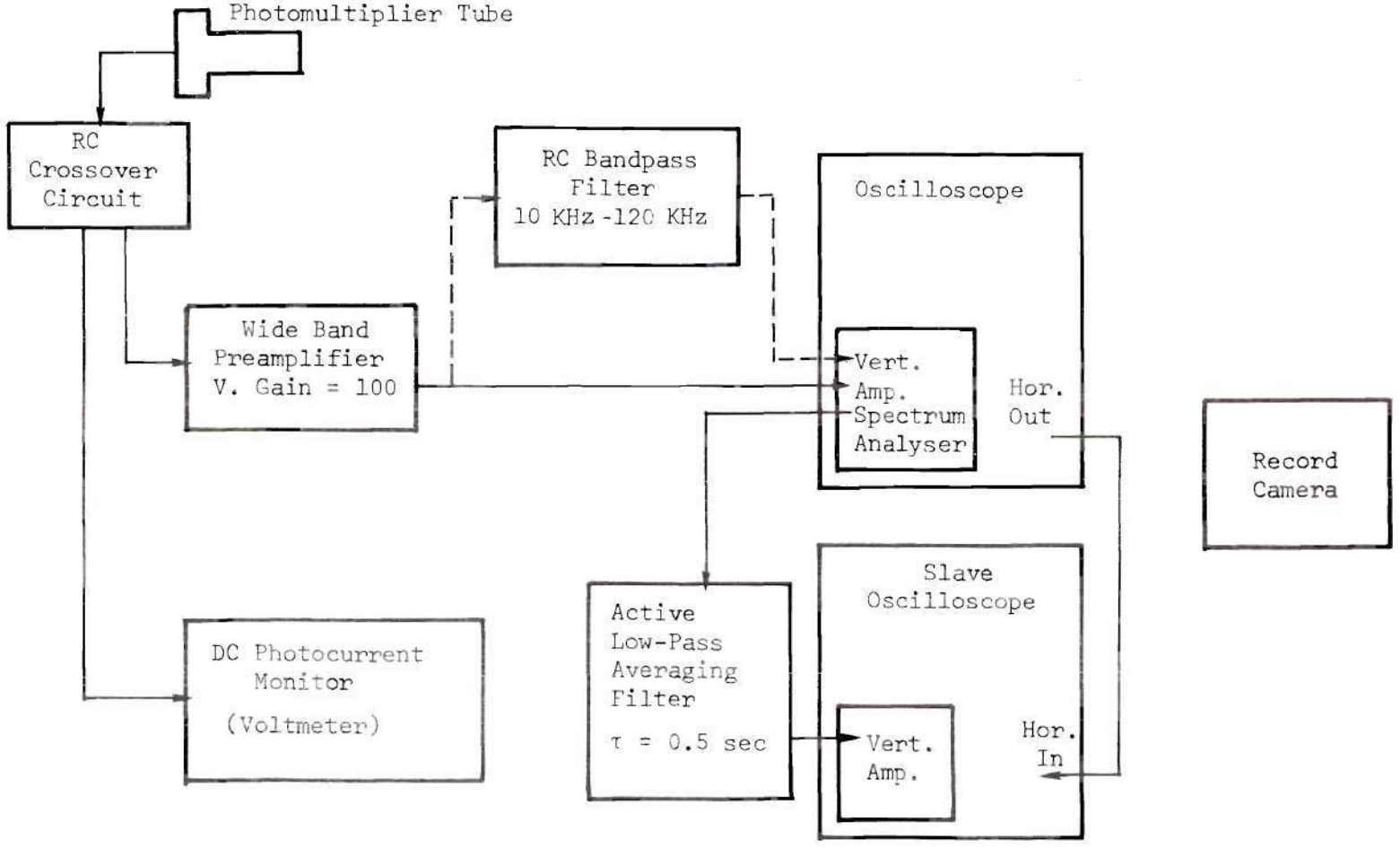

Figure 15. Electronics System Used for Flowmeter Tests.

photomultiplier housing provided a 2000 ohm load for the AC signal over 200 Hz which was delivered to a Tektronix model 1121 wide-band preamplifier whose voltage gain was 100. The DC photocurrent developed a voltage across a 100 K ohm load which was monitored by a vacuum tube voltmeter. The sensitivity of this DC current monitor was 0.1 volt per microampere. The preamplified signal voltage was applied to a Tektronix 1L5 plug-in spectrum analyzer unit housed in a Tektronix 547 oscilloscope. The 1L5 plug-in unit can function either as a spectrum analyzer with a range 50 Hz to 1 MHz or as a vertical amplifier for video displays of the signal. When video display was used, a two-pole RC filter, bandpass between 10 KHz and 120 KHz, was inserted in the signal path to eliminate 60 Hz pickup and some of the broad-band photon shot noise. The video filter was not intended to be optimum in any sense.

Since the signal produced by a laser flowmeter is a noise-like random process, the spectrum display obtained from the spectrum analyzer is only an estimate, which is itself a random process, of the rms voltage spectrum. In order to reduce the variance of the spectrum estimate,[†] the sweep rate of the spectrum analyzer local oscillator was reduced to one sweep per 50 seconds and the vertical output of the plut-in unit was averaged with an active one-pole low-pass filter with a time constant of approximately 0.5 seconds.[††] The averaged spectrum estimate was then displayed on another Tektronix 547 oscilloscope whose

---

[†]For an extensive discussion of analogue averaging of spectral estimates, see Bendat and Piersol.[32]

[††]The design of this filter was provided by R. P. Woodward.

horizontal sweep was slaved to the sweep of the first oscilloscope.[†]

Photographic records of the oscilloscope displays were made on polaroid film as part of the data which was taken. Two of these photographs are presented in Figure 16 as illustrations. The lower trace of 16(a) was a single-trace video presentation of a detected signal and noise. The upper trace was made with the scattering beam covered to show the noise alone. The upper trace of Figure 16(b) is an unfiltered voltage spectrum estimate of the signal and noise from DC to 100 KHz. The lower trace is the averaged spectrum display obtained simultaneously using a dual-beam oscilloscope. The step response of the averaging filter is also shown as another partial trace.

General Procedures

This section describes the manner in which the experimental apparatus was set up and operated, the types of raw data that were recorded, and the calculations performed in the reduction of the data to obtain the results presented in the next section.

System Operation. The smoke source provided with the smoke tunnel produced a dense stream of smoke for a short period of time after which the smoke density decreased rapidly as the smoke oil burned away. In order to decrease the smoke density to the point where the reference beam was not appreciably attenuated and in order to obtain uniform smoke density for periods of several minutes, a variable

---

[†]Initially a single dual-beam oscilloscope was used to display both the unfiltered and the filtered spectrum estimates on the same CRT, but this oscilloscope malfunctioned and had to be replaced with the two units as described.

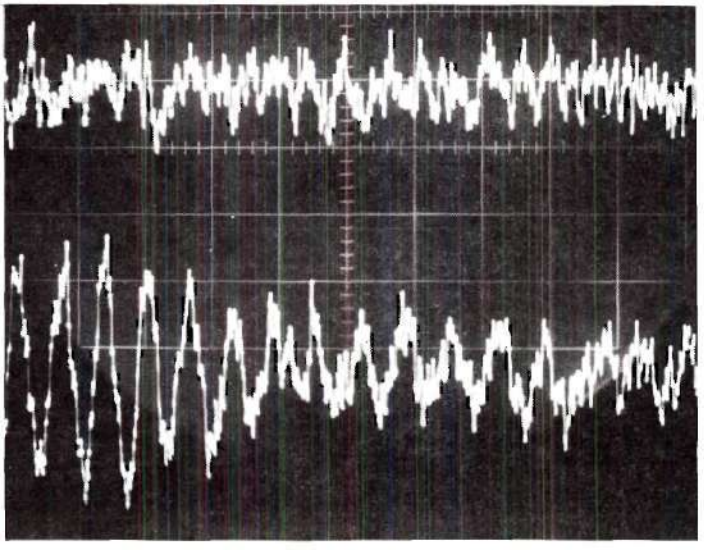

(a) Video Display. Noise Only (Upper); Signal Plus Noise (Lower) Sweep Rate: 50 μsec/division.

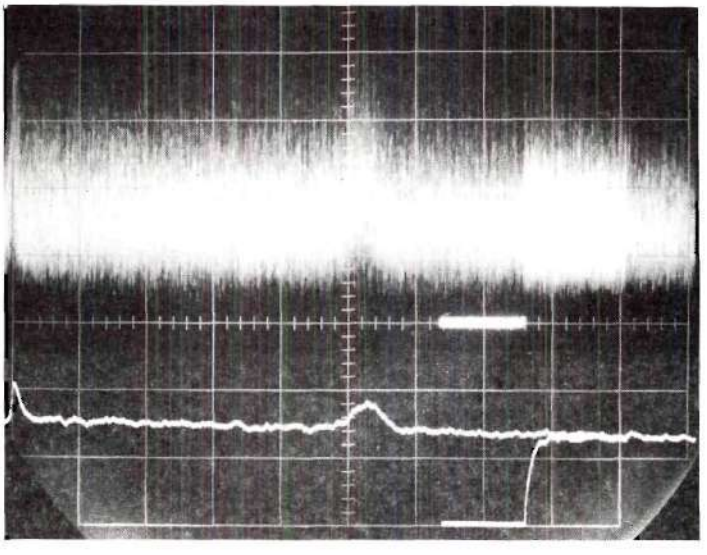

(b) Unfiltered and Filtered Spectrum Display of Signal (53 KHz) Plus Noise. Dispersion: 0-100 KHz; Sweep Rate: 5 sec/division; Filter Time Constant: 0.5 sec.

Figure 16. Flowmeter Signal Displays.

autotransformer was used to reduce the heater voltage of the smoke generator to a lower value. The resulting particle density was of such magnitude that less than one scatterer was present in the measurement volume on the average; this was determined by observation of the video presentation of signal.

The smoke tunnel was very sensitive to room drafts which caused the direction of the three to five-inch diameter smoke stream to wander slowly away from its axis at times. In these instances the spectrum analyzer data were ruined since the scatterer number density at the measurement point would change appreciably during the long time (50 seconds) required for a complete trace. Since it was desired to perform experiments requiring two minutes of constant scatterer number density, precautions were taken to prevent drafts and the few photographic records which obviously showed catastrophic smoke density changes were not used for data. There still remained some small variation in recorded peak signal spectrum values from one trace to the next due to smoke density variations; to further reduce the effects of these variations, most experiments were performed several times to obtain averaged results.

Setting up the optical system was the easiest task of the experimental work. Each element was supported by a separate optical bench holder, but these were merely placed by hand on laboratory tables on either side of the wind tunnel. With the electronic systems and the smoke system all on and properly adjusted, the optical components could be properly placed in position and Doppler signals displayed within

about two minutes. This procedure does not include any attempt to locate the measurement volume at a specific position near a test body in the tunnel since none was used. The point is made to emphasize the ease of use of the simplified heterodyne flowmeter optical system.

The 1/2-second time constant for the active low-pass filter was determined experimentally. In order to obtain maximum averaging, the oscilloscope sweep rate was first set at the slowest position of five seconds per division. A heterodyne flowmeter signal, which was assumed to be the narrowest in bandwidth which would be detected during the experiments, was displayed on the range 0—100 KHz. The filter time constant was then made as long as was possible without attenuating the spectrum pulse amplitude or widening the displayed pulse width.

In addition to the descriptions of the individual experiments and the photographic records of video and spectral displays of the signals, the following types of data were recorded for each photographic record:

HV - The voltage applied to the photomultiplier tube.

I_{dc} - The DC photomultiplier anode current.

VS - The vertical sensitivity of the display in mv/division.

SR - The horizontal sweep rate.

HD - The horizontal dispersion in Hz/division.

CF - The center frequency of the display.

RES - The IF bandwidth of the spectrum analyzer.

In all cases, the spectral resolution was limited by the response of the averaging filter rather than by the IF bandwidth, so this quantity was not used.

Data Reduction. The desired information concerning the heterodyne signal variations was obtained in the form of photographic records such as the lower complete trace of Figure 16(b). The heights and widths of the signal spectrum were determined by measurements made with a hundredths-inch scale with the aid of a 5x magnifier viewer.

A quantity S/I_{dc} was computed for each experiment, where S is the square of the peak rms voltage spectrum of the signal. Because of constant multipliers which have been neglected, S/I_{dc} is *not* the heterodyne signal-to-noise ratio given by the quantity $S_i(f_d)/ei_{dc}$; however, the quantity S/I_{dc} varies proportionally in the same way the shot-noise limited signal-to-noise ratio† varies providing the gain of the photomultiplier tube is not changed between experiments.

The quantity S was measured from the spectrum analyzer display photographs as follows: The value of the noise voltage spectrum N projected to the center frequency of the signal was measured in inches; the value of the peak signal plus noise voltage spectrum P was measured in inches; then S was determined in units of $(mv)^2$ by the formula

---

†Because of the small maximum velocity obtainable using the available smoke tunnel, the Doppler signal frequencies were low enough to fall in the spectral range of laser amplitude fluctuation noise. The existence of this noise was noticed toward the end of the experimental work, but not understood at the time. The theoretical analysis presented at the end of Chapter III was performed after the experimental apparatus was no longer available. Since the proper data was not obtained for comparison of the actual signal-to-noise ratios, including the laser amplitude fluctuation noise, with theoretical predictions also including this noise, an alternate approach was taken. The experimental quantity S/I_{dc} is proportional to the SNR which should have been obtained at higher velocities in the absence of laser amplitude fluctuation noise, and the variation of this experimental quantity should agree with the results of Chapter IV.

$$S = \left(P^2-N^2\right)\left(\frac{1}{0.35}\ \frac{\text{divisions}}{\text{inch}}\right)^2(VS)^2 \qquad (3)$$

where VS, the vertical sensitivity, was given in mv/division. It is permissible to obtain the peak mean-square voltage spectrum value in this manner since the noise and signal are independent random processes. The DC current was a measured quantity, so the ratio S/I_{dc} could be computed.

The half peak power spectrum bandwidth BS was determined from the photographic records of the rms voltage spectra of signals plus noise. First the height H in inches at which the bandwidth was to be measured was calculated according to the formula

$$H = \sqrt{N^2 + \frac{P^2 - N^2}{2}} = \sqrt{\frac{P^2 + N^2}{2}} \qquad (4)$$

where, as before, P is the value measured in inches of the peak signal plus noise voltage and N is the value in inches of the noise voltage projected to the peak signal frequency. The signal bandwidth BS was measured at the height H on the photographic record.† after determining the peak signal frequency f_d from the record, the fractional half power bandwidth BF was computed as

$$BF = BS/f_d \qquad (5)$$

---

†The possible values of H are algebraically restricted to the range $N + 0.5(P-N) \leq H \leq N + 0.707(P-N)$. Actual values were near $N + 0.6(P-N)$ in most cases.

Compensation of Reduced Data. After the experimental apparatus was no longer available,† a systematic trend in the reduced data was detected which indicated that the averaging filter time constant had been chosen too long for the narrower spectra that resulted in some of the experiments. The error was not a gross one, since the filtered spectral pulses were not smeared into the typical impulse response shape produced by an RC low-pass filter, and had thus gone unnoticed during the performance of the experiments. However, some of the narrower spectra had been attenuated and broadened nonnegligibly.

The extent of spectral broadening and attenuation due to the averaging filter was established experimentally with the use of a model F230A Data Royal wave-form generator. Single raised cosine pulses of varying durations were used as the input to the averaging filter. The input and output were simultaneously displayed on a Tektronix 547 oscilloscope with sweep rate set at 5 sec/division (the same sweep rate used in the flowmeter experiments). Figure 17(a) illustrates a typical input and output pulse showing the effect of the filter. The attenuation of the output pulse heights and the increase in output pulse widths were measured; the pulse widths were measured at the 0.6 heights. As shown in Figure 17(b), the factors by which the input pulse widths were less than the output pulse widths were plotted against the measured output pulse widths. The squares of the factors by which the input pulse heights exceeded the output pulse heights were also plotted against the

---

†The smoke tunnel had to be returned to the Aerospace Laboratory for their use.

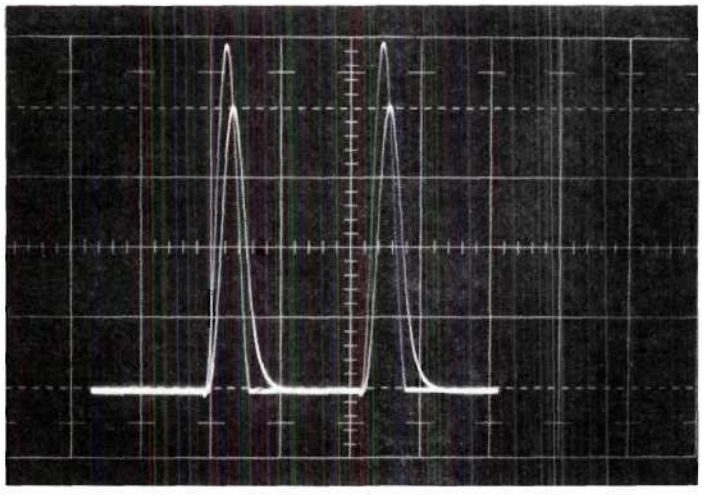

(a) Typical Effect of Filter on Pulse SR = 5 sec/division
(The Lower Amplitude Pulses Have Been Filtered)

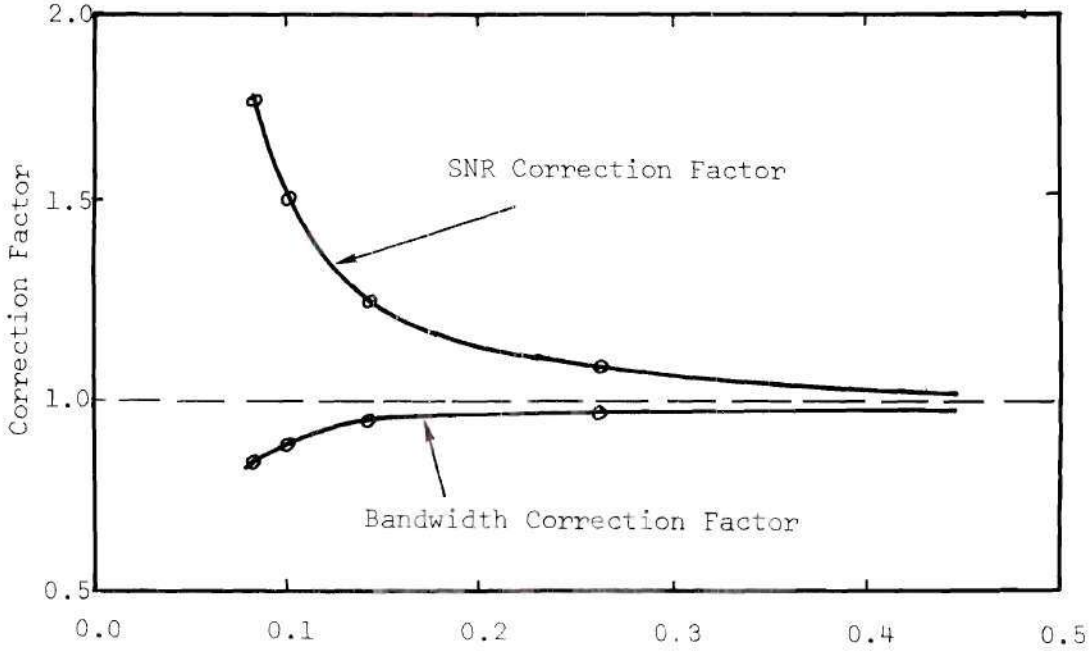

(b) Correction Factors

Figure 17. Compensation for Filter Time Constant

same variable as is shown in the figure. The compensation factors thus obtained were used in the following manner: the average measured spectral width in inches was determined for each optical arrangement and the correction factors determined by Figure 17(b) were then applied to the values of S/I_{dc} and BF which had been previously determined. The compensated results are given as results for the experiments reported below.

Specific Experiments and Results

Four classes of experiments were performed: experiments in which the input-plane distributions were modified by lossy apertures; experiments with Gaussian beams of differing diameters; experiments in which the velocity magnitude and direction were changed; and an experiment to record the variation of the low-pass laser intensity fluctuation noise which was observed during the course of the other experiments. The experiments with apertures were performed to verify qualitatively the predictions of Chapter IV concerning the use of lossy Gaussian apertures. Simple circular and rectangular apertures in a uniform incident plane wave produce relatively the same incident power changes for changes in beams. It is assumed therefore that the SNR and bandwidth changes should be qualitatively the same as those predicted for the Gaussian case.

Experiment 1--Circular Apertures. The velocity is chosen in the x direction. The input distributions are constant phase and equal, except for a multiplying constant and a negligible path length difference. The theory of Chapter IV predicts that if a circular Gaussian

(TEM_{oo}) input distribution is reduced in diameter by a lossy Gaussian attenuation filter by a factor of 2, then the fractional bandwidth will be reduced by a factor of 2 as indicated by (4-57) with $\psi_v = 0$, and the SNR will be reduced by a factor of 4 because of the ξ^2 reduction of incident scattering beam power.

The central portion of the incident 40 mw laser beam was used to illuminate an iris diaphragm located approximately 7.5 inches in front of the focussing lens with the beam splitting flat placed in between the aperture and the lens. Drill bits of diameters 0.06 inches and 0.12 inches were used to set the diameter of the iris diaphragm. The power transmitted by the iris was measured to be 3.0 mw and 11.8 mw, respectively, for the two aperture sizes. Since only the central portion of the incident Gaussian beam was used, the illumination approximated a uniform plane wave.

Two successive traces of the spectrum analyzer were recorded on one photographic record with the 0.06 inch aperture. The aperture was then immediately changed to 0.12 inches and two more traces were recorded on another photographic record, the only other change being a calibrated change of vertical sensitivity of the display. Figure 18(a) is a reproduction of the record for the smaller aperture which showed the poorer reproducibility of the two. The height and width measurements made from the records were the subjective average values for the two traces in each case.

After performing the calculations indicated in the section on general procedures, the fractional bandwidths obtained were BF = 0.14

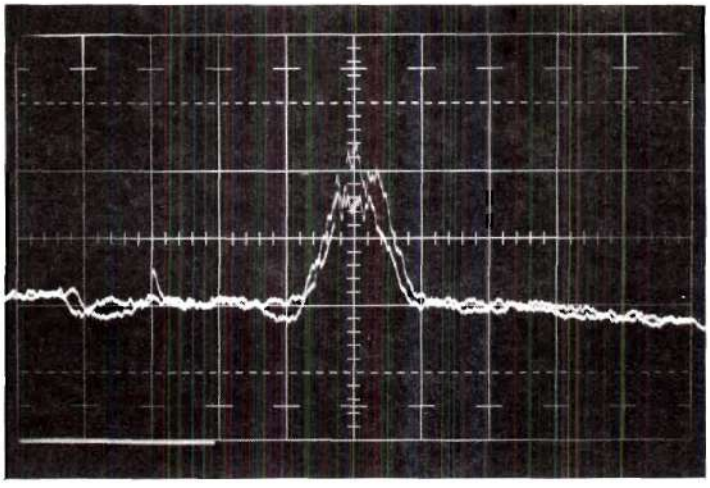

(a) Smaller Circular Aperture (0.06 in.). Two Traces.
Display Center = 30 KHz.HD =5 KHz/division.

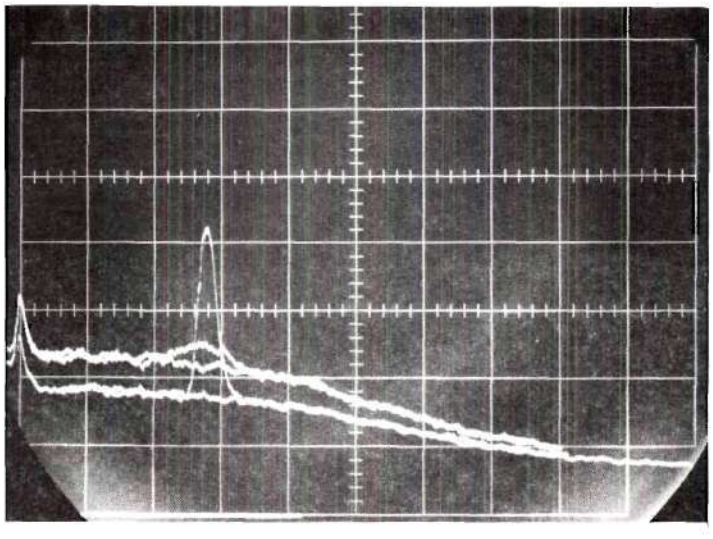

(b) Vertical Slit (Tall Narrow Peak) and Horizontal Slit.
Display Center = 50 KHz. HD = 10 KHz/division.

Figure 18. Typical Spectrum Records - Simple Apertures

and BF = 0.21 with a ratio of 0.65 as compared with the ratio of 0.50 predicted by theory for the Gaussian apertures. The ratio of signal-to-noise ratios, obtained by dividing the S/I_{dc} value for the smaller aperture by that for the larger aperture, was 0.34 as compared to the value 0.25 predicted by theory for similarly related Gaussian apertures.

Experiment 2--Rectangular Apertures. The experiment with simple apertures was also performed using vertical, horizontal, and square rectangular apertures. The velocity was again constant in the x direction.

The theory of Chapter IV predicts that reducing the input beam width with a one-dimensional Gaussian attenuation filter by a factor of 4 should reduce the fractional bandwidth by a factor of 4 without affecting the SNR. On the other hand, reducing the input beam height by a factor of 4 should leave the fractional bandwidth unchanged, but reduce the SNR by a factor of 16.

Rectangular apertures were constructed using 3 x 5 cards, an Exacto knife, and rubber cement. Measurements of these apertures with a 5x magnifier showed them to have the following dimensions: A square aperture was 2.7 mm x 2.7 mm; a vertical slit was 2.7 mm x 0.65 mm; a horizontal slit was 0.50 mm x 2.7 mm. Three sets of comparison experiments were performed: The vertical and horizontal slits were alternated with one of each being used for three photographic records (two traces per record); the vertical slit and the square aperture were used alternately with one of each on each of three records; the square aperture and the horizontal slit were used alternately with one of each on each of two records.

Figure 18(b) is a reproduction of one of the records obtained in comparing the horizontal slit and the vertical slit. When this record was made, two additional traces were made with the scattering beam covered to show the repeatable noise level present in the absence of signal. One observes the presence of the laser amplitude fluctuation noise in this record as a broad low-pass spectrum.

The results of the rectangular aperture experiments are given along with theoretically predicted ratios based on Gaussian attenuation of Gaussian beams in Table 2.

Table 2. Results for Rectangular Aperture Experiment

Record	BF_V	BF_H	BF_V/BF_H	SNR Ratio
1	0.09	0.25	0.36	8.4
2	0.07	0.20	0.35	13.
3	0.08	0.33	0.25	15.
Average			0.32	12.
Predicted			0.24	29.
Record	BF_V	BF_S	BF_V/BF_S	SNR Ratio
4	0.05	0.14	0.34	0.96
5	0.08	0.24	0.32	0.76
6	0.07	0.28	0.26	1.8
Average			0.31	1.2
Predicted			0.24	1.0
Record	BF_S	BF_H	BF_S/BF_H	SNR Ratio
7	0.19	0.19	1.0	6.
8	0.27	0.24	1.1	11.
Average			1.1	8.
Predicted			1.0	29.

The subscripts V, H, S, in the table refer to the vertical, horizontal, and square apertures. The ratio of SNR's column refers to the ratio of the S/I_{dc} values, ordered in the same respective way that the ratio of bandwidths are ordered. The "average" values refer to the arithmetic mean of the column.

Experiment 3--Vertical Slit in One Beam Only. The theoretical expression given by Equation (4-40) with γ given by (4-47) predicts that the fractional bandwidth can be reduced at most by a factor of $\sqrt{2}$ if one of two equal input beams is reduced to zero width while the other stays constant. However, if the velocity is x directed, the fractional bandwidth should be reduced to zero by reducing the width of both input beams simultaneously to zero.

A qualitative test of the implied conclusion that it is inefficient to try to reduce the fractional bandwidth by controlling only one of the two input beamwidths has been made for the case where the velocity is in the x direction. The incident Gaussian laser beam was reduced to a diameter of approximately 0.1 inch by a pair of lenses. In each of two successive photographs two spectrum traces were recorded: one with no apertures in the incident beams and one with a 0.025 inch vertical slit placed past the splitter flat in the reference beam only. In one of the two photographs, the spectrum appears slightly *wider* for the trace taken with the slit in the reference beam, but trace ambiguities make this uncertain. In the second record, with no ambiguity, the spectrum is narrower by a factor of 0.9 for the case of the slit in the reference beam.

In two additional photographic records the case of the slit in the reference beam only was compared with the case of the slit in both beams (slit in front of splitter flat). The average ratio of bandwidths in this comparison was 0.61. This corresponds to a reduction of bandwidth of 0.55 with respect to the incident beam with no slit present. The theory is thus qualitatively verified in predicting the increased effectiveness of keeping the two incident beam widths equal as opposed to altering only one of them.

Experiment 4--TEM_{oo} Gaussian Beams. The theory of Chapter IV is directly applicable to the case where the diameter of a TEM_{oo} input beam is changed without loss by the use of an ideal telescope, i.e. where the total power remains unchanged but input beam waist parameter w_o is changed. For this case the signal-to-noise ratio should not be a function of w_o if the velocity is in the x direction, but the fractional bandwidth should be directly proportional to w_o.

The apertures of the first three experiments were replaced by a collimating, beam-reducing telescope. The telescope was constructed on an optical bench in such a way that the output beam diameter could be rapidly changed by removing one lens and inserting another in another pre-aligned position. The ratio of the focal lengths of the two interchangeable focussing lenses of the telescope was 3.1:1; thus the larger output beam (approximately 0.25 inches in diameter) was 3.1 times wider than the narrower beam. The beams differed in total power by about 2 per cent due to the fact that one of the focussing lenses was a doublet with higher losses than the other lens which was a singlet.

Three photographic records were made. The first two each had a spectrum trace from the narrow beam followed by one from the wide beam. The third record was made with the horizontal dispersion changed to "variable" to expand the presentation and thus give better measurement resolution. Two traces of each signal were recorded on the third record with excellent reproducibility, so the results from this record were counted twice in the average results. The average ratio of fractional bandwidths was 0.31 as compared with the predicted value of 1/3.1 = 0.32. The predicted ratio of SNR's was 1.0 but the average ratio obtained experimentally was 2.7 with the narrower beam producing the larger SNR.

Experiment 5--Cylindrical Lens. An attempt was made to verify the predictions of Chapter IV concerning the predicted advantages of using elliptical Gaussian beams, obtained by use of cylindrical lenses. This experiment could not be performed since the cylindrical lenses which had been obtained proved to be worthless for constructing a one-dimensional telescope with which to alter the incident beam. The distortion of the beam by these cylindrical lenses was so great that no pattern resembling an elliptical Gaussian beam could be produced.†

Experiment 6--Velocity Magnitude. Theory predicts that the signal bandwidth should be proportional to the velocity magnitude; i.e. the fractional bandwidth should remain constant. The SNR should

---

†The author was somewhat naive about the availability of well-corrected cylindrical lenses. The ones obtained were from Edmund Scientific and probably were designed as magnifiers for reading telephone books.

be inversely proportional to the velocity magnitude, so long as the scatterer number density remains constant.

The narrow beam producing telescope of Experiment 4 was used to provide an input beam, and the velocity of the air in the smoke tunnel was varied as much as possible by varying the voltage applied to the tunnel exhaust fans. According to calculations based on the center signal frequency, the velocity range of the tunnel was from 1 to 2 feet per second.

It should be pointed out that the smoke input rate was not changed when the tunnel air speed was changed. A first reaction might be that this implies that the smoke density would halve if the total air intake were doubled. This would be true if the air and smoke were passed through a mixing chamber before reaching the test section. The design of the tunnel was such, however, to quickly still all motion of the intake air relative to itself so that coherent smoke streams could be formed. It is considered most likely, therefore, that the density of scatterers at the center of smoke stream remained relatively unchanged while the diameter of the smoke stream changed as the exhaust fan speed was varied.

Two photographic records were made, each with one spectrum trace with the velocity turned down and one with the velocity turned up. For the first record the signal frequency maxima were at 20.0 KHz and 37.8 KHz for the low and high velocities, respectively, which corresponds to a velocity ratio of 1.89. The ratio of the S/I_{dc} value at the low velocity to the value at the high velocity was 1.9 while the ratio of

the fractional bandwidths was 1.07 as compared with predicted values of 1.89 and 1.00, respectively. For the second record, the signal frequencies for the low and high velocities were 19.6 KHz and 38.3 KHz for a velocity ratio of 2.00. The ratio of S/I_{dc} values was again 1.9 while the ratio of fractional bandwidths was 1.06 as compared with predicted values of 2.00 and 1.00.

Experiment 7--Velocity Direction Effects. The effect of rotation of the velocity vector in the xy plane is now considered for the case of a TEM_{oo} mode beam incident. The symbol ψ_v indicates the angle between the x axis and the velocity vector. The v_x component of the velocity, and hence the center signal frequency f_d, varies as $\cos\psi_v$ as the velocity vector is rotated. The theory of Chapter IV indicates that the total signal bandwidth† BS and the SNR factor S/I_{dc} should not vary as a function of ψ_v.

The size of the wind tunnel prevented rotation of the velocity vector about the axis of the incident beam. To effect the same relative rotation, the optical flat, which previously produced two parallel beams in the horizontal plane, was mounted in a precision rotatable mount so that the plane of the scattering and reference beams could be rotated about the axis of the source beam. Since the reflection coefficients of the optical flat were critically dependent on the incident beam polarization, a polarization rotator was used to maintain fixed polarization direction relative to the splitter flat. The velocity

---

†The variation of both f_d and BS will be considered separately here instead of just their ratio, BF.

vector was thus rotated with respect to a coordinate system fixed to the plane of the scattering and reference beams.

Three photographic records were made, each with spectrum traces at three different values of ψ_v. After two records had been made, it was determined that the 0^o reference setting on the rotation mounts were approximately 3^o from parallel to the velocity vector so 3^o were added to the angle values which had been recorded, and the last record was made with a new reference setting. Table 3 shows the results; values are shown for the center signal frequency f_d, the ratio of f_d to the zero-angle frequency f_{do} (should equal $\cos\psi_v$), the S/I_{dc} value, and the bandwidth BS. No compensation for the averaging filter time constant has been applied to obtain the results in Table 3 since the correction factors required were near one and nearly the same for all traces. Since the absolute magnitude of the S/I_{dc} values are meaningless, the power of 10 has been omitted.

Experiment 8--Variation of the Laser Amplitude Fluctuation Noise. During the performance of the heterodyne experiments the presence of the laser amplitude fluctuation noise in the detected signal was recognized but its variation with the reference beam power was not fully understood. That increasing the reference beam power could decrease the SNR had not been anticipated since none of the literature on optical heterodyne SNR theory had indicated such a possibility. The theory which was presented in Chapter III indicates that the white quantum noise power density increases linearly with increasing reference beam power, but the laser intensity noise power density increases as the square of the reference beam power.

Table 3. Effects of Velocity Rotation

Record 1--Single Traces

ψ_v	$\cos\psi_v$	f_d(KHz)	f_d/f_{do}	S/I_{dc}	BS(KHz)
3°	1.00	32.0	1.00	2.5	2.6
63°	0.45	14.5	0.45	3.0	3.1
78°	0.21	7.0	0.22	2.6	3.0

Record 2--Two Trace Averages at Each Position

ψ_v	$\cos\psi_v$	f_d	f_d/f_{do}	S/I_{dc}	BS
3°	1.00	32.0	1.00	2.5	3.2
63°	0.45	14.5	0.45	2.3	3.0
78°	0.21	6.5	0.20	2.3	3.3

Record 3--Single Traces

ψ_v	$\cos\psi_v$	f_d	f_d/f_{do}	S/I_{dc}	BS
0°	1.00	31.5	1.00	1.9	3.3
60°	0.50	15.5	0.49	1.9	3.3
80°	0.17	5.0	0.16	2.0	3.0

An experimental test was made to see how the noise spectra varied with a change of reference beam power. The smoke source was turned off so that no signal was detected, only noise. The horizontal dispersion of the spectrum analyzer was increased to 100 KHz/division. Two spectrum traces were recorded with the optical splitter flat rotated to slightly different positions to give one trace at a detected DC current level four times less than that occurring for the other trace;

i.e., the reference beam power was varied by a factor of four. The record is reproduced in Figure 19.

The photographic record and other non-recorded observations indicated the presence of nearly white noise above 150 KHz whose rms voltage density varied by a factor of 2, corresponding to a linear power density change by a factor of 4. This noise is assumed to be photon noise. The variation of the low-pass noise has been calculated at 40 KHz. This value is sufficiently far from the zero-frequency transient to avoid averaging filter effects. The procedure was to square the measured values of rms low-pass noise plus white noise and subtract the projected squared white noise level to obtain the power density of the low-pass noise, assumed independent of the white noise. The result indicated an increase in the low-pass noise power spectrum by a factor of 14.3 as compared with the factor 16 predicted by theory.

Discussion of Results

The experimental results agree qualitatively in most cases with the predictions of theory. Most of the variance in the results of repeated experiments can be attributed to fluctuations in the smoke density which would not have been present had the smoke been uniformly mixed with the air. Considering the experimental conditions, it is felt that the quantitative agreement between the experimental results and the theoretical predictions was quite good with regard to the variations of the fractional bandwidth.

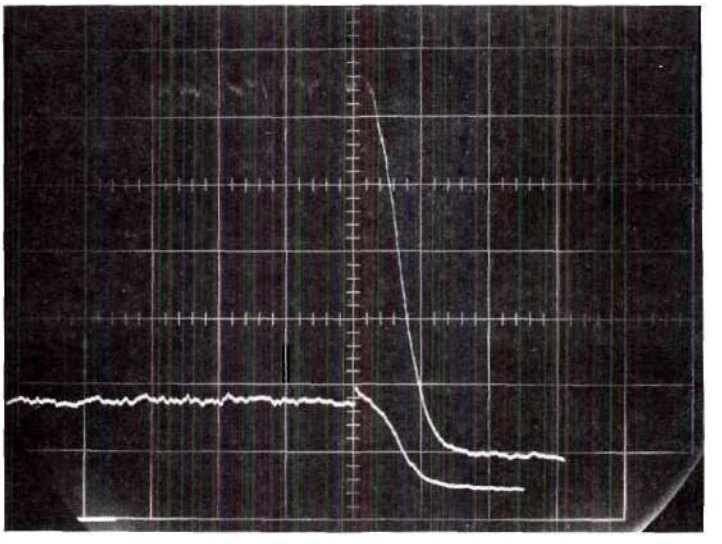

Horizontal Dispersion = 100 KHz/division
Zero Frequency at Center
Reference Beam Power for Upper Trace is
Four Times that of Lower Trace.

Figure 19. Noise Voltage Spectral Density Comparison for Change in Reference Beam Power.

The quantitative agreement between experiment and theory was not as good concerning the signal-to-noise ratio. Part of the reason for this may be attributed to slow variations in the smoke density since the SNR is proportional to this quantity; however, a review of the results reveals that the most severe quantitative disagreements occurred in experiments in which the height dimension of the input beam was changed. For example, reduction of the TEM_{oo} mode beam diameter without loss of total incident power should not have altered the SNR, but experimentally the SNR increased. In all cases involving reduction of the height dimension of the input distribution, the SNR was greater than the predicted value for the distribution with the reduced height dimension.

The reason for the quantitative disagreement in cases involving variations of the y dimension of the input distribution has been found. The cause was a small vertical misalignment of the two intersecting focussed beams which resulted from not having the focussing lens squarely perpendicular to the two incident parallel beams. A small vertical displacement of one focussed beam with respect to the other is equivalent to a linear phase error in the y direction; this case was treated in Chapter IV where it was shown that the reduction of SNR by the alignment error becomes less when the y dimension of the input distribution is reduced.

The misalignment effect was discovered after the results were compiled. The type of disagreement of experimental results and theory indicated the possibility of vertical misalignment, but this should not

have been possible according to the idealized derivation concerning the simplified flowmeter optics. In order to check the possibility of vertical misalignment, the same splitter flat, focussing lens, and optical window which had been used in the experiments were set up again. The only difference was that two nearly equal reflected beams were used instead of the two transmitted beams which have very unequal intensities. The beam intersection region was imaged with magnification by a microscope objective; the focussed beams did not completely overlap. It was found, however, upon close inspection that the focussing lens was not perpendicular to the incident beams. When the lens was positioned perpendicularly, the two focussed beams intersected perfectly.

It is felt that in carrying out the heterodyne experiments the focussing lens was slightly misplaced in angular position since it was not known at the time that a slight angular rotation of the lens could partially misalign the system. This misalignment was possible because the lens was not well-corrected for off axis-incident rays, a possibility not analyzed in the idealized derivation.

Feasibility Experiments with an Interference Flowmeter

The interference flowmeter concept has been demonstrated experimentally to be feasible. Three different experimental arrangements are reported briefly which illustrate some of the flexibility and potential of the system.

Transverse Velocity of a Rough Surface

Figure 20 is a schematic diagram of the experimental system used to measure the velocity of a rough surface mounted on a record changer

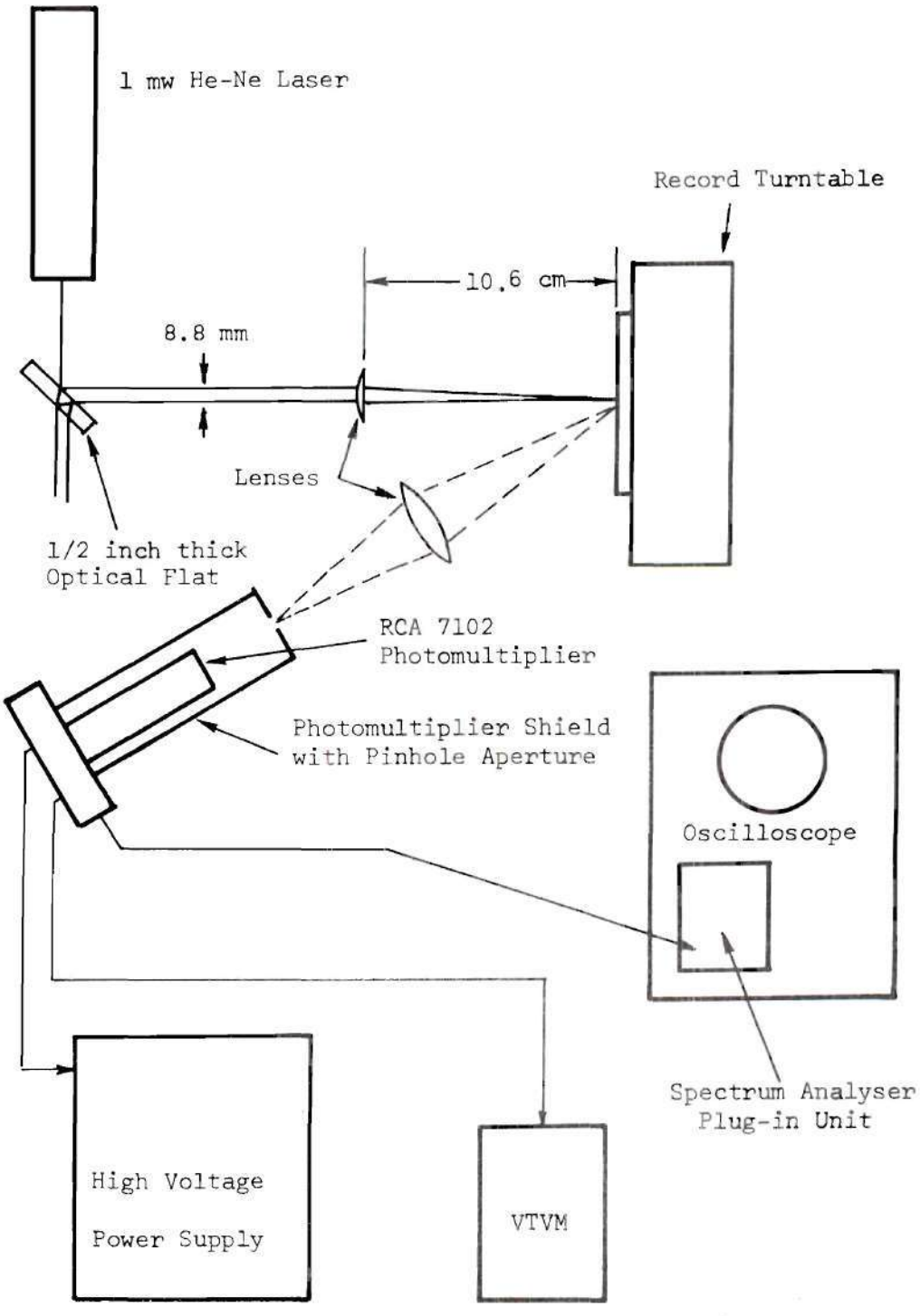

Figure 20. Measurement of the Tranverse Velocity of a Rough Surface

turntable. One observes that the laser used was an inexpensive 1 mw laser. The beam splitting optical flat was an uncoated one obtained from Edmund Scientific. Since most of the optical power was lost by transmission, the two beams incident on the focussing lens were each less than 0.1 mw in power. The record turntable was placed so that the focussed beams intersected at the mounted rough surface 4.3 cm above the axis of the turntable. A two-inch diameter collecting lens, placed about the same distance from the turntable as the focussing lens, focussed the scattered light through a pinhole to an RCA photomultiplier tube. The detected signal was displayed with a Tektronix oscilloscope and a Tektronix 1L5 spectrum analyzer plug-in unit. This experiment was performed earlier than the heterodyne experiments and no spectrum averaging filter was used at the time.

The results of the experiment showed that the roughness of the surface is an important factor which should be studied further analytically (the high scatterer density case). No velocity signal could be obtained when the surface was white paper. A velocity signal was easily detected when the surface was replaced with very fine sandpaper, even though the sandpaper was of a dark color and hence scattered less total light. The signal was detectable as a pip on the spectrum analyzer whose frequency position was proportional to the rate of revolution of the turntable. When the turntable selector was changed from 45 rpm to 78 rpm, the center signal frequency changed by the ratio 78/45 within 0.7 per cent. The actual velocity of the surface at the measurement point was calculated at 78 rpm to be 35.1 cm/sec; the

measured velocity was calculated to be 32.8 cm/sec, an error of approximately 6.5 per cent. This error is attributed to lack of precision in measuring the beam separation and distance to the surface from the lens plane and also includes any error in the turntable rate.

Velocity of a Smoke Stream--Forward Scatter

The same components shown in Figure 19 were also used to measure the velocity of a smoke stream, but the collecting lens was placed directly in the forward direction beyond the smoke stream with small pieces of black tape stuck to the lens to block the incident beams. The smoke stream was produced by placing lighted cigarettes in a cardboard box with an intake blower. The smoke exited the box through a 1/4-inch diameter pipe placed near the intersection of the focussed beams.

The forward scatter system produced signal pulses with ripple frequencies in the range 200 KHz to 1 MHz depending on the smoke blower speed. The signal was displayed both as a video presented and a spectrum presentation. The signal spectrum was rather broad due to turbulence but changed its center frequency in the appropriate direction when the fan speed was changed.

The most significant result of this experiment is that it produced much better signal-to-noise ratio than did a simplified optical heterodyne experiment using the same system components. This is doubly significant since the uncoated optical flat is much more efficient with the laser source power when the transmitted beam and the internal reflection reference beam are used. Too many system parameters are

involved to state categorically that at short ranges the forward-scatter interference flowmeter will always give higher SNR's than will a heterodyne system with the same source power and signal bandwidth; however, this experiment indicates great promise in this respect.

Velocity of a Smoke Stream--Backscatter

After the heterodyne studies had been completed with the 50 mw laser and the constant velocity smoke tunnel, an interference flowmeter was set up to demonstrate the feasibility of using the backscattered radiation from smoke. The electronics used for detection were the same as those used for the heterodyne experiments as shown in Figure 15. The optical system used is illustrated in Figure 21. The optical flat used to produce the two parallel reflected beams was the inexpensive uncoated flat; the power in each beam was less than 2 mw.

The collection optics were inefficient. Due to the very low intensity of the image of the scattering region, the full two-inch aperture of the collecting lens was used; the image of the beam intersection region was just visible on a white card with all the room lights out after the eyes were dark adapted. Unfortunately, the collecting lens exhibited large amounts of spherical aberration and very limited depth of focus at this large aperture. Due to the poor resolution of the image and the lack of a precision adjustable holder it was not possible to use a very small pin-hole aperture matched to the small intersection volume size. The small aperture used, after some trial and error, was a 1/16" x 1/64" vertical slit. As a result of the poor image focus and relatively large aperture, significant amounts of light

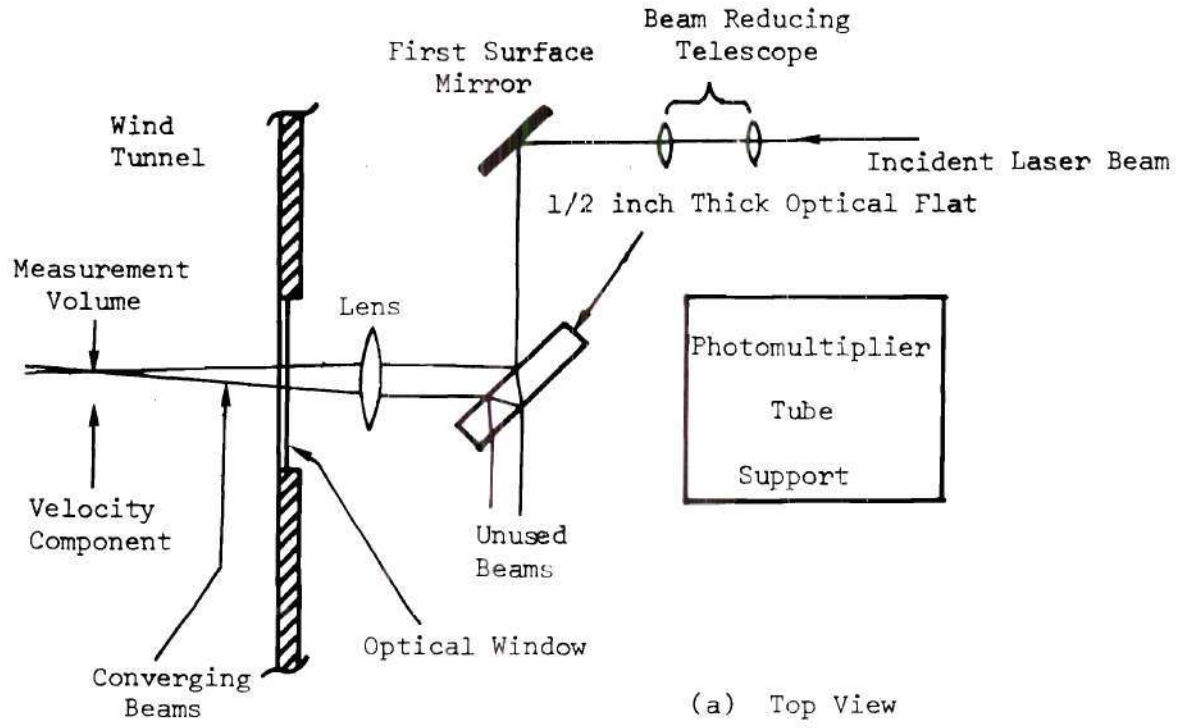

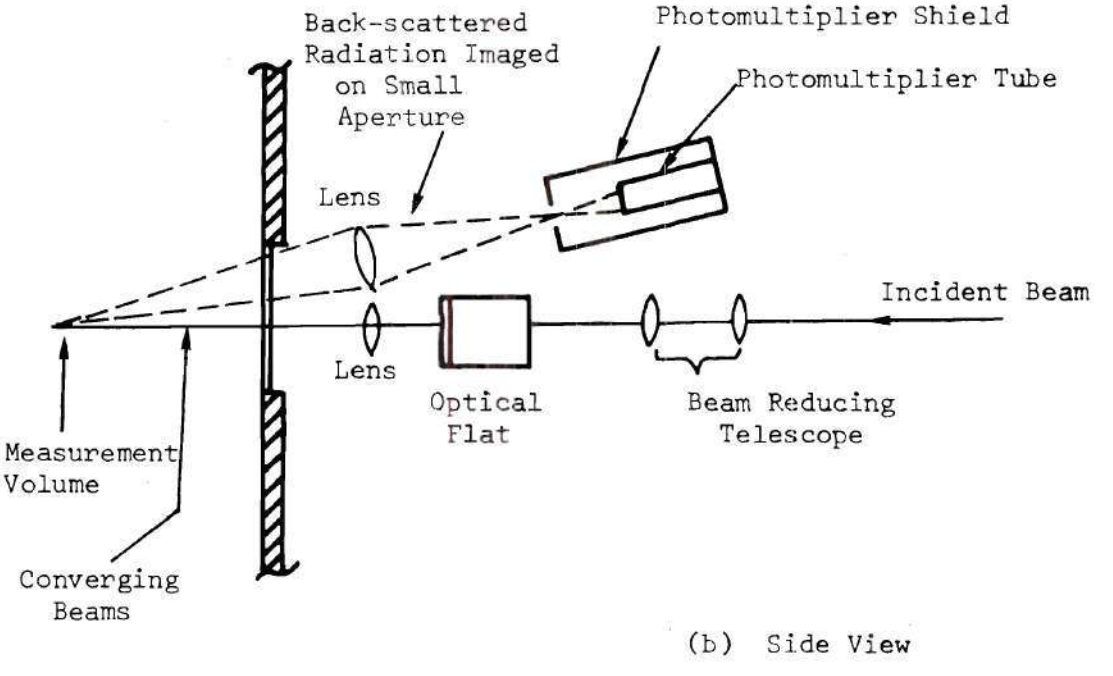

Figure 21. Interference Flowmeter--Backscatter from Smoke

reached the photomultiplier tube from particles not in the beam intersection region, producing useless low-pass signal and additional quantum noise.

In spite of the crudeness of the collecting optics the signal was detected with signal-to-noise ratio as high as was obtained in most of the heterodyne experiments. This was true even though the incident scattering power was much less than was used in the heterodyne experiments and the back scattered radiation was considerably weaker than the forward scattered radiation used in the heterodyne case. Figure 22(a) is a photographic record made of one of the signal pulses which occurred as a particle passed through the measurement region. Figure 22(b) shows a spectrum analyzer trace of signal plus noise and a second trace of dark current noise only obtained by covering the photomultiplier aperture. A large low-pass spectrum in the signal trace indicates the presence of scatterers not in the measurement region.

Considering the fact that a photodetector with less dark current noise would have improved the SNR, the fact that most of the available laser power was not used, and the fact that the collection optics were crude, one draws the conclusion that in some applications the interference flowmeter *is* capable of giving better signal-to-noise ratios using the weak back scattered light than can be obtained with a heterodyne flowmeter using the strong forward scattered light.

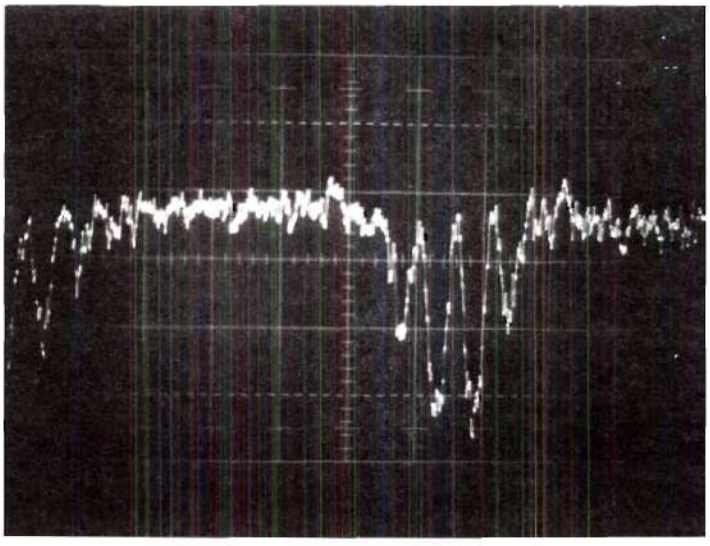

(a) Single Sweep Video Presentation of Signal, 0.1 ms/division.

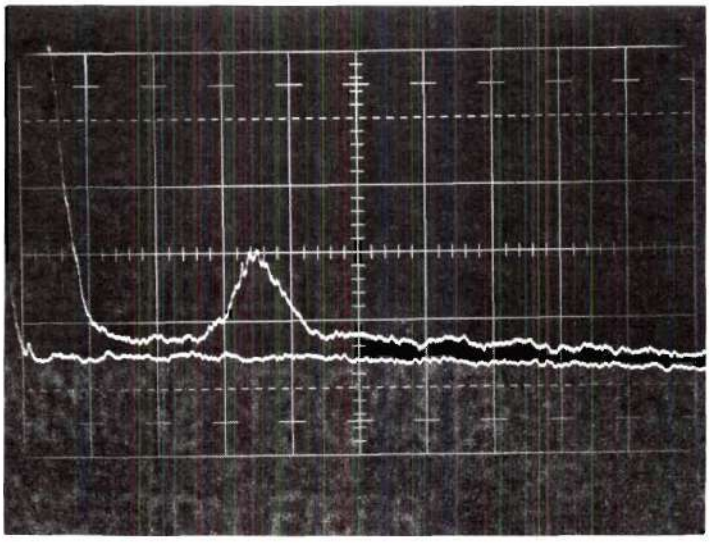

(b) Spectrum of Signal Plus Noise (Upper Trace); Dark Current Noise Alone (Lower Trace). Range is 0-100 KHz with Dispersion = 10 KHz/division.

Figure 22. Typical Signals from Interference Flowmeter

CHAPTER VIII

SUMMARY, CONCLUSIONS, AND RECOMMENDATIONS

The objective of this research has been to provide increased understanding of the interacting limitations of laser flowmeter systems imposed by the optical subsystem and the statistical nature of the signal which is produced at the photodetector. The research was to have been restricted to optical heterodyne flowmeters, employing a strong reference beam; the theoretical work led to the discovery of the interference flowmeter, however, which has also been investigated.

Summary and Conclusions

A generalized analysis of heterodyne flowmeter optical systems which does not depend on specific lens choices, apertures, and element positions, was presented in Chapter II. The generalized analysis was made possible by the discovery of a theorem concerning optical heterodyne detection systems in which the reference beam is sufficiently intense to produce a quantum-noise limited detected signal: "the effects on the signal current of any number of transmission filters in different z planes of the signal and/or reference waves may be replaced by a single equivalent reference beam with all filters removed." Using the generalized model of the optical system illustrated in Figure 4, a system response function for the flowmeter signal current was determined in terms of the scattering constant of a scatterer and the complex amplitudes of the incident scattering beam and equivalent reference beam

at the position of the scatterer. The form of the response function showed that the measurement volume is the region of intersection of the incident scattering beam and the *equivalent* reference beam. The size of the equivalent reference beam in the beam intersection region is *not* the same as the size of the actual reference beam in a Goldstein type system if apertures obstruct part of the reference beam before detection.

The flowmeter response function was expressed in terms of the complex amplitudes of the equivalent scattering and reference beams incident in the input planes in Figure 4. It was concluded that the optimum class of input-plane distributions for both the scattering and reference beams is the class of even, constant-phase, low-pass functions whose two-dimensional Fourier transforms are also constant-phase. Such an aperture distribution cannot actually be realized on a finite aperture, but this is of no practical consequence.

A definition of the flowmeter measurement region dimensions must be somewhat arbitrary since the region can never have sharp boundaries. The variation of the "height," "width," and "length" of the measurement region, as defined in the text and illustrated in Figure 5, was given by Equations (72) through (74) of Chapter II. It was shown that the height of the measurement region is inversely proportional to the height of the input distributions; and the width *and length* of the measurement region are inversely proportional to the width of the input distributions. This conclusion differs from a published opinion that the length of the measurement volume is proportional to the square of the f/number of the focussing lens.

The statistical aspects of heterodyne flowmeter signals and noise were presented in Chapter III. For the case of constant flow velocity the signal was found to be a wide-sense stationary random process whose mean, autocorrelation, and power spectrum were determined. The properties of the signal process were obtained by first deriving the mean and autocorrelation of a three-dimensional Poisson shot noise process. The signal power spectrum was determined in terms of a multiple convolution integral of the complex amplitude functions of the incident beams in the input planes of the generalized flowmeter. The result as given by Equation (3-66) showed that the signal bandwidth is reduced by decreasing the dimensions of the input-plane distributions at the expense of increased measurement volume dimensions.

Optical heterodyne detection noise theory was used with the statistical signal properties, which had been derived, to obtain expressions for the signal power to quantum noise power ratio (SNR) at the photodetector. The SNR was shown to be proportional to the scatterer number density, the effective mean scattering cross section, and the incident optical scattering power; and to be inversely proportional to the sine of the scattering angle.[†]

Chapter III is concluded with a derivation of the effect of laser intensity fluctuation noise on the optical heterodyne signal-to-noise

---

[†]This dependence on scattering angle results from the variation of the effective scattering volume with angle; variation due to the radiation patterns of the scatterers is included in the effective mean-square scattering cross section.

ratio. All discussions of optimum optical heterodyne SNR theory, which have been found in the literature, indicate that increasing the reference beam power will increase the SNR monotonically to a maximum constant value if an ideal non-saturable photodetector is assumed. It has been shown, however, that the detected laser intensity fluctuation noise power increases more rapidly than does the detected signal power and quantum noise power; if the signal spectrum lies within the low-pass spectral region of the reference beam intensity fluctuation noise, the SNR will be degraded by increasing the reference beam power.

In Chapter IV it was concluded that the class of constant-phase elliptical Gaussian input plane distributions is optimum for flowmeter applications. This subclass of the class of functions deduced in Chapter II was chosen because it can be efficiently produced by a laser operating in the TEM_{oo} mode and because it was heuristically shown to simultaneously minimize both the scattering volume dimensions and the signal bandwidth to the extent allowed by the Fourier transform uncertainty principle. Although it was not used in Chapter IV, a derivation of the propagating mode of an elliptical Gaussian beam has been presented in an appendix since the result will be useful to others.

The integral expressions of Chapter III for the heterodyne signal power spectrum and SNR were evaluated analytically to obtain algebraic expressions for the signal bandwidth and SNR for the case of elliptical Gaussian input-plane distributions. It was shown that the heights of the input-plane distributions should be chosen equal in order to obtain the maximum SNR for a fixed measurement region height.

The effects of small phase errors in the input plane distributions have been shown to be equivalent to small system misalignments. Within the approximations used in the derivations, small x-dependent phase errors were shown not to affect the SNR, however, y-dependent linear phase errors were shown to reduce the SNR exponentially, with the exponent being dependent on the vertical dimensions of the input plane distributions.

Chapter IV was concluded with a detailed analysis of heterodyne flowmeters with elliptical Gaussian input plane distributions in which the scattering angle is small and the velocity direction is transverse to the bisector of the scattering angle. This special case is pertinent to the measurement of high-speed flow in wind tunnels. It was shown that for this case the horizontal dimensions of the input-plane distributions should be equal in order to maximize the SNR obtainable with fixed measurement region width. Simplified algebraic expressions for the measurement region dimensions, the signal bandwidth, and the SNR were presented in Equations (4-52) through (4-54). From the results of this analysis it was concluded that optimum choices for the input plane distributions are equally-dimensioned elliptical distributions whose minor axes are essentially parallel to the direction of the flow velocity.

Chapter V described a simplified practical laser flowmeter optical system which is applicable when velocities are to be measured at short distances with a small scattering angle. This system, illustrated in Figure 7, requires almost no heterodyne alignment, is

insensitive to vibration, and automatically insures that the reference and scattering beam will have the desired equality of functional form in the input planes. The system was shown to be analytically equivalent to the generalized flowmeter model; it provides simple implementation for the optimum theoretical systems previously discussed.

In Chapter VI a new type of laser flowmeter was presented which has been designated as an interference flowmeter. Two coherent beams of equal intensity intersect to produce a sinusoidally varying intensity pattern in space. A scatterer passing through the region of beam intersection with constant velocity radiates light *in all directions* whose intensity varies sinusoidally in time with instantaneous frequency proportional to one vector component of the scatterer velocity.

Although the interference flowmeter signals are similar in many ways to those of the heterodyne flowmeter they have several unique dissimilarities. No heterodyne conversion gain is present, so a critically aligned spatial filter is required to prevent radiation from scatterers not in the beam intersection region from reaching the photodetector. For high scatterer number densities the system response is not linear as is the heterodyne flowmeter response. The SNR is limited either by photodetector dark current noise or by dependent quantum noise, as compared with the heterodyne flowmeter limitation by independent quantum noise; however, the analysis of the interference flowmeter SNR was not carried far enough to establish the conditions under which interference flowmeters will produce SNR's greater than those produced by equivalent heterodyne flowmeters. A major advantage of the interference flowmeter

is the flexibility of use which derives from the fact that photodetection optics are not required to be placed in the forward-scatter direction. Several new applications were discussed which are not possible with heterodyne flowmeters; for example, the back-scattered radiation may be used to measure transverse velocities near an opaque test model in a wind tunnel which would block the signal radiation in a heterodyne flowmeter.

Experimental work was reported in Chapter VII. The variation of the heterodyne flowmeter SNR and signal bandwidth was measured for lossy and lossless variations of the input beam dimensions and for variations of the flow velocity magnitude and direction. The experimental results supported the predictions of the heterodyne flowmeter theory. The experiments were performed with a simplified heterodyne flowmeter optical system, theoretically described in Chapter V, and the predicted stability and ease of heterodyne alignment was obtained.

Three feasibility experiments with interference flowmeter systems were also reported in Chapter VII. The transverse velocity of a rough surface was measured by back-scattered radiation. The velocity of smoke was measured using both forward-scattered and back-scattered radiation. The signal-to-noise ratio of the back-scatter experiment with smoke was comparable with those obtained with the forward-scatter heterodyne system in spite of the fact that an order of magnitude less scattering power was available and the fact that the back-scattered radiation was considerably less intense than the forward-scattered radiation.

Recommendations for Future Work

Not all of the theoretical results of this dissertation were verified experimentally. In particular, predictions concerning improved heterodyne flowmeters using elliptical Gaussian beams could not be verified since the cylindrical lenses acquired for that purpose did not prove to be of sufficient quality. Experimental verification of the predictions concerning the measurement region dimensions would also be desirable.

The interference flowmeter has shown such promise that it deserves further theoretical and experimental study.

Nowhere in the literature has anyone considered the problem of determining the optimum heterodyne flowmeter *electronics* from a statistical communications theory point of view. For the case of time-varying flow, the flowmeter signal is a *randomly-sampled* amplitude and frequency modulated signal. The randomness of the signal insures a certain statistical error in the measurement process even in the absence of all noise (which is never the case). If a theoretical optimum detection system cannot be found, there should at least be a study of the expected magnitude of the system error for different specific types of detection systems. The statistical work presented in Chapter III should serve as a starting point for such research.

APPENDIX

APPENDIX A

HETERODYNE REFERENCE BEAM AS AN EQUIVALENT SPATIAL FILTER

In this appendix it will be proved that the effect of any spatial filter arrangement, consisting of thin transmission filters, on the signal detected by an optical heterodyne receiver may be duplicated by using an equivalent reference beam. The proof is obtained by demonstrating the method of determining the equivalent reference beam.

Figure 23(a) illustrates a heterodyne receiver in which the signal wave, u_s, is processed by n transmission filters, $t_1(x,y)$, $t_2(x,y)\ldots\ t_n(x,y)$, before being mixed with a reference wave u_r. The time variation of the signal wave is not shown explicitly. The effect of the beam splitter is to attenuate each beam by a constant and rotate the direction of propagation of the reference beam. Neglecting the attenuation factors, an equivalent reference beam may be postulated to exist in the input ($z = 0$) plane which propagates to the detector surface without being affected by the filters. This equivalent reference beam has complex amplitude in the input plane determined by inverse propagation as:

$$u_r(x,y,0) = h^*(x,y,z_d) * u_r(x,y,z_d) \qquad (1)$$

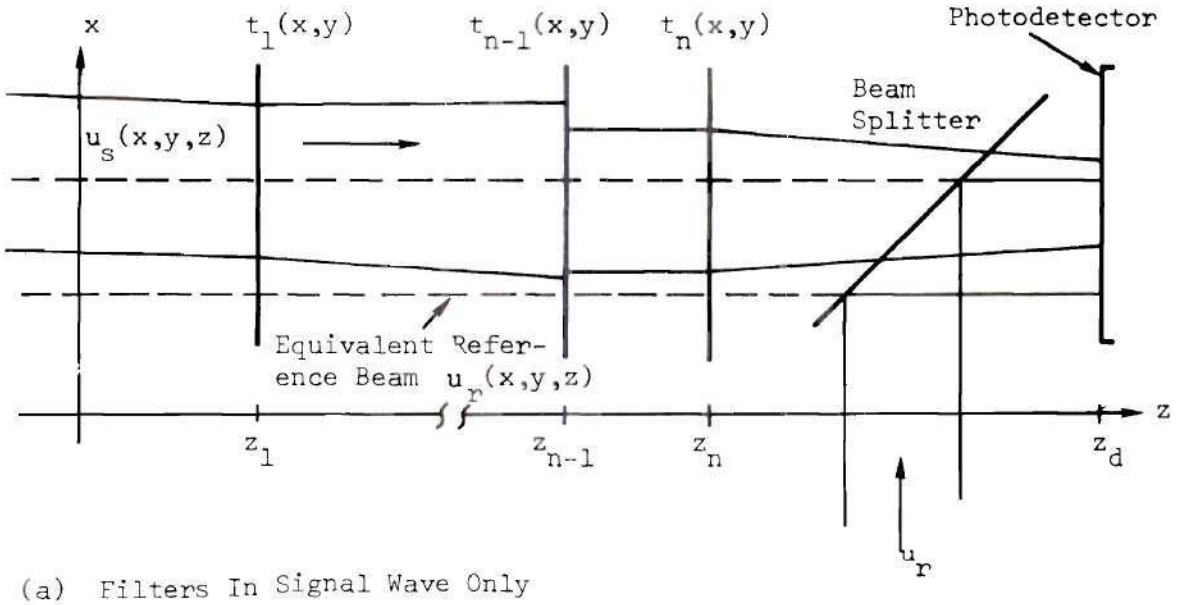

(a) Filters In Signal Wave Only

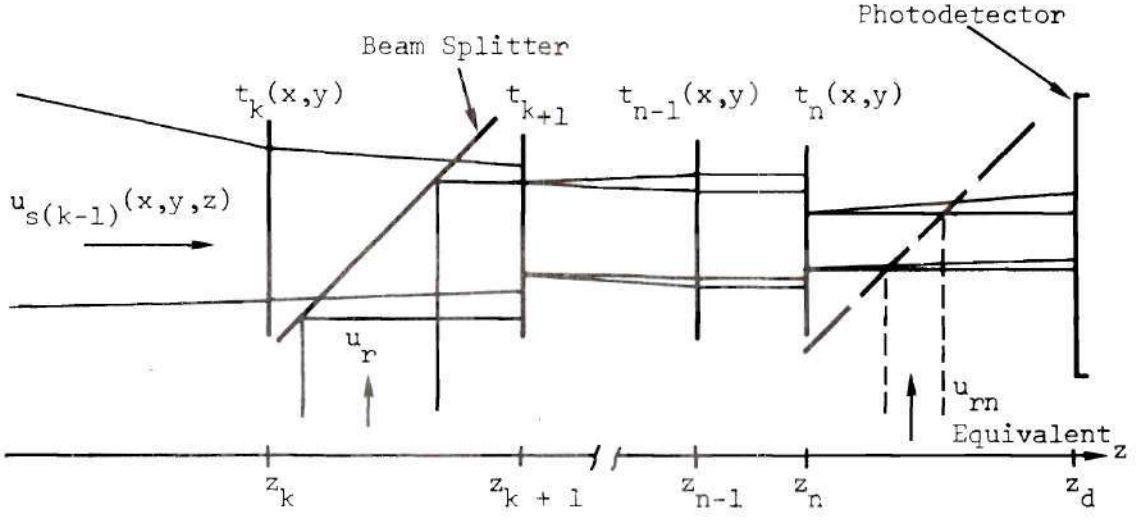

(b) General Case: Filters Before and After Mixing

Figure 23. Equivalent Heterodyne Reference Beams

The complex signal current i_s is calculated as:

$$i_s = N\iint u_{sn}(x,y,z_d)\ u_r^*(x,y,z_d)\ dxdy = N\iint u_{sn}(x,y,z_n^+)\ u_r^*(x,y,z_n^+)\ dxdy \quad (2)$$

with the right hand equality following from the fact that the detector placement is immaterial after the last filter. Now the function $u_{sn}(x,y,z_n^+)$ is given by

$$u_{sn}(x,y,z_n^+) = t_n(x,y)\ u_{s(n-1)}(x,y,z_n^-) \quad (3)$$

so

$$i_s = \iint [u_{s(n-1)}(x,y,z_n^-)][t^*(x,y)\ u_r(x,y,z_n^-)]^* dxdy \quad (4)$$

The grouping of the last expression is chosen to point out that the same signal current would have been obtained had the reference beam been passed through a conjugate filter $t^*(x,y)$ at the same distance from the photodetector. Going one step further, an equivalent reference beam u_r^1, having no filter present, may be determined as

$$u_r^1(x,y,z_n) = t_n^*(x,y)\ u_r(x,y,z_n) \quad (5)$$

so at the input plane the complex amplitude of the equivalent reference beam is

$$u_r^1(x,y,0) = h^*(x,y,z_n) * [t_n^*(x,y)u_r(x,y,z_n)] \tag{6}$$

If now $u_r(x,y,0)$ is replaced by $u_r^1(x,y,0)$ and the filter $t_n(x,y)$ is removed entirely, the complex signal current is not altered at all. The detector surface may now be moved up to the position immediately past $t_{n-1}(x,y)$ without affecting i_s, since $t_n(x,y)$ is no longer present. This situation duplicates the original one with one filter removed. The same steps may be used recursively with the modification of the equivalent reference beam at each step given by

$$u_r^{k+1}(x,y,0) = h^*(x,y,z_{n-k}) * [t^*_{n-k}(x,y)\, u_r^k(x,y,z_{n-k})] \tag{7}$$

until $u_r^n(x,y,0)$ is determined and all filters have been removed.

Having determined the final equivalent reference beam, $u_r^n(x,y,z)$, such a beam may be added to the incident signal wave at any plane after the signal wave has been generated and the filtered wave will be detected by any photodetector surface of infinite extent which follows. The required photodetector shielding has no effect so long as negligible reference beam power is obstructed.

In most heterodyne receiver configurations some spatial filters will be placed after the beams have been mixed as shown in Figure 23(b). A photodetector shield which does obstruct part of the reference beam is an example. In this more general case, the equivalent input reference beam may still be determined. To do this one first calculates the reference beam complex amplitude at the photodetector plane as

follows:

$$u_r(x,y,z_{k+1}^-) = h(x,y,z_{k+1}) * u_r(x,y,0) \tag{8}$$

$$u_{r(k+1)}(x,y,z_{k+1}^+) = u_{r(k+1)}(x,y,z_{k+1}^-)\, t_{k+1}(x,y) \tag{9}$$

$$u_{r(k+1)}(x,y,z_{k+2}^-) = u_{r(k+1)}(x,y,z_{k+1}^+) * h(x,y,z_{k+2} - z_{k+1}) \tag{10}$$

This process is continued until $u_{rn}(x,y,z_d)$ is determined in terms of $u_r(x,y,0)$ and the (n-k) filters. Having done this, an equivalent reference beam which does not pass through the filters may be assumed to be added by a beam splitter, shown dashed in Figure 23(b), in front of the last filter. The equivalent complex amplitude at the input plane is

$$u_r^o(x,y,0) = h^*(x,y,z_d) * u_{rn}(x,y,z_d) \tag{11}$$

The situation is now identical to that shown in Figure 23(a) and the process may be continued as previously described. Thus it has been shown that the general spatial filter arrangement shown Figure 23(b), which includes all possible combinations of thin lens and apertures with dimensions much larger than the optical wavelength, can be eliminated by using a single unobstructed reference beam.

Some other observations should be made. The equivalence shown here is for the signal current and does not hold for the DC current

which is proportional to the total reference beam power. One observes, however, that the iterative procedure given above for determining the equivalent reference beam always attenuates or leaves unchanged the total reference beam power. This is true because $|t(x,y,|\leq 1$ for any passive filter. Since the quantum noise is proportional to the reference beam power, the use of the equivalent reference beam corresponds to the maximum possible signal-to-noise ratio for a given signal wave and spatial filtering choice.

APPENDIX B

ELIMINATION OF THE R_{i2} TERM FROM THE SIGNAL AUTOCORRELATION

The signal autocorrelation $R_i(\tau;\bar{v})$ was presented in Equation (3-44) as the sum of two integral expressions which have been denoted $R_{i1}(\tau;\bar{v})$ and $R_{i2}(\tau;\bar{v})$. The first term, $R_{i1}(\tau;\bar{v})$ was expressed in terms of separable input-plane distributions in (3-57). The corresponding expression for $R_{i2}(\tau;\bar{v})$ is presented below and then shown to vanish when practical restrictions are imposed.

From Equation (3-49), (3-55), and (3-56) one obtains

$$R_{i2}(\tau;\bar{v}) = \frac{MN^2E[C_p^2]e^{-j2\pi f_d\tau}}{\lambda F|\sin\theta|} \tag{1}$$

$$\cdot \int U_{ioy}(f_y)U^*_{roy}(f_y)U_{ioy}(f_y + C_y\tau)U^*_{roy}(f_y + C_y\tau)df_y$$

$$\cdot \int U_{iox}(f_{x'})U_{iox}(f_{x'} + C_{x'}\tau)e^{-j4\pi F\tan(\theta/2)f_{x'}}df_{x'}$$

$$\cdot \int U^*_{rox}(f_{x''})U^*_{rox}(f_{x''} + C_{x''}\tau)e^{-j4\pi F\tan(\theta/2)f_{x''}}df_{x''}$$

Attention is now restricted to the last two integrals of (1). Details are presented only for the first of these, denoted by $q_2(\tau)$, since the

other one vanishes in a similar manner. Thus

$$q_2(\tau) = \int U_{iox}(f_{x'})U_{iox}(f_{x'} + C_{x'}\tau)e^{j2\pi f_{x'}a} df_{x'} \qquad (2)$$

where

$$a = -2F \tan(\theta/2) \qquad (3)$$

Equation (2) is recognized as an inverse Fourier transform with the result that the shifting and convolution theorems may be used to obtain

$$q_2(\tau) = u_{iox}(a) * u_{iox}(a)e^{-j2\pi aC_{x'}\tau} \qquad (4)$$

The temporal Fourier transform of $q_2(\tau)$ will be denoted by $Q_2(f)$. If $Q_2(f)$ is zero for all frequencies, then $q_2(\tau) = 0$. Thus after interchanging the order of integration one has

$$Q_2(f) = \int u_{iox}(b)u_{iox}(a-b) \int e^{-j2\pi bC_{x'}\tau} e^{-j2\pi f\tau} d\tau \; db \qquad (5)$$

$$= \int u_{iox}(b)u_{iox}(a-b)\, \delta(f + C_{x'}b)db \cdot$$

Using the property of delta functions that

$$\delta(f+C_{x'},b) = \frac{1}{|C_{x'}|}\,\delta(b+f/C_{x'},) \tag{6}$$

and the sifting property, one evaluates (5) as

$$Q_2(f) = \frac{1}{|C_{x'}|}\,u_{iox}(a+f/C_{x'},)u_{iox}(-f/C_{x'},) \tag{7}$$

Recalling (3), the result is

$$Q_2(f) = \frac{1}{|C_{x'}|}\,u_{iox}[f/C_{x'} - 2F\tan(\theta/2)]\,u_{iox}[-f/C_{x'},] \tag{8}$$

Figure 24 re-illustrates the optical input geometry. The figure illustrates the fact that it is physically not possible for the input beam radii to exceed F tan (θ/2) in the xz plane at the lenses since the lenses would then necessarily simultaneously occupy the same space. This restriction is removed in the optical system of Chapter V, but it is still undesirable for the beams to overlap at the focussing lens. This is true because the signal spectrum would then be excessively broad. Since the radius of an incident beam with constant phase in the input plane is less in the input plane than at the lens plane, it is assumed that

$$u_{iox}(x') = 0 \quad , \quad x' \leq -F\tan(\theta/2) \tag{9}$$

Thus

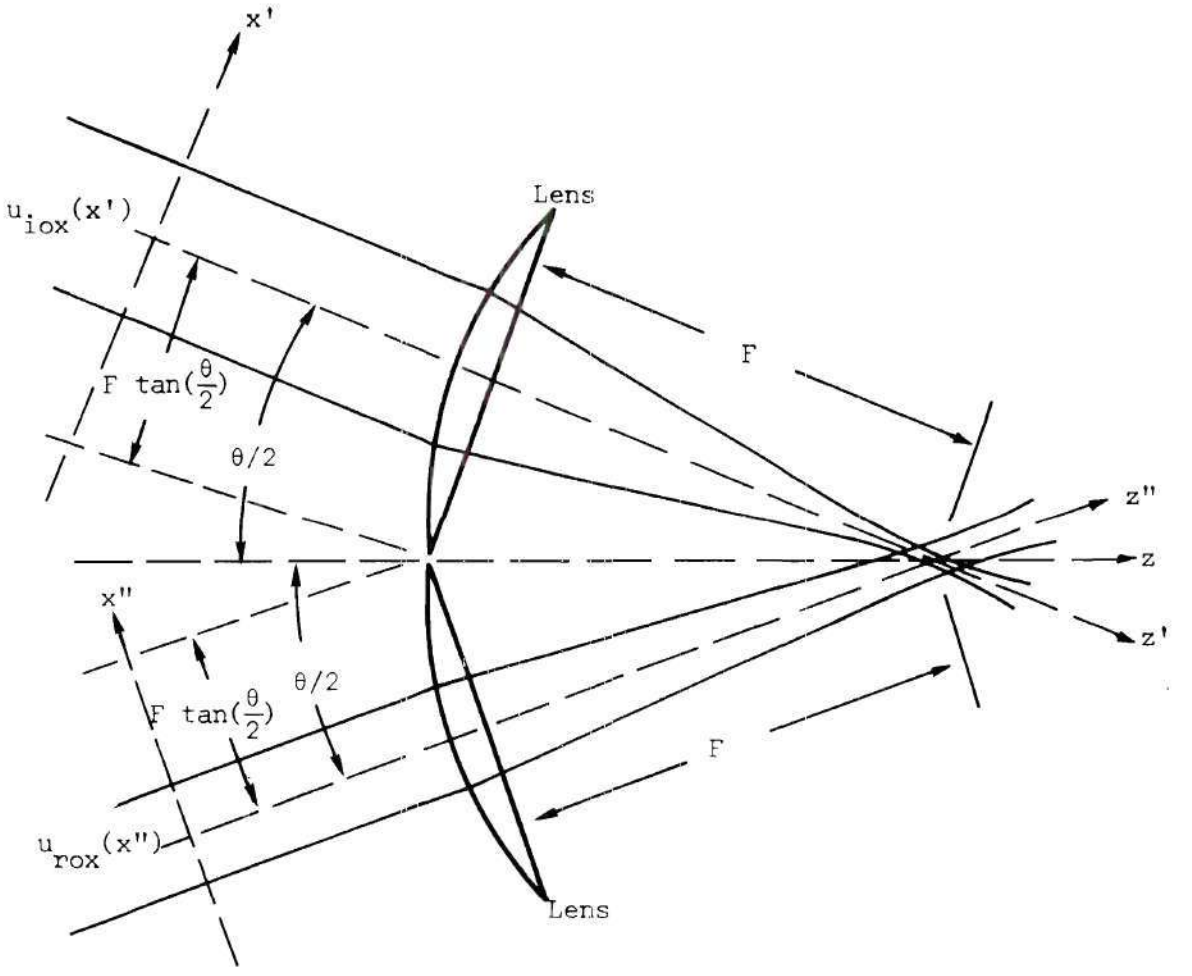

Figure 24. Heterodyne Flowmeter Input Geometry

$$u_{iox}(-f/C_{x'}) = 0 \quad , \quad f \geq C_{x'} F \tan(\theta/2) \tag{10}$$

and

$$u_{iox}[f/C_{x'} - 2F \tan(\theta/2)] = 0 \quad , f \leq C_{x'} F \tan(\theta/2) \tag{11}$$

so $Q_2(f) = 0$ for all values of f.

This result implies that $R_{i2}(\tau,\bar{v})$ is zero for practical flowmeters.

APPENDIX C

EFFECT OF BROADBAND LOW-PASS LASER INTENSITY FLUCTUATION NOISE ON THE OPTICAL HETERODYNE SNR

This appendix gives a brief theoretical derivation which includes the effect of the laser intensity fluctuation noise on the heterodyne SNR. The results show that the effect of laser intensity fluctuation noise is to produce low-pass noise in the photodetector output which increases as the square of an increase in reference beam power while the detected signal power and quantum-noise power increase is only linear. The intensity fluctuation noise would affect the detection of any type of signal modulation because the noise is additive in the output photocurrent.

The analysis will be simplified by the assumption that at the photodetection plane the signal and reference beams are perfectly aligned and equal in spatial variation. The complex envelope of the reference wave is given by

$$u_r(x,y,t) = \sqrt{P_r}\, u(x,y,t) \tag{1}$$

and the complex envelope of the signal wave is

$$u_s(x,y,t) = \sqrt{P_s}\, s(t)u(x,y,t) \tag{2}$$

where P_r and P_s are the total average powers of the reference beam and signal beam, respectively, with

$$P_r >> P_s \ ; \tag{3}$$

and where s(t) is an independent, narrow-band, complex modulation process with

$$E[s(t)] = 0 \tag{4}$$

and

$$E[s^2(t)] = 1 \tag{5}$$

The function u(x,y,t) is the common factor of both u_r and u_s which contains the matched spatial variation and the undesired laser noise modulation. This function is assumed to satisfy

$$\iint |u(x,y,t)|^2 \, dxdy = 1 + n(t) \tag{6}$$

where n(t) is an independent, zero-mean intensity fluctuation noise process with autocorrelation

$$R_n(\tau) = E[n(t)n(t + \tau)] \tag{7}$$

and low-pass power spectrum

$$S_n(f) = T[R_n(\tau)] \tag{8}$$

The intensity fluctuation is assumed to be only a small per cent of the total average source power so that

$$E[n^2(t)] \ll 1 \tag{9}$$

The current produced by the photocathode is

$$i(t) = N\iint \left| \sqrt{P_r}\, u(x,y,t) + \sqrt{P_s}\, s(t)u(x,y,t) \right|^2 dxdy \tag{10}$$

$$\approx N[1 + n(t)]\,(P_r + \sqrt{P_r P_s}\,[s(t) + s^*(t)])$$

$$\approx N\left[P_r + P_r n(t) + \sqrt{P_r P_s}\; s^r(t)\right]$$

$$= i_{dc} + i_{dc} n(t) + i_s(t)$$

The last result of (10) is obtained by neglecting two small terms and by defining a real, zero-mean signal process $s^r(t)$ given by

$$s^r(t) = s(t) + s^*(t) \tag{11}$$

One observes that the processes $n(t)$ and $i_s(t)$ are uncorrelated.

The autocorrelation $R(\tau)$ of the detected photocurrent is

$$R(\tau) = i_{dc}^2 + i_{dc}^2 R_n(\tau) + R_i(\tau) \tag{12}$$

where $R_i(\tau)$ and $R_n(\tau)$ are the autocorrelations of the detected signal current and the intensity noise process $n(t)$ respectively.

The power spectrum $S(f)$ of the photocurrent, including the independent white photon noise which has been omitted to this point, is

$$S(f) = i_{dc}^2 \delta(f) + i_{dc}^2 S_n(f) + S_i(f) + ei_{dc} \tag{13}$$

Assuming that the wide-band low-pass intensity noise is essentially constant in power density over the bandwidth of the narrow-band signal spectrum, the total signal power to noise power in the "noise bandwidth" is

$$SNR = \frac{S_i(f_c)}{ei_{dc} + i_{dc}^2 S_n(f_c)} \tag{14}$$

where f_c is the center signal frequency.

In the case of the heterodyne flowmeter the center frequency of the signal is f_d and the power spectrum of the signal is $S_i(f,\bar{v})$. Even though the scattered wave in a heterodyne flowmeter is not spatially matched to the reference wave as was the signal wave considered in this

appendix, it is assumed that the intensity fluctuation noise is added to the quantum noise in a heterodyne flowmeter in the same way. An increase in reference beam power produces a linear increase in $S_i(f_d;\bar{v})$ and in i_{dc}; hence the SNR decreases with increasing reference beam power because of the $i_{dc}^2 S_n(f_d)$ term if $S_n(f_d)$ is non-zero.

APPENDIX D

PROPAGATION OF THE ELLIPTICAL GAUSSIAN BEAM

It is assumed that the complex amplitude distribution in the front focal plane of a spherical lens of focal F and large diameter is given by

$$u_o(x,y) = \frac{e^{-\left[\frac{x^2}{w_{ox}^2} + \frac{y^2}{w_{oy}^2}\right]}}{\sqrt{\frac{\pi}{2} w_{ox} w_{oy}}} \tag{1}$$

where w_{ox} and w_{oy} are real constants. The beam power is normalized to unity, i.e.,

$$\iint |u(x,y)|^2 \, dxdy = 1 \tag{2}$$

The back focal plane distribution may be obtained directly as a scaled Fourier transform of $u_o(x,y)$ as indicated in the text. In order to obtain the propagating field, Equation (2-24) is used. Thus

$$u(x,y,z) = \frac{e^{jKz}}{\lambda F \sqrt{\frac{\pi}{2} w_{ox} w_{oy}}} \tag{3}$$

$$\cdot \iint e^{-\left[\frac{a^2}{w_{ox}^2} + \frac{b^2}{w_{oy}^2}\right] - \frac{jKz}{2F^2}(a^2 + b^2) - j\frac{2\pi}{\lambda F}(ax + by)} \; dadb$$

where the z = 0 plane is the back focal plane of the lens. The integral is separable and only one factor, I_x, need be considered. Hence one evaluates

$$I_x = \int e^{-\left[\frac{1}{w_{ox}^2} + \frac{jKz}{2F^2}\right]a^2 - j2\pi a f_x} \; da \tag{4}$$

where $f_x = \frac{x}{\lambda F}$. The integral is the Fourier transform of a complex Gaussian function $e(x,\sigma_x^2)$ where

$$e(x,\sigma_x^2) = e^{-\frac{x^2}{2\sigma_x^2}} \tag{5}$$

with

$$\frac{1}{\sigma_x^2} = \frac{2}{w_{ox}^2} + j\frac{Kz}{F^2} \tag{6}$$

It is known† that, if Re $[1/\sigma_x^2] > 0$, then

†See Fourier transform pair 708, Table 1, Fourier Integrals by Foster and Campbell.[30]

$$I_x = T[e(x,\sigma_x^2)] = \sqrt{2\pi}\,\sigma_x\, e^{-\frac{(2\pi F_x)^2\sigma_x^2}{2}} \tag{7}$$

The magnitude and phase of σ_x can be calculated from (6) as

$$\sigma_x = \frac{w_{ox}\, e^{-j\frac{1}{2}\tan^{-1}\left[\frac{Kzw_{ox}^2}{2F^2}\right]}}{\sqrt{2}\left[1+\frac{K^2z^2w_{ox}^4}{4F^4}\right]^{1/4}} \tag{8}$$

while σ_x^2 is obtained from (6) as

$$\sigma_x^2 = \frac{w_{ox}^2 F^2(2F^2 - jKzw_{ox}^2)}{4F^2 + K^2z^2w_{ox}^4} \tag{9}$$

A new constant w_x is now defined as

$$w_x = \frac{2F}{Kw_{ox}} = \frac{\lambda F}{\pi w_{ox}} \tag{10}$$

where

$$K = \frac{2\pi}{\lambda} \tag{11}$$

Thus the factor $\sqrt{2\pi}\ \sigma_x$ in (7) becomes from (8)

$$\sqrt{2\pi}\ \sigma_x = \frac{\lambda F\ e^{-j\frac{1}{2}\tan^{-1}\left[\frac{\lambda z}{\pi w_x^2}\right]}}{\sqrt{\pi}\ w_x\left[1+\left(\frac{\lambda z}{\pi w_x^2}\right)^2\right]^{1/4}} = \frac{\lambda F\ e^{-j\phi_x(z)}}{\sqrt{\pi w_x}\ \sqrt{W_x(z)}} \tag{12}$$

where

$$\phi_x(z) = \frac{1}{2}\tan^{-1}\left[\frac{\lambda z}{\pi w_x^2}\right] \tag{13}$$

and

$$W_x(z) = w_x\sqrt{1+\left[\frac{\lambda z}{\pi w_x^2}\right]^2} \tag{14}$$

Now from (9) the exponent, $-(2\pi f_x)^2\ \sigma_x^2/2$, in (7) becomes

$$-\frac{(2\pi f_x)^2\ \sigma_x^2}{2} = -\frac{x^2}{W_x^2(z)} + \frac{jKx^2}{2R_x(z)} \tag{15}$$

where $R_x(z)$, the radius of phase curvature, is defined by

$$R_x(z) = z\left[1 + \left(\frac{\pi w_{ox}^2}{\lambda z}\right)^2\right] \tag{16}$$

and $W_x(z)$, the beam radius, is given by (14) as before.

Returning to (3), the field beyond the lens is now determined as

$$u(x,y,z) = \frac{e^{jKz}}{\lambda F\sqrt{\frac{\pi}{2} w_{ox}w_{oy}}} \cdot \frac{(\lambda F)^2}{\pi\sqrt{w_x w_y}\ \sqrt{W_x(z)W_y(z)}} \tag{17}$$

$$\cdot e^{-\left[\frac{x^2}{W_x^2(z)} + \frac{y^2}{W_y^2(z)}\right] + j\frac{K}{2}\left[\frac{x^2}{R_x(z)} + \frac{y^2}{R_y(z)}\right] - j\left[\phi_x(z) + \phi_y(z)\right]}$$

Once again using (10), the premultiplying constant may be reduced somewhat, so that one obtains

$$u(x,y,z) = \frac{e^{jKz}}{\sqrt{\frac{\pi}{2} W_x(z)W_y(z)}} \tag{18}$$

$$\cdot e^{-\left[\frac{x^2}{W_x^2(z)} + \frac{y^2}{W_y^2(z)}\right] + j\frac{K}{2}\left[\frac{x^2}{R_x(z)} + \frac{y^2}{R_y(z)}\right] - j\left[\phi_x(z) + \phi_y(z)\right]}$$

where the terms $\phi_x(z)$, $W_x(z)$, and $R_x(z)$ are given by (13), (14), and

(16) respectively. The corresponding y terms are identical, but with y subscripts.

Anyone familiar with the TEM_{oo} Gaussian laser mode will recognize (18) as a generalization of the circular Gaussian laser beam. Equation (18) reduces to the scaled Fourier transform of the input distribution in the z = 0 plane.

It is interesting to note that the major axis of the beam ellipse is rotated 90° in the transformation from the front focal plane to the back focal plane, but the aspect ratio remains the same, i.e.,

$$\frac{w_{ox}}{w_{oy}} = \frac{w_y}{w_x} \tag{19}$$

One also observes that the geometric mean radii $w_o = \sqrt{w_{ox} w_{oy}}$ and $w = \sqrt{w_x w_y}$ also obey the same inverse radius law, i.e.,

$$w_o = \frac{\lambda F}{\pi w} \tag{20}$$

Because of the above relations, it is possible to obtain the symmetric situation in which the input plane radii and the focal plane radii have the same dimensions, i.e.,

$$w_{ox} = w_y \quad , \quad w_{oy} = w_x \tag{21}$$

This occurs when the mean radius is given by

$$w_o = \sqrt{\frac{\lambda F}{\pi}} \tag{22}$$

with the result that the beam is <u>circular</u>, at the lens with

$$W_x(-F) = W_y(-F) = \sqrt{w_{ox}^2 + w_{oy}^2} \tag{23}$$

BIBLIOGRAPHY

1. Y. Yeh and H. Z. Cummins, "Localized Fluid Flow Measurements with An He-Ne Laser Spectrometer," Applied Physics Letters, Vol. 4, No. 10, p. 176, (May 1964).

2. J. W. Foreman, Jr., E. W. George, J. L. Jetton, R. D. Lewis, J. R. Thornton, and H. J. Watson, "Fluid Flow Measurements with a Laser Doppler Velocimeter, IEEE Journal of Quantum Electronics, Vol. QE-2 No. 8, 260, (August 1966). See also NASA Reports N65-26015, N66-22338.

3. H. J. Watson, R. D. Lewis, and J. R. Thornton, "Laser Doppler Velocimeter Measurements of Velocity Profiles in Liquids," Brown Engineering Research Laboratories Technical Note R-224, October 1966.

4. J. W. Foreman, Jr. and J. R. Thornton, "Frequency Distribution in the Laser Doppler Velocimeter Heterodyne Signal," Brown Engineering Research Laboratories Technical Note R-225, October 1966.

5. J. W. Foreman, Jr., "Optical Path Length Difference Effects in Photomixing with Multimode Gas Laser Radiation," Applied Optics, Vol. 6, No. 5, 821, (May 1967).

6. E. Rolfe and R. M. Huffaker, "Part 1. Laser Doppler Velocity Instrumentation for Wind Tunnel Turbulence and Velocity Measurements," NASA Report N68-18099.

7. E. Rolfe, J. K. Silk, S. Booth, K. Meister, and R. M. Young, "Laser Doppler Velocity Instrument" NASA Report CR-119.

8. N. E. Welch and W. T. Tomme, "The Analysis of Turbulence from Data Obtained with a Laser Velocimeter," AIAA Fifth Aerospace Sciences Meeting, New York, N.Y., January 23-26, 1967.

9. J. I. Shipp, R. H. Hines, W. A. Dunnill, "Development of a Laser Velocimeter System" Arnold Engineering Development Center Report No. AEDC-TR-67-175.

10. W. A. Dunnill, J. I. Shipp, R. H. Hines, "Range Extension and Component Resolution of the Laser Velocimeter," Arnold Engineering Development Center Report No. AEDC-TR-67-195.

11. J. D. Fridman, R. M. Huffaker, and R. F. Kinnard, "Laser Doppler System Measures Three-Dimensional Vector Velocity and Turbulence," Laser Focus, Vol. 4, No. 21, 34, (November 1968).

12. R. J. Goldstein and D. K. Kreid, "Measurement of Laminar Flow Development in a Square Duct Using a Laser Doppler Flowmeter," Transactions of the ASME, Journal of Applied Mechanics, December 1967, p. 813.

13. R. J. Goldstein and W. F. Hagen, "Turbulent Flow Measurements Utilizing the Doppler Shift of Scattered Laser Radiation," Physics of Fluids, Vol. 10, No. 6, 1349, (June 1967).

14. David L. Morrow, Application of a Laser Doppler Velocity Meter to Fluid Flow and Particle Size Distribution Measurements, A Master's Thesis, Dept. of Chemical Engineering, Case Western Reserve University, June 1968.

15. Robert L. Bond, Contributions of System Parameters in the Doppler Method of Fluid Velocity Determination," A Ph.D. Dissertation, University of Arkansas, 1968.

16. Monte Ross, Laser Receivers, Devices, Techniques and Systems, John Wiley and Sons, Inc., New York, N. Y., 1966.

17. B. M. Oliver, "Thermal and Quantum Noise," Proceedings of the IEEE, Vol. 53, 436 (May 1965).

18. M. C. Teich, "Infrared Heterodyne Detection," Proceedings of the IEEE, Vol. 56, No. 1, 37 (January 1968).

19. A. E. Siegman, "The Antenna Properties of Optical Heterodyne Receivers," Proceedings of the IEEE, Vol. 54, No. 10, 1350 (October 1966).

20. R. N. James, W. R. Babcock, H. S. Seifert, "A Laser-Doppler Technique for the measurement of Particle Velocity," AIAA Journal Vol. 6, No. 1, 160. (January 1968). For full details see "Application of a Laser-Doppler Technique to the Measurement of Particle Velocity in Gas-Particle Two Phase Flow," by same authors, Air Force Rocket Propulsion Lab., Edwards Air Force Base, California TR-66-119 (May 1966). Also, Stanford University Department of Aeronautics and Astronautics Report SUDAAR 265 (June 1966).

21. J. W. Goodman, Introduction to Fourier Optics, New York, McGraw-Hill, 1968.

22. A. Papoulis, Systems and Transforms with Applications in Optics New York, McGraw-Hill, 1968.

23. A. Vander Lugt, "An Analysis of Coherent Optical Systems Using Operational Notation," Chapter 5, University of Michigan Engineering Summer Conference, Introduction to Optical Data Processing, 1968.

24. G. W. Stroke, An Introduction to Coherent Optics and Holography, New York, New York, Academic Press, 1966.

25. M. Born and E. Wolf, Principles of Optics, New York, Pergamon Press, 1964.

26. J. W. Goodman, "Statistical Properties of Laser Sparkle Patterns," Systems Techniques Laboratory, Stanford Electronics Laboratories, Stanford University Technical Report No. 2303-1, December 1963. (Also has report numbers SSD-TDR-64-58 and SEL-63-140).

27. E. Parzen, Modern Probability Theory and its Applications, New York, John Wiley and Sons, 1960.

28. A. Papoulis, Probability, Random Variables, and Stochastic Processes, New York, McGraw-Hill, 1965.

29. H. Kogelnik and T. Li, "Laser Beams and Resonators," Proceedings of the IEEE, Vol. 54, 1312, (October 1966).

30. R. N. Foster and G. A. Campbell, Fourier Integrals for Practical Applications, D. Van Nostrand, New York, 1948.

31. M. J. Mazumder, "Signal-to-Noise Ratio and Instrumental Broadening of the Doppler Shifted Signal in Velocity Measurement," Informal Status Progress Report for NASA Grant SC-NGR-04-001-015 for period ending June 30, 1968. NASA Accession No. X69-10039.

32. J. S. Bendat and A. G. Piersol, Measurements and Analysis of Random Data, John Wiley and Sons, Inc., New York, 1966.

VITA

William Taylor Mayo, Jr. was born in Tallahassee, Florida, on November 11, 1941. He is the son of William Taylor Mayo and Elizabeth Blalock Mayo. He was married to Mary Ann Jennings of Tallahassee, Florida, on August 3, 1963, and has one son.

He attended public school in Tallahassee, Florida, where he graduated from Leon High School in 1959. In 1964 he received his B.E.E. Degree and in 1966 his M.S.E.E. Degree, both from Georgia Institute of Technology. He was awarded the M.A. Ferst Award by the Georgia Tech Chapter of Sigma Xi for his Master's thesis research in 1966.

As an undergraduate he worked as a co-op student for the Martin Company, Orlando, Florida, and as a Research Assistant at Georgia Institute of Technology. He held a summer position in 1964 with the Martin Company before returning to graduate school where he held an NSF Co-operative Fellowship for 3 years. From September, 1967, until June, 1968, he held a Graduate Teaching/Research Assistantship in the school of Electrical Engineering, Georgia Tech. He is presently employed by the Systems Sciences Research Laboratory of the Lockheed-Georgia Company, Marietta, Georgia.